University of São Paulo

Institute of Astronomy, Geophysics and Atmospheric Sciences

Department of Atmospheric Sciences

Mercel José dos Santos

Impact of the Rivers and the Seasonal Flooding on the Local Climate of the Central Amazon

Impacto dos Rios e da Inundação Sazonal no Clima Local da Região Central da Amazônia

São Paulo

2017

Mercel José dos Santos

Impact of the Rivers and the Seasonal Flooding on the Local Climate of the Central Amazon

Impacto dos Rios e da Inundação Sazonal no Clima Local da Região Central da Amazônia

Thesis presented to obtain the degree of Doctor of Sciences at the Institute of Astronomy, Geophysics and Atmospheric Sciences.

Major field: Meteorology
Advisor: Maria Assunção Faus da Silva Dias
Co-advisor: Edmilson Dias de Freitas

Final version. The original copy is available in the library.

São Paulo

2017

I would like to dedicate this Ph.D. thesis to my family.

Acknowledgements

this research would be impossible without the supercomputers.

I deeply thank my parents, Miguel José (dad), Vilma Gonzaga (mother), Melquesedequi (brother), Marcos Alex (bother) and Maria Camila (sister) for the unconditional love, encouragement and support. I love all of you.

I would like to offer my **special thank** to my girlfriend **Deyse Rodrigues** who always stood by me encouraging me to overcome all difficulties. Deyse has always said to me "keep calm my love, everything is gonna be alright". My adorable girlfriend, I am so grateful for your unconditional love, encouragement, and motivation. I love you.

Esta tese foi escrita em LaTeX com a classe IAGTESE, para teses e dissertações do IAG.

"Minhas raízes estão no ar, minha casa é qualquer lugar. Se depender de mim eu vou até o fim. Voando sem instrumentos, ao sabor do vento. Se depender de mim eu vou até o fim ..."

Humberto Gessinger

Resumo

O cenário da Amazônia central promove desenvolvimento de circulações locais haja visto que o mesmo é composto por superfícies que possuem capacidades térmicas diferentes (floresta, corpos d'água e a área urbana de Manaus). A inundação sazonal modifica a paisagem local e altera as condições hídricas do solo. Estudos sobre as circulações locais da Amazônia central e sua relação com as terras alagadas são escassos. Sendo assim, este trabalho investiga o papel dos rios e da inundação sazonal no desenvolvimento de circulações locais e na ilha de calor da cidade de Manaus. Os padrões locais de vento e umidade foram analisados com os dados das estações meteorológicas dos aeroportos de Manaus, enquanto que a variabilidade espacial e temporal da precipitação local foi analisada com dados estimados por satélite (TRMM e CMORPH). Os dados observacionais mostram que ventos dos rios para a cidade são comumente observados durante o dia e transportam ar mais úmido. No período noturno e no início da manhã, ventos que sopram da cidade de Manaus para os rios são frequentes e transportam ar mais secos. Esse padrão de vento geralmente verificado na região central da Amazônia evidencia as circulações de brisas fluviais. As estimativas por satélite mostram que durante o dia os máximos de precipitação ocorrem sobre a superfície da terra, enquanto que mínimos valores são observados sobre os rios. No período noturno, a precipitação é ligeiramente mais elevada sobre os rios quando comparada com a superfície terrestre. Os processos físicos envolvidos na formação das brisas fluviais foram analisados em um estudo numérico de um caso ocorrido em Julho de 2011. Este estudo de caso também permitiu analisar o impacto da inundação sazonal nas brisas fluviais. Os resultados deste estudo mostram que as brisas fluviais na Amazônia central desenvolvem-se devido ao distinto particionamento de energia apresentado pelas superfícies aquáticas e terrestres que promovem um marcante gradiente horizontal de temperatura.

A inundação sazonal altera o particionamento de energia das superfícies, provocando diminuição da temperatura do ar na região dos rios e consequentemente intensificação das brisas fluviais durante o dia. As brisas fluviais quando intensificadas propagam-se mais rapidamente sobre a superfície terrestre, perduram por mais tempo e promovem movimentos verticais mais intensos que alteram o transporte vertical de calor e massa. Experimentos numéricos também foram conduzidos para verificar a influência dos rios e da inundação sazonal no clima local de Manaus. Os resultados mostram que os rios promovem desenvolvimento de brisas fluviais que advectam ar mais frio sobre a área urbana de Manaus reduzindo a intensidade da ilha de calor no período vespertino. Esse efeito é mais intenso nos experimentos numéricos nos quais a inundação sazonal é adicionada uma vez que a mesma intensifica as brisas fluviais.

Palavras chaves: Brisa Fluvial, Ilha de Calor Urbana, Inundação Sazonal, Rios, OLAM.

Abstract

The landscape of the central Amazon promotes the development of local circulations since it is dominated by several land cover types (forest, water bodies, and the urban area of Manaus) of different thermal capacity. The seasonal flooding modifies this landscape and alters the hydric soil conditions. In this thesis, we in analyze the role of the rivers and the seasonal flooding of the central Amazon on local circulations development and the urban heat island of Manaus. Long-term data sets were analyzed to assess the local wind patterns and their role on spatial-temporal distribution of the moisture and precipitation. These data sets are wind direction and dew point temperature from weather stations and satellite estimates of precipitation (TRMM and CMORPH). The station data results show that onshore wind commonly occurs in the daytime and transport moist air from the rivers to the Manaus City. At night and in the morning, the offshore winds are frequent and transport drier air from Manaus City to the river regions. This diurnal pattern of winds is an evidence of the river breeze action. The rainfall data shows reduced values over rivers and maximum over land. At dawn and in the morning this pattern is opposite, i.e., maximum values of accumulated precipitation are found over the rivers and reduced values are observed over land. The physical processes involved in the river breeze formation were analyzed by simulating a case that occurred in July 2011. This case study also allowed to verify the impact of seasonal flooding on the river breezes. The results of this study reveal that the river breezes in the central Amazon are triggered because the different energy partitioning of the water and land surface leads to a remarkable horizontal thermal gradient. The seasonal flooding alters the surface energy partitioning causing a temperature decrease over the river region and intensification of the river breezes in the daytime. The intensified river breezes propagate more rapidly through the upland region,

take longer to dissipate and promote stronger upward vertical motion altering the heat and mass transport. Numerical experiments were also carried to accesses the impact of the rivers and the seasonal flooding on the local climate of Manaus. The results show that the rivers promote development of river breezes that advect cooler air into the urban area of Manaus reducing the urban heat island intensity in the afternoon. This effect is more intense when the seasonal inundation is taken into account since the seasonal flooding intensifies the river breezes.

List of Figures

List of Tables

List of Abbreviations

ABL   — Atmospheric Boundary Layer

AEG   — Eduardo Gomes

APP   — Ponta Pelada

CaMa-Flood   — Catchment-Based Macro–scale Floodplain

CFSV2   — NCEP Climate Forecast System Version 2

CMORPH   — CPC MORPHing technique

CPC   — Climate Prediction Center

DEM   — Digital Elevation Model

DRP   — Diurnal Cycle of Residual Precipitation

GCM   — General Circulation Model

GOES   — Geostationary Operational Environmental Satellite

HAND   — Height Above the Nearest Drainage

HINDU   — sensible heat released by industry

HTRAF   — Sensible heat released by traffic

ITCZ   — Intertropical Convergence Zone

JRA   — Japanese ReAnalysis

LEAF   — Land Ecosystem-Atmosphere Feedback model

LEINDU   — Latent heat released by industry

LETRAF   — Latent heat released by traffic

LST   — Land Surface Temperature

LT   — Local Time

MATSIRO   — Treatment of Surface Interaction Runoff

MODIS   — Moderate Resolution Imaging Spectroradiometer

MUA	—	Manaus Urban Area
MUHI	—	Manaus Urban Heat Island
NCEP	—	National Centers for Environmental Prediction
NDV	—	Normalized Difference Vegetation Index
NE	—	northeastern sector
NW	—	northwestern
OLAM	—	Ocean-Land-Atmosphere Model
PBL	—	Planetary Boundary Layer
SAMS	—	South American Monsoon System
SRTM	—	Shuttle Radar Topography Mission
SST	—	The Sea Surface Temperature
SW	—	southwestern
TEB	—	Town Energy Budget
TRMM	—	Tropical Rainfall Measuring Mission
TRMM LBA	—	Tropical Rainfall Measuring Mission Large-Scale Biosphere-Atmosphere
UHIC	—	Urban Heat Island Circulation
UHI	—	Urban Heat Island
UHII	—	Urban Heat Island Intensity
VFC	—	Vegetation Fractional Coverage
VP	—	vapor pressure
WST	—	Water Surface Temperature
WTD	—	water table depth

List of Symbols

P_{3r} — 3-hourly average of accumulated rainfall

P'_{3r} — Precipitation tendency

ϕ — Latitude

λ — Longitude

β_0 — Intercept of linear regressions

β_1 — Slope of linear regressions

β_2 — Slopes of linear regressions

R'_{3r} — Residual mean precipitation

H_0 — Null hypothesis in t-test

H_a — Alternative hypothesis in t-test

$\mu_d = 0$ — Difference of the mean rainfall between samples

N' — Sample size in t-test

ρ — Correlation between the samples

σ_{pred} — Standard deviation of predicted values

σ_{obs} — Standard simulated of predicted values

r — Correlation coefficient

MB — Mean Bias

RMSE — Root-Mean-Square Error

$RMSE_{UB}$ — Root-Mean-Square Error with bias removal

Contents

Chapter 1

Introduction

The Amazon region has the largest tropical rainforest in the world with an area of about 5,500,000 km^2. This forest has a great importance for the biodiversity and the climate since it holds million species of plants and animals and stores more than 100 billion tons of carbon. Thus, the Amazon conservation has been a subject of worldwide interest. The large water bodies is another important factor of the Amazon region since they have a great importance to the local economy, transportation, and electricity generation. The Amazon river, for example, has an extent of about 6,400 km and is the main way to access the cities and communities that are located near the coast. Some members of these communities are fishermen and their survival depends on the rivers. People in South American also depends on the electricity generated by the several hydroelectric dams spread over the Amazon. The extent and the water levels of the rivers are greatly affect by the interannual variability of the rainfall (Marengo, 2009; Papa et al., 2010; Marengo et al., 2012; Espinoza et al., 2013; Marengo et al., 2013; Satyamurty et al., 2013) causing serious consequence for the local population. During a drought period, for example, the low levels of the rivers make it difficult to navigate.

The water bodies of the Amazon also play an important role on the local climate due to their impact on the the local circulations development. This subject has been studied since 1990s when Molion and Dallarosa (1990) showed a spacial bias of precipitation near the Amazon rivers using data from few weather stations. These authors observed that total precipitation near the river margin is 30 % lower than values measured 30 km far fom the river and suggested that this pattern is caused by occurrence of river breezes. Further, studies carried out with a dense rain gauge network (Fitzjarrald et al., 2008) and satellites (Paiva et al., 2011) show that the spatial variation of precipitation near the water bodies

presents a considerable diurnal variation. In the daytime, maximum precipitation occurs far from the rivers whereas small rainfall values are founded over the water bodies. In the night period, the maximum of precipitation occurs over and very close to the water bodies. Numerical studies for the eastern Amazon have confirmed that the rivers promote development of local circulations (Silva Dias et al., 2004; Lu et al., 2005) and this affects the local distribution of precipitation Saad et al. (2010).

The intensity of local circulations triggered by rivers is greatly influenced by the large scale flow, coast shape, terrain, water surface temperature and the water size (Zhong et al., 1991; Crosman and Horel, 2010; Silva Dias et al., 2004). In this context, Silva Dias et al. (2004) showed that the river breeze in the eastern Amazon is stronger when the temperature of the rivers is colder during the daytime and warmer in the nighttime. Zhong et al. (1991) compared the river breeze intensity of two rivers in Florida, USA, (Indian and Banana rivers) and showed that local circulation triggered by the Indian river is stronger since it is wider. The extent of the water bodies in the Amazon region is affected by the seasonal flooding, suggesting that this phenomena can influence the local circulation and consequently the local climate. The seasonal flooding also influences the local climate by inundating the local vegetation and affecting the surface energy partitioning (Borma et al., 2009; Dadson et al., 2010; Schedlbauer et al., 2011). Inundation in Amazonian has maximum extent during May to June and occurs over the floodplain areas mostly located around rivers and lakes (Hess et al., 2003).

In the central Amazon, where the Negro and Solimões rivers encounter, the scenario promotes development of a particular case of river breezes since it is dominated by water bodies, forest, and the Manaus urban area. The floodplain areas in this region are large and located around Amazon and Solimões rivers and over the Negro River (Hess et al., 2003). The evidence of river breeze in the central Amazon was shown by Oliveira and Fitzjarrald (1993) by analyzing wind data collected in the field campaigns. The urban area of Manaus is another important factor of the central Amazon since it promotes the development of an Urban Heat Island – UHI (Maitelli and Wright, 1996; Souza and Alvalá, 2012). Acordding to Souza and Alvalá (2012) this UHI is remarkable with intensity reaching 3.5 °C in the dry season.

1.0.1   Objectives

The rivers play an important role in the local climate as highlighted above. In this study, we analyze the river breeze development in the central Amazon, its response to the seasonal flooding, and its influence on the local climate of Manaus. These analyses allow to answer to following specific questions:

- How frequent is the river breeze occurrence in the central Amazon?

- Do the local circulations in the central Amazon affect the moisture transport?

- Does the river breeze affect the diurnal cycle of precipitation in the central Amazon?

- How are the river breezes triggered in the central Amazon and how do they affect the convection?

- Does the seasonal flooding affect the river breeze intensity and its response to the local convection?

- Does the roughness variation over the floodplain/upland forest interface alter the river breeze?

- What are the rivers impact on the UHI of Manaus?

- Does the seasonal flooding affect the UHI of Manaus?

The answer to these questions are presented in the next chapters. In chapter 2 we analyze long-term data sets of wind direction, dew point temperature and precipitation to investigate the local wind patterns and its influence on the moisture transport and the spatial-temporal distribution of precipitation. In chapter 3, we address the impact of the seasonal flooding on the river breeze by means of numerical experiments carried out with OLAM (Ocean-Land-Atmosphere Model) coupled with land surface models. Numerical simulations are also used in chapter 4 to investigate the influence of the rivers and the seasonal flooding on the UHI of Manaus. Finally, chapter 5 shows main conclusions of this research and future works.

Chapter 2

Observational analyses of Local circulations and its Influence on Moisture, and Precipitation

This chapter is based on the paper titled as **Influence of local circulations on wind, moisture, and precipitation close to Manaus City, Amazon Region, Brazil** that was published by the author of this thesis on the **Journal of Geophysical Research: Atmospheres**

2.1 Introduction

The Amazon region is one of the major areas of the earth occupied by tropical evergreen forest (Lapola et al., 2008), being an appreciable source of water vapor for the local atmosphere (Zeng et al., 2012) and regional area, particularly for the Central Brazil region (Rao et al., 1996). The Amazon region comprises huge water bodies such as the Amazon, Negro, Solimões, and Tapajós rivers, which play a fundamental role on Amazonian hydrological cycle (Marengo, 2005, 2006) and are essential to river breeze formation (Silva Dias et al., 2004; Lu et al., 2005; Fitzjarrald et al., 2008). The river breeze circulations are thermally induced wind patterns, resembling the sea breeze, generated by the different surface temperature between the hot land and the cool water during day time which produces a horizontal pressure difference. At night the situation is reversed and the land breeze may be observed. The local circulations affect the moisture transport (Silva Dias et al., 2004), as well as the spatial and temporal distribution of precipitation in the Amazon region (Fitzjarrald et al., 2008; Paiva et al., 2011). However the detailed long term average of the circulation and moisture relationship has not been analyzed before in this region.

The local circulations in the Negro and Solimões confluence region (Central Amazonian)

have been studied by Oliveira and Fitzjarrald (1993). The rivers (Negro, Solimões, and Amazon) in this region ($2-4^{\circ}$ S, $62-58^{\circ}$ W) assume particular characteristics concerning orientation, shoreline curvature, and water surface temperature (Figure 2.1a), which may affect the intensity of the local circulations. Another important feature of the Central Amazonian region is the Manaus Urban area, with approximately 517 km^2 (Figure 2.1a). Some authors (e.g., Maitelli and Wright, 1996; Souza and Alvalá, 2012) have demonstrated the existence of the the Urban Heat Island (UHI) effect of the Manuas City. Souza and Alvalá (2012) pointed out that the temperature difference between the urban and forest region in the wet season (December-May) is lower than in the dry season (June-November), and the daily cycle of the temperature difference has a peak in the morning (08 A.M. local time) and another in the afternoon (between 03 and 05 P.M. — local time). The UHI of the Manaus City likely affects the severity and propagation velocity of the river breeze circulation. According to Freitas et al. (2007), the UHI of São Paulo metropolitan area accelerates the sea breeze front propagation before reaching the urban region, as well as intensifies the updraft and slows the propagation when the sea-breeze front is over the urban area.

The topography around the confluence region has different characteristics depending on river bank sides (Figure 2.1b). Whereas in the southern side of the Amazon and Solimões rivers the elevation is low and rather flat, in the northern side of the Amazon River the topography is more complex, characterized by valleys (the tributaries of Amazon River) and relatively high hills (peaks ranging between 150 and 240 m). In both Negro River flanks, the terrain is considerably high (about 75 m), which may conduce to the channeling of large-scale wind flow over the rivers as observed over Amazon and Tapajós confluence region (Fitzjarrald et al., 2008).

The way in which the river breeze interacts with the urban heat island, the rain forest and even with topography is a challenging problem that has implications on the ability to model the rainfall distribution and amounts. This is particularly important in a tropical environment where large scale forcing is much weaker than in mid-latitudes and in equatorial regions like Central Amazon. In these regions surface forcing has been seen to affect the distribution of cloudiness, and eventually rainfall, associated with deforestation (Cutrim et al., 1995; Durieux et al., 2003; Saad et al., 2010).

In the vicinity of the Amazon and Solimões rivers (i.e., in the low and flat areas), there

are lakes and permanent wet lands as wide as the rivers (Figure 2.1a). The width of the Amazonian and Solimões rivers is about 5 km, whereas the Negro river width ranges from 3 to 22 km. The width of the lakes located around the Amazonian rivers is about 10 km. The influence of the river width on the breeze circulation was shown by Zhong et al. (1991) in two rivers in Florida, US, by means of numerical atmospheric model experiments. The authors showed that the breeze circulation of the Indian River is stronger than the breeze of the Banana River, since the Indian river is wider than the Banana river.

The surface temperature of the Amazon River and neighboring lakes are similar, especially at night. Thus, the region of increased temperature observed at night over and around the Amazon river is wider than those observed over the Negro and Solimões rivers (Figure 2.1c). The Amazon River water surface temperature is also higher at night. At daytime the Water Surface Temperature (WST) of the Negro river is the coldest, specially in the wet season. The seasonal variation of the rivers WST (Figure 2.1d) is well defined with maximum values occurring in the wet and minimum in the dry season. The rivers WST is a fundamental element for land/water temperature gradient existence that is indispensable for developing the river breeze. Silva Dias et al. (2004) studied the influence of the WST on river-breeze circulation by numerical modeling. The authors showed that higher values of WST promoted stronger river-breeze circulation at nighttime, whereas the colder WST supported stronger circulation at daytime.

The large-scale flow of the Amazonian region is basically composed by southeast and northeast trade winds, which are modulated by the subtropical high pressure systems of the North and South Atlantic. This large-scale pattern is changed during a *friagem* event, which occurs when a frontal system reaches the Central Amazon. Marengo et al. (1997) observed reduction of the temperature and wind values over Manaus City during a *friagem* event. The large-scale flow affects the development and the localization of the river breeze circulation. In this context, Silva Dias et al. (2004) observed reversal of the wind caused by the river breeze circulation of the Tapajós River during weak trade winds conditions (i.e., *friagem* event). Lu et al. (2005) showed that this kind of reversal did not occur during the strong trade winds conditions in the dry season (period from 1 to 15 August 2001).
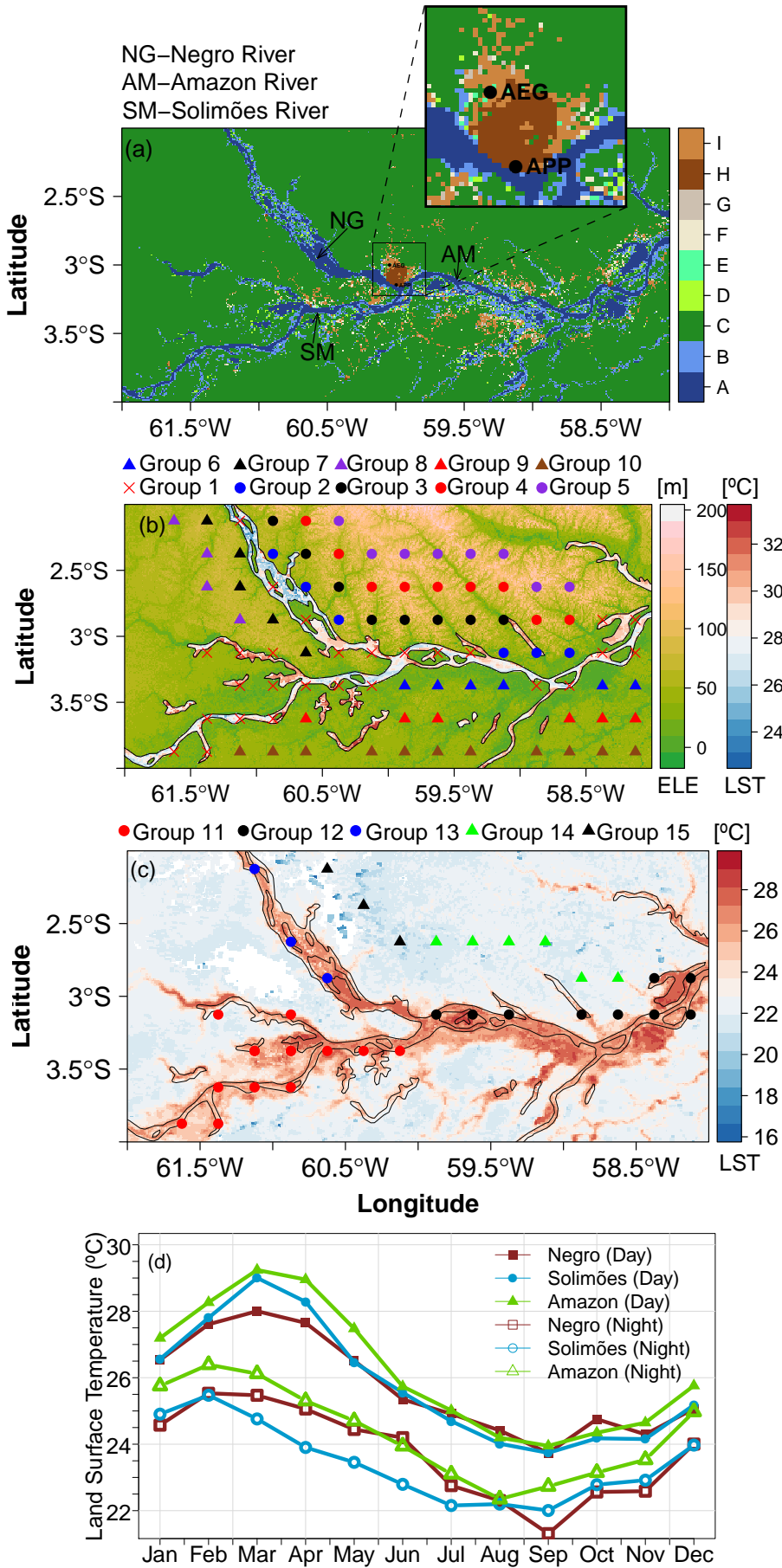
Figure 2.1: (a) Land cover map of the region (A = Water, B = Permanent Wetlands, C = Evergreen Broadleaf Forest, D = Mixed Forests, E = Croplands, F = Woody Savannas, G = Savannas, H = Urban and Builtup, I = Cropland/Natural Vegetation Mosaic) from Moderate Resolution Imaging Spectroradiometer (MODIS) and spatial location of the airports weather stations (Eduardo Gomes, AEG, and Ponta Pelada, APP, stations), (b) elevation (ELE) on the land domain, 8 day average (between 5 and 12 May 2012) of land surface temperature (LST) from MODIS in the daytime over the rivers domain, and groups of grid points with the same distance of the riverbanks, (c) 8 day average at nighttime (the period and source is the same as in Figure 1a) and groups of grid points that have the same distance from the margins and form a virtual line parallel to a river, and (d) intra-annual variability of the surface temperature of the rivers during the day and nighttime.

The purpose of this paper is to assess the local wind patterns, and their role on spatial-temporal distribution of the moisture and precipitation close to the Manaus City region. Section 2.2 details the meteorological data and the statistical analyses. Section 2.3.1 presents results and discussions about the pattern of the wind direction observed in Manaus City, by using long-term data sets that allow quantitative estimates with detail that has not been obtained before in analysis of short periods. The role of wind on moisture transport over Manaus is shown in section 2.3.2. The spatial and temporal variability of the precipitation is discussed in section 2.3.3. Finally, the conclusions are presented in section 2.4.

2.2 Data and Methodology

The data used here consists of 35-years of hourly data (1978-2012) of surface weather stations from two Manaus airports, Eduardo Gomes (AEG) and Ponta Pelada (APP), as well as 15 years (1998 - 2012) of rainfall estimates from TRMM and CMORPH over Central Amazonia. Figure 2.1a shows the spatial location of the weather stations. Specifically, the data set from weather stations are wind direction and dew point temperatures,measured at 10 and 2 m height, respectively. The wind direction was considered only when the wind velocity was greater or equal to 0.5 m/s. The dew point temperature data were used to calculate vapor pressure (e.g. Bolton (1980) relationship), which was used as an atmospheric moisture indicator. By means of the wind direction and vapor pressure data we analyzed the patterns of wind and moisture, and how these patterns are influenced by

local circulations over the regions of Manaus airports that encompass the urban area of Manaus and are close to the encounter of Negro and Solimões rivers that turn into the Amazon River.

The TRMM estimates used here are the precipitation rate (mm h^{-1}) over the global belt region that extends from 50º N to 50º S, which is called 3B42 product version 7. The grid space of TRMM-3B42 is about 25 x 25 km^2 at equator and has 3-hourly temporal resolution (Huffman et al., 2007). The CMORPH also was a rainfall rate (mm h^{-1}) estimates but with better spatial (about 8 x 8 km^2 at equator) and temporal (30 minutes) resolution. These estimates are made for a global belt area extending from 60ºN to 60º S (Joyce et al., 2004). These data were used to analyze the influence of the river breeze circulation on the spatial and temporal distribution of precipitation near the Negro and Solimões rivers confluence region (Figure 2.1a). Some statistical characteristics of rainfall from satellite estimates (TRMM-3B42 and CMORPH) and rain gauge measurements over the Amazon basin were analyzed by Buarque et al. (2011). The authors found a strong (moderate) correlation between mean annual rainfall calculated from TRMM (CMORPH) estimates and the rain gauge measurements, as well as they verified moderate correlation between the mean 95 % quantiles of daily rainfall from satellite estimates and gauge observations. Silva et al. (2009) performed comparisons between TRMM-3B42 and S-band radar precipitation estimates during the Tropical Rainfall Measuring Mission Large-Scale Biosphere-Atmosphere (TRMM LBA). They show that TRMM-3B42 rainfall estimates reproduce well some characteristics of the diurnal cycle i.e., maximum precipitation at 21 UTC and highest values in the nighttime when the rainfall is predominantly stratiform. However, the quantitative analyses shown that TRMM LBA underestimated the precipitation in about 50 %.

The satellite estimates were used to calculate 3-hourly accumulated precipitation. With these data we made 3-hourly average of accumulated rainfall (P$_{3r}$) providing the diurnal cycle of precipitation over the region under study. These averages allow the assessment of spatial distribution of the rainfall diurnal cycle close to the rivers. As the Central Amazon has an intrannual variability of the precipitation characterized by high rainfall values from December to May (wet season) and reduced rainfall from July to November (dry season) (e.g., Ribeiro and Adis, 1984), we calculated P$_{3r}$ for the dry and wet seasons to verify how the local circulations affect spatial distribution of the precipitation in each rain regime.

Monthly daily cycle of precipitation without spatial trend also was calculated and used to verify (by means of a statistical t-test) the river proximity effect. Fitzjarrald et al. (2008) and Paiva et al. (2011) have stressed that the daily patterns of precipitation on the regions far away from the rivers have different phases regarding the rainfall diurnal cycle from those over and very near to the rivers. Thus, the 3-hourly spatial tendency was calculated for each month by means of multiple linear regression according to the following equation $P'_{3r} = \beta_0 + \beta_1\phi + \beta_2\lambda$. Where P'_{3r} is the precipitation tendency (dependent variable), ϕ (Latitude) and λ (Longitude) are predictor variables, β_0 is the intercept, β_1 and β_2 are the slopes. Therefore the residual mean precipitation used in the analysis is $R'_{3r} = P_{3r} - P'_{3r}$, where P_{3r} is the 3-hourly averages of accumulated rainfall. The spatial trend was removed to emphasize the maximum and minimum precipitation values of the diurnal cycle.

The statistical t-tests were peformed for grouped points according to the distance from river banks, as shown in Figure 2.1b. From the monthly daily cycle of residual precipitation we made averages of the grid point values in each time, resulting in temporal series for each groups. These group temporal series were used to calculate averages in two different ways: i) average of the monthly daily cycle of residual precipitation, referred as mean residual rainfall, ii) average at each 3-hours, providing the mean Diurnal Cycle of Residual Precipitation (DRP) for each group. Then, the Student's t-test was applied to verify whether mean residual rainfall and DRP differ between some groups. In the tests we considered the difference of the mean rainfall (mean residual rainfall and DRP) between some groups ($\mu_d = 0$) as null hypothesis (H_0), $\mu_d \neq 0$ as alternative hypothesis (H_a) and $\alpha = 0.05$. The sample size (N') used in these t-tests was calculated according to the falowing equation $N' = N(1 - \rho)/(1 + \rho)$. Where N is the original sample size and ρ is the correlation between the groups. Similar aproach was applied by Paiva et al. (2011).

The rivers close to Manaus City region have different morphological characteristics, like width, orientation, and water surface temperature that may influence the local circulations and precipitation in many ways. Hence we grouped points that form a virtual line parallel to the river banks to verify the influence of these morphological characteristics on the river breeze and consequently on the precipitation patterns. Then we also applied Student's t-test (detailed above) for each group of pairs constituted by the points with the same distance from the rivers but parallel to the Amazon and Negro rivers, respectively, to verify whether the rainfall regime of the groups differs from each other.

Finally, we analyzed the monthly daily cycle of residual precipitation for groups which have rainfall regime statistically different.

2.3 Results

2.3.1 The observed wind features

The wind direction pattern was analyzed by polar plots of wind frequency. In these diagrams the wind frequency is shown as a function of the direction (azimuth) and local time — distance from the center —, allowing to assess the diurnal cycle of the wind direction. The null wind relative frequency values in these diagrams show that there is no wind blowing in the correspondent direction and time. The relative frequency is defined as the number of times that wind was from a given direction at a given time divided by the total number of records. If the wind magnitude was less than 0.5 m/s the data was not cosidered (representing 43 % of the complete dataset for Ponta Pelada and 56 % for Eduardo Gomes). Figure 2.2 shows the relative frequency of the wind for each direction and local time for the Eduardo Gomes airport station data, for each month. In this Figure, it is also possible to see that there is a preferential wind direction in each season. In the rainy season (Figure 2.2a to e and Figure 2.2l), the wind flows more frequently from the northeastern sector (NE), while in the dry season (Figure 2.2f to k) the highest values of wind frequency are observed on the southeastern sector (SE). In the months of April (Figure 2.2d), September (Figure 2.2i), and October (Figure 2.2j) the predominant direction of the wind oscillates around 90 °. The majority of the frequencies, which change between the NE and SE sectors, are linked to the seasonal variability of the trade winds. In the rainy season, the large scale circulation pattern intensifies the northeastern trade winds over the Amazon region because the North Atlantic subtropical high is stronger than the South Atlantic subtropical high. The opposite pattern, which increases the southeastern trade winds, occurs in the dry season.

The relative high values noticed on southwestern (SW) and northwestern (NW) sectors in the diurnal time period, which occurred more frequently during the dry season, may be due to the river breeze action associated to the Negro River. At daytime, under cloudless and weak large-scale flow conditions, which provide a strong thermal contrast between land and water surface, the river breeze wind may be excited and reported as southwestern and

northwestern winds at Eduardo Gomes airport weather station. Silva Dias et al. (2004) showed that the river breeze wind on the eastern side of the Tapajós was sufficient to overcome large-scale wind flow during an Amazonian *friagem* event. In this event the large scale flow was characterized by weak trade winds. At nighttime and dawn the wind frequency values are almost null on NE sector, indicating that the land breeze occurrence over the Eduardo Gomes airport region is rare.
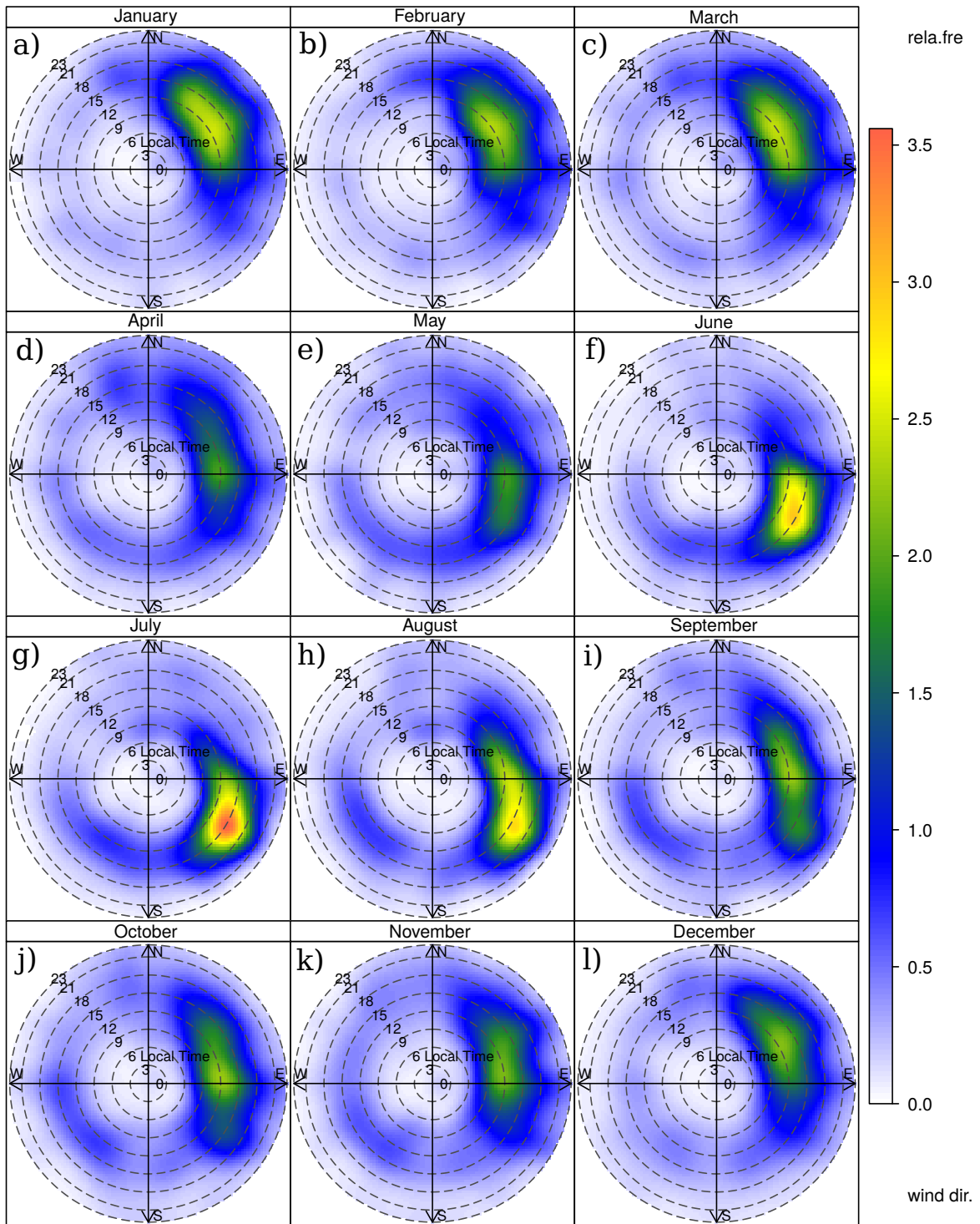
Figure 2.2: Monthly relative frequency of wind direction (10^4) as a function of the direction (azimuth) and local time (distance from the center, i.e., the dashed lines) for Eduardo Gomes airport weather station.

The seasonal variability of the wind frequency over Ponta Pelada airport region is similar to the one of the Eduardo Gomes airport region; in other words, the northeastern

wind is the most frequent in the rainy season (Figure 2.3a to e and 2.3l), while in the dry season (Figure 2.3f to k) the most persistent wind comes from the southeast. This pattern is associated to the trade winds seasonality, as previously explained.

The diurnal variation of the wind direction over Ponta Pelada airport region is also expressive (Figure 2.3). At nighttime and dawn we verified maximum values of wind frequency on NE and NW sectors (e.g high frequency of wind toward rivers), whereas the values around zero were observed on the SE and SW sectors, indicating that winds blowing from river towards the land are less frequent. These features, which are less evident in the wet season, are modulated by land breeze circulation that is induced by the thermal gradient between Manaus city and the river water surfaces. During the day, the river breeze circulation is also better defined in the dry season. In this season, between 9 and 18 local time, southern and southeastern winds (away from the rivers) are the most frequent, whereas northeastern and northwestern (toward the rivers) are the most infrequent. Between June (Figure 2.3f) and August (2.3h) there was no wind from the north over Ponta Pelada airport region during the day, because the river breeze and large scale winds blew from south. Oliveira and Fitzjarrald (1993) observed a similar behavior of diurnal wind direction cycle over Manaus city and Ducke Reserve during the dry (between April 13 and May 13, 1987) and wet (between July 15 and August 5, 1985) seasons.
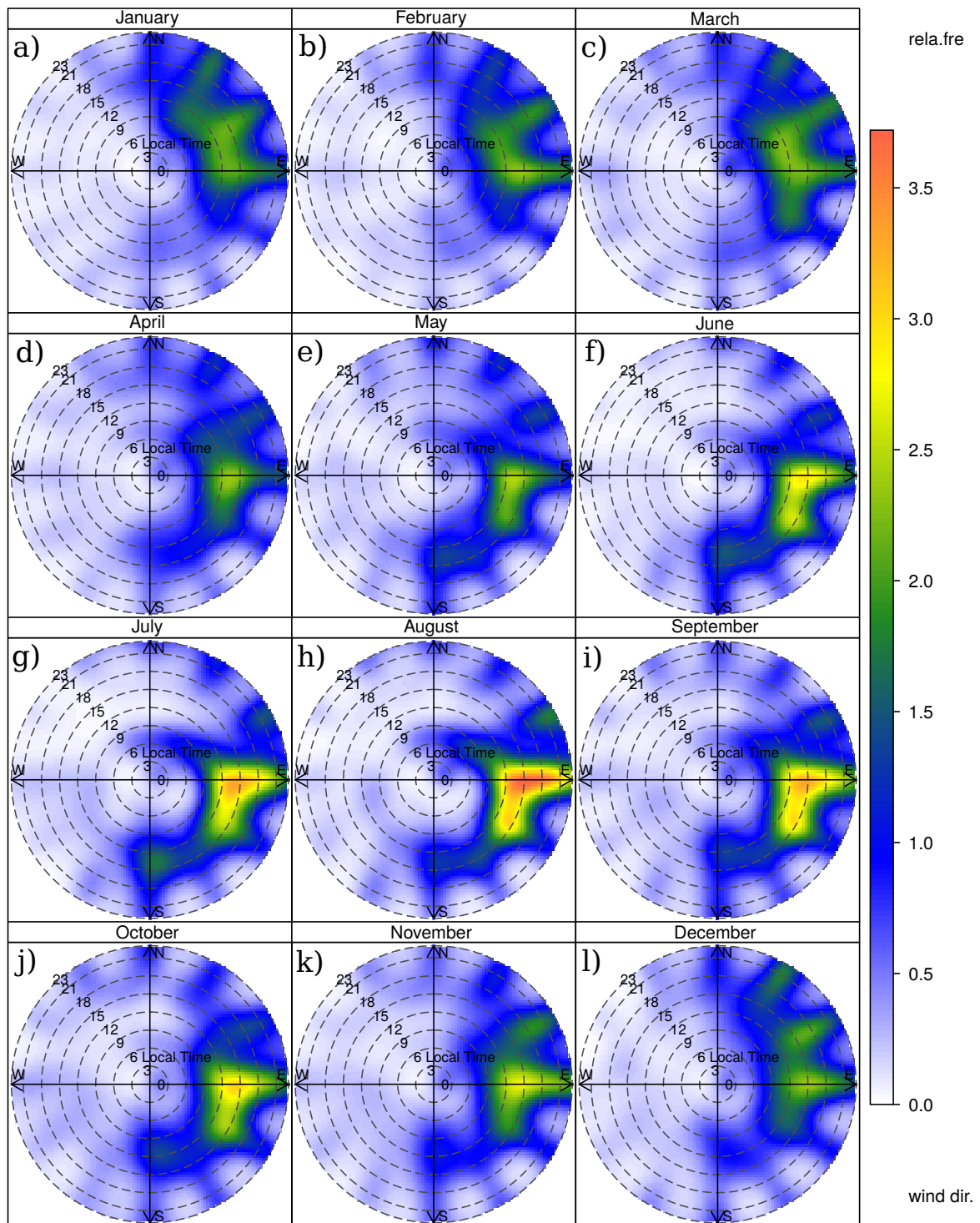
Figure 2.3: Same as in Figure 2.2 but for Ponta Pelada Airport weather station.

2.3.2   The moisture pattern and transport by the wind

On the previous section we analyzed the daily and seasonal cycle of wind direction over the regions of Manaus airports. Herein we focus on the impact of the wind direction

oscillation on the moisture transport over these regions. But first we present the daily and seasonal cycle of moisture over the regions.

Figures 2.4a and 2.4b show the daily cycle of vapor pressure (VP) for each month over the two airports. These figures show that, in both stations, the maximum values occur in the wet season, and minimums in the dry season. A similar seasonal behavior of VP was observed by Culf et al. (1996) over a region close to Manaus City. This seasonal cycle is modulated mainly by the seasonal oscillation of the Hadley cell, as well as by the South American Monsoon System (SAMS). The SAMS, which is characterized by a seasonal reversal of low level wind — verified only when the strong annual mean wind is removed, supports the moisture increasing in the Amazon wet season and the moisture decreasing the dry season. (Rao et al., 1996; Zhou and Lau, 1998; Gan et al., 2004; Raia and Cavalcanti, 2008). In the dry season, the descending branch of Hadley Cell is over the north of the Southern Hemisphere, while the ascending branch (e.g Intertropical Convergence Zone - ITCZ- region) is over the Northern Hemisphere. This subsidence promotes entrainment of drier air from free atmosphere into the Planetary Boundary Layer (PBL), which promotes the reduction of atmospheric moisture near the surface (Betts et al., 2002).
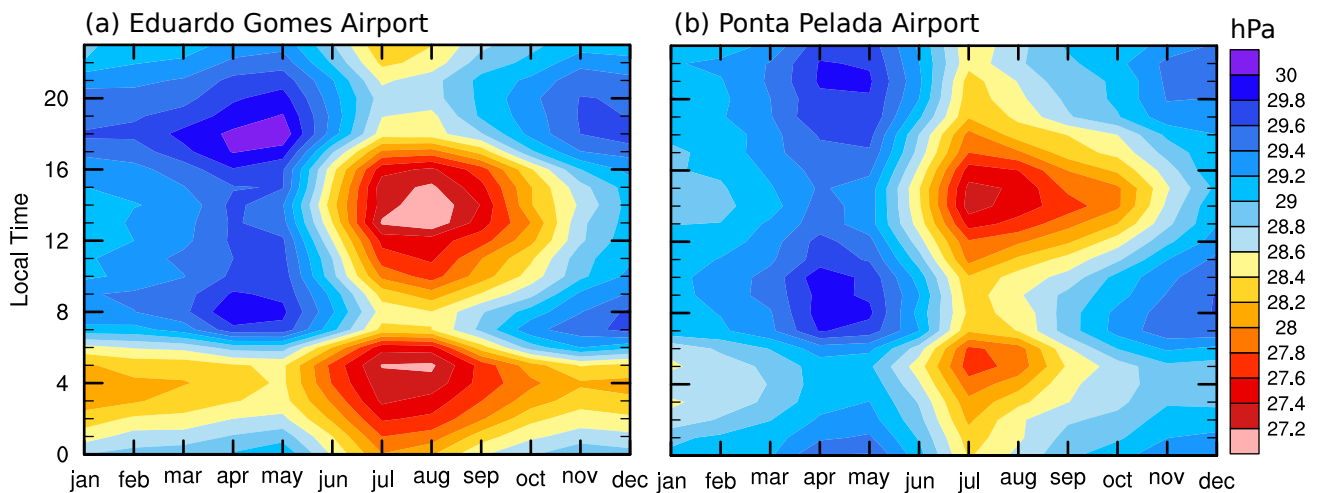
Figure 2.4: Daily cycle of vapor pressure for each month.

The main characteristics of the daily cycle of VP (in both stations) are the minimum values observed before sunrise and in the afternoon, as well as the maximum values that come about in the morning and in the evening as seen in Figures 5 and 6. Minimum values at dawn occur due to the vapor condensation, since the mean saturation deficit at this time is very close to zero (results not shown). Culf et al. (1996) observed occurrence

of saturation at night over all days of April, May, and June 1991-1993 on measurement performed over a pasture region (experimental site located near Manaus City). In the other months, the authors observed less frequent saturation events.

The increasing of VP after sunrise, observed in both stations data, occurs due to the enhancement of evapotranspiration that is triggered by the solar energy absorbed by the surface at this time. The VP reduction around midday happens owing to upward movements of thermally induced turbulence, which transport water vapor from the mixed layer to the atmospheric entrainment zone at a rate greater than the evaporation and transpiration rate. Martin et al. (1988) and Betts et al. (2002) also emphasized these relationships by analysing the vertical moisture flux (w'q') and specific humidity over Manaus Region and Rondônia.

Figures 2.5 and 2.6 show the daily cycle of VP as a function of wind direction at the Eduardo Gomes and Ponta Pelada airport weather stations, allowing to assess the influence of wind direction oscillation on the moisture transport over the airports regions. It can be seen from Figure 2.5a and 2.5b that when the wind direction is between 180 and 360 ° high values (about 30 hPa) of VP are observed from the morning until midnight while minimum values are seen at dawn, which differs from the climatological daily cycle (Figure 2.4a). This increase of VP after sunrise until midnight happens because of the southwesterly and northwesterly winds, which transport moist air from Negro River towards Eduardo Gomes airport region. When the wind comes from the Amazonian Forest or urban region (Manaus City), the daily cycle of VP is similar to the mean daily cycle (e.g Figure 2.4a) i.e., minimum values happen before sunrise and in the afternoon, whereas the maximum values occur in the evening. This decrease of VP in the afternoon in the dry season is stronger than that observed in the rainy season and it occurs because the winds from the forest and urban regions transport relatively drier air.

In the wet season, when the wind comes from the Forest or Manaus City, there is not a considerable difference on diurnal cycle of VP or in the magnitude of VP; while in the dry season, even though the same diurnal pattern is observed, there is a notable difference on the magnitude of the values and it depends on whether the wind is northeasterly or southeasterly. When the wind blows from the south, the VP values between 11:00 A.M. and midnight (local time) are much smaller than the values observed when the wind comes from the north.
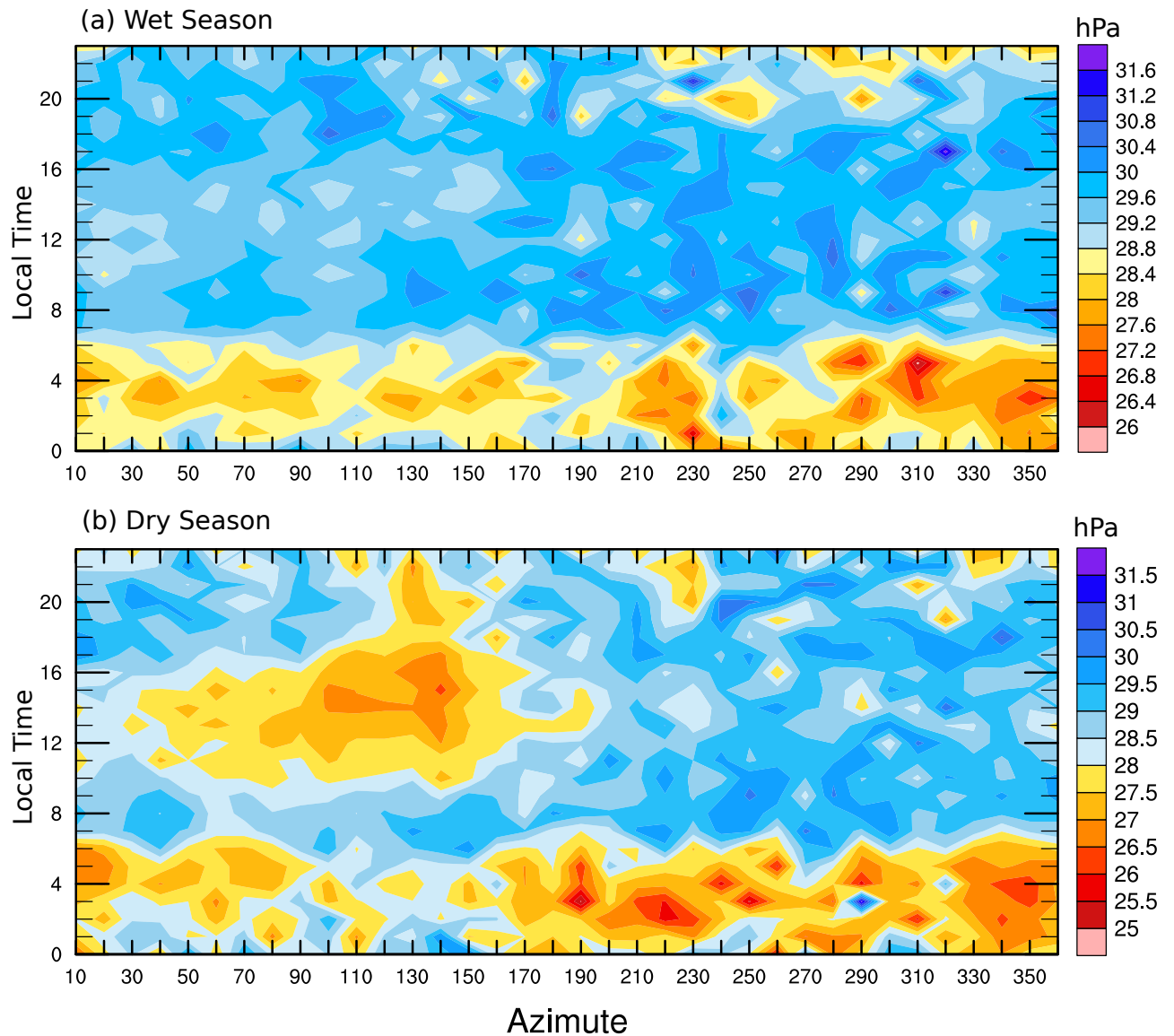
Figure 2.5: Daily cycle of VP as a function of wind direction (azimuth) for Eduardo Gomes weather station.

Over Ponta Pelada airport weather station the onshore wind is more often reported, because this weather station is located near the margin of a convex coastline (Figure 2.1a). Thus, the onshore wind transports moister air to Ponta Pelada airport region, whereas the transport of drier air from Manaus City occurs mostly under northern wind circumstances. These phenomena can be seen through the 2.6a and 2.6b, where the diurnal cycle of VP for wet and dry season is, respectively, shown. These figures clearly show that when the wind blows from the rivers (e.g., wind direction between 80 and 300 °), the VP values are substantially greater than the values observed when wind comes from the urban region.
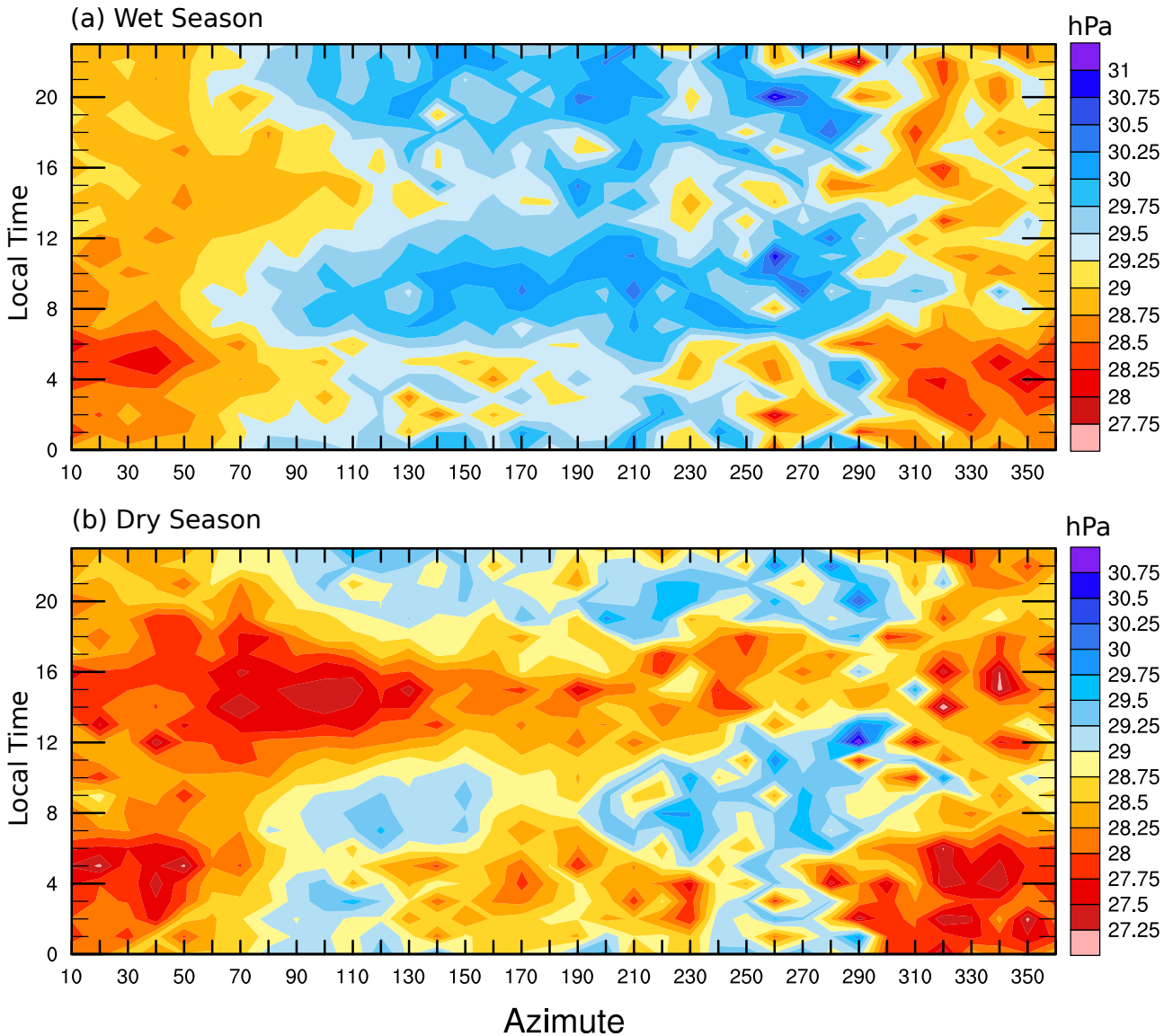
Figure 2.6: Same as in Figure 2.5 but for Ponta Pelada Airport weather station.

2.3.3   Spatial and temporal distribution of the precipitation

The influence of local circulations on the spatial distribution of precipitation was analyzed by 3-hours averages of accumulated precipitation calculated for the dry and wet seasons. The spatial distribution of the precipitation in the afternoon and in the evening (Figure 2.7) showed minimum values on the river regions and maximum over the land that may be due to a combination of cooler surface over the river/warm surface over land which favors convection over land plus the action of the river breeze, which transports moist air toward the land, leading to convergence, cloud development and consequently precipitation (Fitzjarrald et al., 2008). Reduced precipitation over the rivers is also a result of the downward

movement (subsidence), which is likely observed over the rivers and is promoted by the river breeze circulations, hampering the cloud development and precipitation (Silva Dias et al., 2004). Similar spatial distribution of the rainfall for the same period was shown by Paiva et al. (2011) in regions close to Amazonian rivers. This spatial characteristic of the precipitation at nighttime is less evident, mainly after 8:00 P.M. (local time), where there is no evidence of local circulations on the precipitation field. The river breeze circulation at this time, transition period from river to land breeze, is not so obvious because the thermal gradient between land and river surfaces is very weak.

The highest values of precipitation in the afternoon were observed on the western part of the studied region, specifically near the eastern margin of the Negro River. The maximum rainfall on the eastern margin of the Negro River probably occurred due to two combined effects: i) the large magnitude of the river breeze wind associated to Negro River, since the day time surface temperature of Negro River is coldest, mainly, in the wet season (Figure 2.1d) and ii) the river breeze wind, in the eastern side of the Negro River, converges with offshore synoptic-scale flow. These factors promote the vertical transport of air and, consequently, cloud development and precipitation.

In the western side of the Negro River, the maximum precipitation happened far away from the margin because convergence, induced by of the roughness of the forest, occurs far away from the river, since the synoptic-scale flow on the western side is onshore (i.e., almost always, the river breeze and synoptic-scale wind have the same direction).

At dawn and in the morning the maximum values of accumulated precipitation were found over the rivers, mainly over and around the Amazon River (Figure 2.8), and it happens due to the wind convergence over the rivers, which is caused by the action of the land breeze. The increase of the precipitation over and surrounding the Amazonian rivers at dawn has also been observed by some authors (Fitzjarrald et al., 2008; Paiva et al., 2011). In the vicinity and over the Amazon River the increase in accumulated precipitation was much more expressive because its water surface temperature at nighttime is the hottest comparing to the other rivers (Figure 2.1c and d). At night, the hot waters contribute to raise the land/water thermal gradient and, thus, to promote a more intense land breeze circulation. The permanent wet land regions situated around the Amazon River (Figure 2.1a), mainly on its southern side, is another factor that contributes to enhancement of the land breeze, since these marsh surfaces have similar temperature at night (Figure 2.1c)

and are as wide as the rivers.
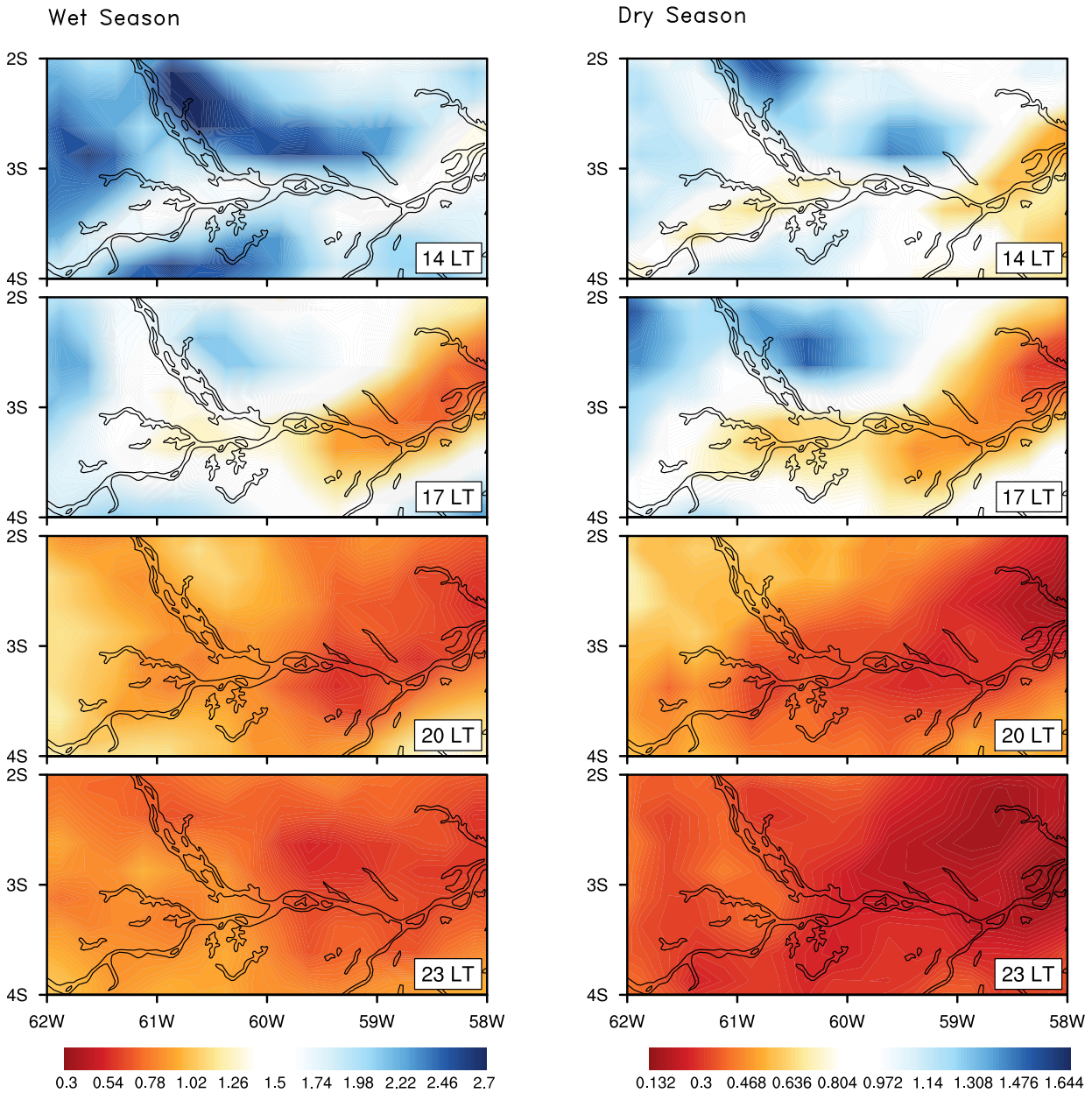
Figure 2.7: Spatial distribution of average accumulated precipitation from TRMM (in millimeters) in the afternoon and evening for central Amazonian. LT means local time.

The spatial precipitation pattern in the dry and wet season is very similar except at dawn and in the morning. In the dry season, characterized by cloudless condition, the pattern of maximum rainfall over the rivers and reduced over the land was only verified in the morning, mostly at 11:00 A.M. (local time) (Figure 2.8). The cloudless condition contributes to development of local circulations. Probably, the decreased WST observed in the dry season (Figure 2.1d), which promotes weaker land/water temperature gradient at night, can reduce the intensity of the land breeze circulation in this period and thus can

also reduce the convergence and precipitation over the rivers.

On the Negro River margins, in the rainy season, the average of precipitation at 5:00 A.M. (local time) (Figure 2.8) shows an opposite spatial pattern to that observed during the afternoon time (Figure 2.7). Figure 2.8 illustrates that in the closeness to the western Negro River margin the accumulated precipitation values are greater than on the eastern side nearby the margin. These features might be attributed to the displacement of the land breeze convergence (caused by the northeasterly wind in the wet season) that would occur over the Negro river, and thus the subsidence (associated to the river circulation) would promote decreased precipitation on the eastern side of the river.

The aforementioned analysis were also made using CMORPH data. The results were very similar to those obtained from TRMM satellite estimates, especially in the afternoon, as shown the Figure 2.9. The main difference between 3-hourly average of accumulated precipitation from TRMM and CMORPH was in respect to the magnitude values, where the TRMM has larger values than CMORPH in general. Buarque et al. (2011) found that these two data sets are well correlated with raingage data for yearly totals. The fact that the rainfall distribution is similar in Figures 7 and 9 renders confidence that the results present reliable estimates of the rainfall distribution.

As previously shown, the daily cycle of precipitation over the studied region changes according to the distance from the river margins due to the presence of the local circulations. Consequently, we created groups of grid points constituted by points with the same distance from the rivers (Figure 2.1b). Then, we tested (i.e., Student's t-test) mean residual rainfall and DRP for each group pairs to set up groups with the same rainfall patterns, as well as to assess how the river proximity — in different margin sides of the rivers — affects the daily precipitation cycle.
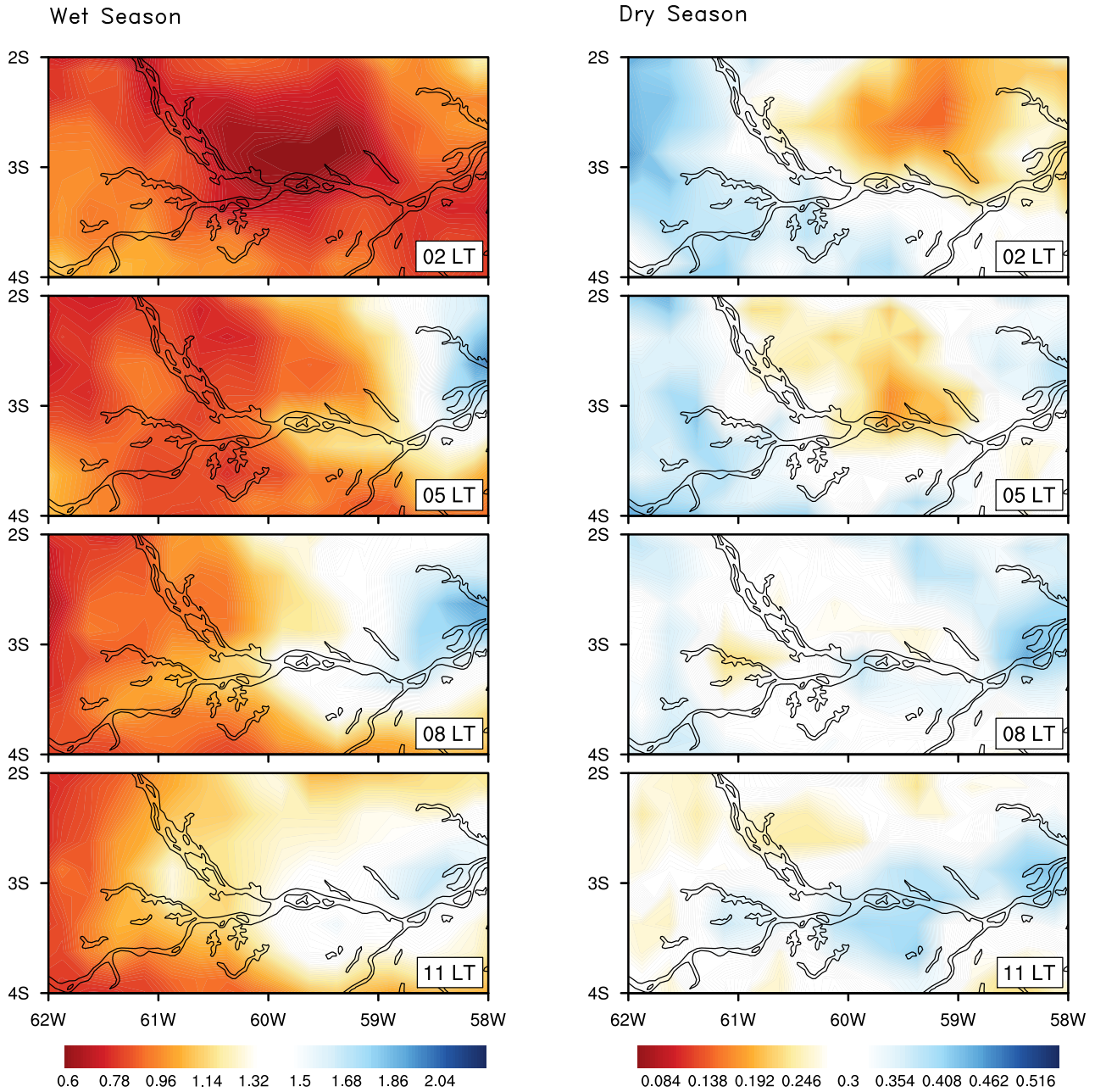
Figure 2.8: Same as in Figure 2.7 but at dawn and in the morning.

The statistical characteristics of these groups and the t-test results are shown on Table 2.1. Over the rivers and on the land regions (very close to the river margins) the mean residual rainfall is statistically the same. In other words, the Student's t-test shows that mean residual rainfall for the groups 1, 2, 6, and 7 are equal. However, the mean residual rainfall over the regions situated about 25 km away from the rivers is different with respect to the cycles observed on the river and margin regions, as shown in the group 1/group 3 t-test. These t-tests also show that the groups situated about 25 km afar from the rivers margins (group 3) and the groups located farther from margins (e.g., group 4, 8, and 9

placed about 50 km, group 5 and 10 at about 75 km) have the same mean residual rainfall.
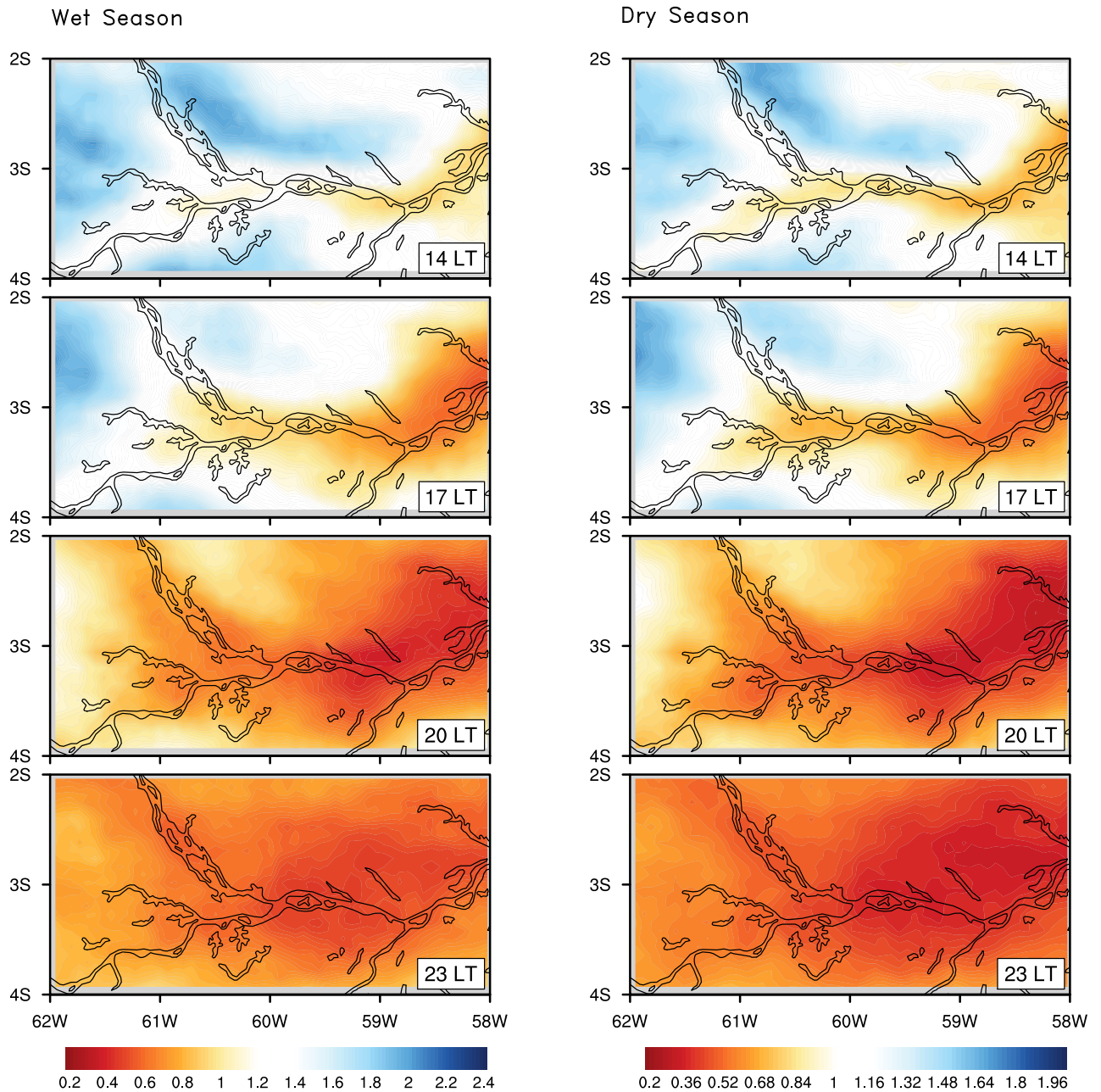
Figure 2.9: Same as in Figure 2.7 but based on rainfall estimates from CMORPH.

The 3-hours average of accumulated precipitation (Figures 2.7, 2.8, and 2.9) also showed that there is a spatial displacement of the minimum and maximum values during the day, previously discussed, which can be related to the WST and rivers morphological characteristics such as width and orientation. Thus, we also applied Student's t-tests for the group pairs (e.g., groups 11/12 and 11/13), which are composed by grid points situated over the different rivers (Negro, Solimões and Amazon), to assess whether the precipitation

patterns over the rivers differ from each other. The Student's t-tests showed that the mean residual rainfall of these pair of groups is the same (Table 2.1). Clusters of grid points that have the same distance from the margins and form a virtual line parallel to a river (e.g., the group pairs 8/9 and 14/15) were tested to assess whether the rivers characteristics can affect precipitation regime on the regions far away from margins. The results indicated that mean residual rainfall of the group 14 and 15 are statistically equal, whereas the group 8 and 9 have different means.

Table 2.1 - The Student's t-test results of the mean residual rainfall for the group pairs[a]

Tested Groups	Mean Difference	Standard Deviation	ρ	N'	p.value [b]
group 1 - group 2	-0.03	0.15	0.23	59	**0.07**
group 1 - group 3	-0.06	0.30	-0.44	252	0.0
group 1 - group 6	-0.02	0.08	0.77	12	**0.19**
group 1 - group 7	0.00	0.11	0.61	23	**0.39**
group 3 - group 4	-0.02	0.13	0.82	9	**0.32**
group 3 - group 5	-0.01	0.21	0.25	57	**0.36**
group 3 - group 8	0.02	0.27	-0.34	196	**0.15**
group 1 - group 9	-0.08	0.21	-0.53	318	0.0
group 3 - group 9	-0.01	0.25	-0.06	110	**0.32**
group 3 - group 10	-0.03	0.21	0.31	50	**0.17**
group 11 - group 12	-0.02	0.14	0.72	15	**0.32**
group 11 - group 13	-0.01	0.19	0.0	95	**0.24**
group 14 - group 15	-0.04	0.20	0.26	56	**0.10**
group 8 - group 9	0.04	0.14	0.12	75	0.016

[a] Where ρ is the correlation.

[b] P values greater than 0.05 (null hypothesis accepted) indicate that mean residual rainfall between the group paires are statistically equals; otherwise, the means are different.

The statistical test results aforementioned reveal that the river proximity and morphological characteristics affect the mean rainfall. However, groups with the mean residual rainfall can have the DRP with different phase and/or amplitude, as shows the Table 2.2.

Figure 2.10 shows the monthly diurnal cycle of residual precipitation for grid-points clusters statistically distinct in respect to mean residual rainfall. Figure 2.10a indicates that over the rivers and on the regions close to the margins the positive values occur between 2:00 P.M. and 11:00 P.M. (local time), and the reduced precipitation (negative

Table 2.2 - t Test P Values of the Mean Diurnal Cycle of Residual Precipitation for Each Group Pairs [a]

Tested Groups	02h	05h	08h	11h	14h	17h	20h	23h
group 1 - group 2	**0.37**	**0.24**	**0.05**	0.01	**0.25**	**0.29**	0	0.04
group 1 - group 3	**0.37**	0.0	0.0	0.0	**0.08**	**0.25**	0.0	0.01
group 1 - group 6	**0.34**	**0.36**	**0.35**	**0.34**	**0.28**	**0.29**	**0.09**	
group 1 - group 7	**0.16**	0.02	**0.34**	0.03	0	**0.11**	**0.33**	**0.16**
group 3 - group 4	0.02	b	**0.05**	**0.19**	b	**0.09**	b	**0.06**
group 3 - group 5	0.0	0.0	0.0	**0.08**	**0.32**	0.01	0.0	0.04
group 3 - group 8	0.02	0.0	0.0	0.0	**0.39**	0.0	0.0	**0.26**
group 1 - group 9	0.0	0.0	**0.36**	0.0	0.0	0.0	0.0	0.0
group 3 - group 9	0.0	0.0	0.01	**0.11**	**0.09**	0.0	0.0	0.0
group 3 - group 10	0.0	0.0	0.0	0.03	**0.32**	0.0	0.0	0.0
group 11 - group 12	**0.37**	**0.11**	**0.14**	0.02	**0.11**	**0.14**	**0.36**	**0.26**
group 11 - group 13	0.01	0.03	**0.09**	**0.06**	0.0	0.0	0.01	0.0
group 14 - group 15	0.0	0.0	**0.08**	**0.08**	**0.04**	**0.04**	**0.3**	0.0
group 8 - group 9	0.01	**0.39**	**0.33**	**0.09**	**0.21**	**0.37**	**0.11**	0.0

[a] Bolded cells indicate the groups that have equal averages. For nonbolded, the averages are different.

b Represents the cases wherein the degree of freedom is zero.

values) occurs in the afternoon and in the evening. On the regions 25 km farther away from the rivers the maximum precipitation happens in the afternoon, and minimum is observed at dawn (Figure 2.10b). The Figures 2.10c and 2.10d show that the diurnal variations of precipitation for the groups 8 and 9 are similar to that shown in the Figure 2.10a and 2.10b respectively. Figure 2.10c also shows that although the group 8 is placed about 60 km far from the rivers, its precipitation pattern is similar to that groups placed over the rivers due to the interaction between synoptic and local scales flows, as discussed in the previous paragraphs.
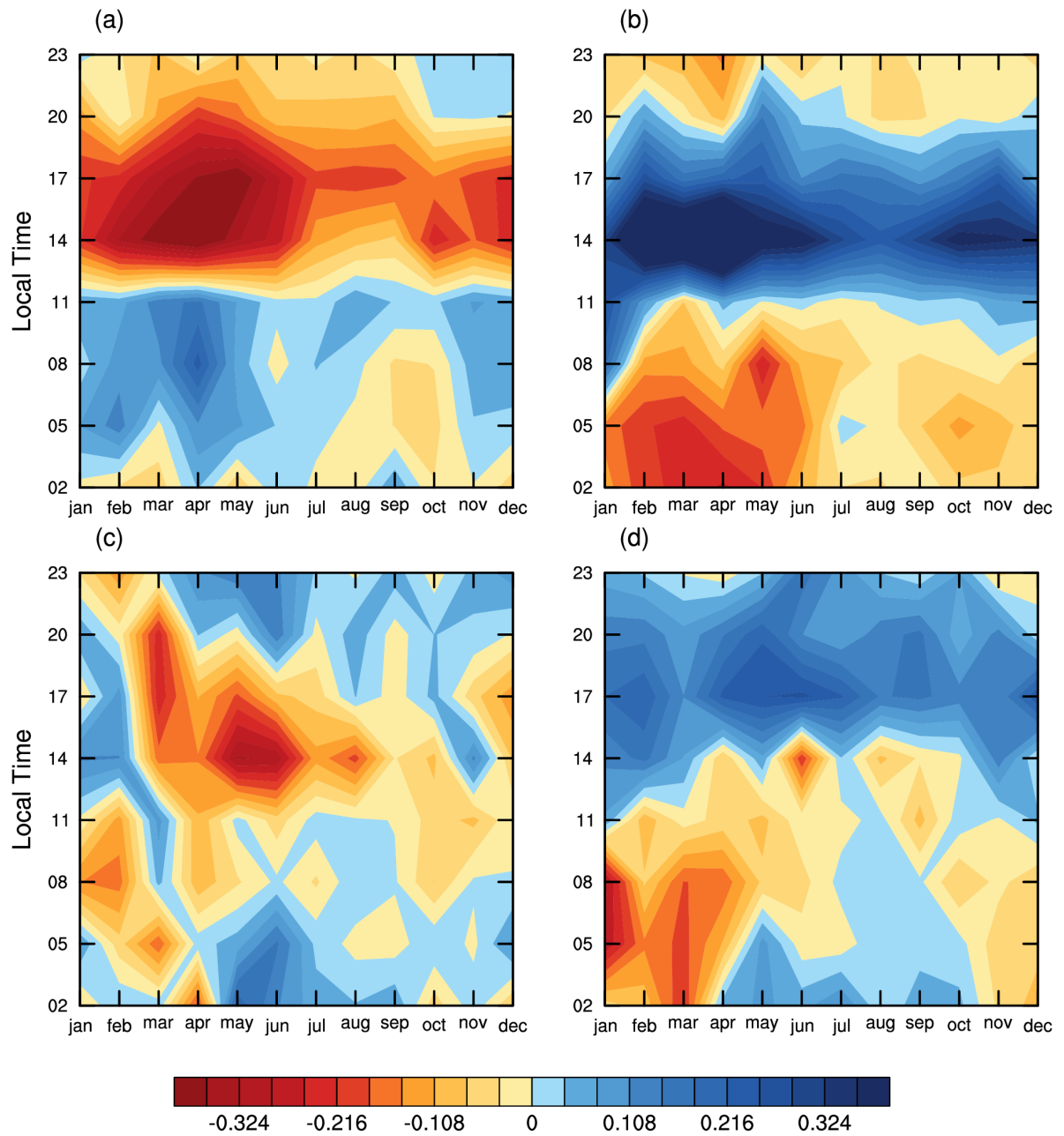
Figure 2.10: Monthly diurnal cycle of residual mean precipitation in millimeters. (a) group 1, (b) group 3, (c) group 8, and (d) group 9.

2.4 Conclusions

The existence of the river breeze circulation associated with large Amazon rivers has been studied in the literature focusing on case studies (Oliveira and Fitzjarrald, 1993; Silva Dias et al., 2004; Fitzjarrald et al., 2008) and numerical simulations (Oliveira and Fitzjarrald, 1994; Silva Dias et al., 2004; Lu et al., 2005) of particular events. Here we present long term evidence based on 35 years of hourly weather station data and on 15 years of satellite estimates of rainfall.

The behavior of the local circulations and their role on moisture transport have been investigated using vapor pressure and wind direction data from the Manaus airports weather stations. The use of the long-term surface data and different satellite rainfall data sets renders details and confidence in the results that have never previously been obtained in limited time periods. At Eduardo Gomes weather station, expressive occurrences of southwestern and northwestern wind in the daytime, which are very likely excited by the breeze of the Negro River, are verified. When the winds assume these directions an increase of vapor pres- sure after sunrise until midnight is observed. Therefore, it indicates that the river breeze winds transport moisture air from the Negro River to the Manaus City during the daytime. Low frequency of northeast wind observed at night in this weather station indicates that a land breeze event rarely occurs.

At Ponta Pelada airport the northeastern and northwestern winds (e.g., winds toward to rivers) are commonly verified at night, which are evidences of the land breeze action. These winds transport drier air from Manaus city to the Amazon river regions as showed in the vapor pressure analysis. In the daytime, between 9:00 and 18:00 local time, winds away from the rivers (southern winds) are frequent, suggesting action of the river breeze. The vapor pressure analysis showed that under this wind conditions moister air is transported toward Manaus city, increasing the air humidity over the region. In both airport weather stations, these evidences of the local circulations and their impact on the moisture transport are more obvious in the dry season.

The influence of the local winds on spatial/temporal pattern of the precipitation was analyzed using data from satellite estimates (TRMM and CMORPH). The 3-hours average of accumulated precipitation show a spatial tendency varying according to the hour of the day. In the afternoon and in the evening maximum precipitation values are observed

over the land as a possible consequence of the warmer land surface and the river breeze action; whereas reduced rainfall values are verified over the rivers as a probable result of the subsidence associated to river breeze circulations. This spatial distribution in the dry and wet season is very similar. At dawn and in the morning the maximum values of accumulated precipitation are found over the rivers, mainly over and around the Amazon River, where the water surface temperature is the hottest in the night time. In the dry season, the increased precipitation values over the river only appear in the morning, mostly at 11:00 A.M. (local time).

Statistical tests showed that the mean rainfall on the river regions is equal to that observed over the land areas very close to the river margins and is different from that observed over the regions situated about 25 km or more away from the rivers. These regions located about 25 km afar from the river margins have the same mean rainfall from those located farther from margins, i.e., areas placed about 50 and 75 km from the margins. The rainfall regime over the regions situated farther than 25 km from eastern margin of Negro River differs from that observed on the regions located in the same distance in respect to the northern margin of the Amazon River.

The intrannual analysis has shown that the influence of the local circulations on the rainfall daily cycle is much more evident in the rainiest quarter (March, April and May). This is a novel result for the impact of local circulation on rainfall close to rivers in he Amazon region.

The results presented here indicate that raingages located close to the margin of large rivers, because logistically they are more conveniently placed and maintained, are biased towards lower values than the ones that would be obtained farther inland, because of the impact of the river breeze. In Buarque et al. (2011) (c.f. their figure 1b) it is shown that the raingage distribution is preferentially along the large rivers. The impact of local circulation on the rainfall data obtained at the margins of large rivers indicates that these data cannot be extrapolated to represent, as an average, the Amazon hydrological cycle.

Local circulations in the Manaus region are especially relevant not only with respect to rainfall but also regarding atmospheric transports. In the ongoing experiment GoAmazom (Artaxo et al., 2013) the interaction of the urban plume with the Amazon Forest is being examined in detail from different perspectives ranging from ecological processes to the atmospheric chemistry. The underlying surface features and resultant local circulations

potentially impact the urban plume, its dimensions and time evolution. In this respect, ongoing research is being conducted using very high resolution numerical simulations incorporating detailed surface features and using the results presented here as a validation.In particular, surface water hydrology models may be an important addition to the overall modeling framework. Application into the monitoring and prediction of the urban plume is the expected result besides profound understanding of the physical processes involved.

Chapter 3

Seasonal Flooding Causes Intensification of the River Breeze in the Central Amazon

The text and results presented in this chapter will be submitted as a paper to the **Journal of Geophysical Research: Atmospheres**.

3.1 Introduction

The center of the Brazilian state of Amazonas is dominated by evergreen broadleaf forests, deforested areas including the city of Manaus, rivers, and lakes (Figure 3.1a). This landscape supports the development of local circulations because of the the thermal capacity difference between water and land surfaces. These circulations are capable of triggering convection near the river and lake margins in the daytime and consequently affect the spatial and temporal distributions of precipitation (Fitzjarrald et al., 2008; Paiva et al., 2011; Dos Santos et al., 2014; Tanaka et al., 2014; Burleyson et al., 2016).

One type of local circulation, the river breeze, is associated with frequent onshore winds in the daytime and offshore winds in the nighttime (Oliveira and Fitzjarrald, 1993; Dos Santos et al., 2014). According to Dos Santos et al. (2014) the river breeze is more frequent during the dry season (June — December) when there is less cloud cover and more incoming solar radiation. Large amounts of incoming solar radiation at the surface are associated with strong gradients of surface temperature when the landscape is heterogeneous such as close to large water bodies, and this causes development of local circulation. In fact, onshore winds near the Amazon river margins are part of river breeze circulations, and are mainly associated with calm large scale wind conditions, as showed by Silva Dias et al. (2004) in a numerical study for the eastern Amazon.

Observational data for this region is scarce, but observations from analogous contexts suggest that the river breeze may be a critical component of the local climate (Dos Santos et al., 2014; Tanaka et al., 2014; Burleyson et al., 2016). Numerical simulations can help assess the importance of the river breeze for the climate of Amazonas and have the potential to provide mechanistic understanding of breeze formation, inland propagation, and impact on local convection. Such a numerical investigation has not yet been carried out with the required realistic details. For example, rivers in the central Amazon are well-known to exhibit seasonal flooding (Sippel et al., 1994; Hess et al., 2003; Prigent et al., 2007; Sorribas et al., 2016), but the impact of flooding on the river breeze circulation is unknown.

Inundation in the central Amazon occurs throughout the year, but with maximum extent during May to June (named here as the "high-inundation period"). The smallest inundation extent happens during September — October (Sippel et al., 1994; Hess et al., 2003; Sorribas et al., 2016). Inundation is normally observed over floodplain areas near the Amazon and Solimões rivers (Figure 3.1b) where the topography is very flat. Moreover, large floodplain areas also exist along the Negro River. When these floodplain areas are inundated, land-atmosphere exchanges are affected because the surface water changes the net surface radiation and favors direct evaporation. The latent heat fluxes increase during the inundation period whereas the sensible heat fluxes decrease (Borma et al., 2009; Schedlbauer et al., 2011). Furthermore, Wu et al. (2016) observed that the latent heat fluxes increase with the surface water level. This surface flux response of the inundation is expected to be stronger in the vicinity of the Amazon and Solimões rivers due to the low vegetation cover observed over these places (Figure 3.1c) (Mahmood et al., 2011; Wang et al., 2014).

During the high-inundation period of the central Amazon, when the surface energy fluxes are expected to be greatly altered, the atmospheric boundary layer over the flooded areas can be affected. In the daytime, for example, the air temperature over the floodplain region is expected to be cooler than the temperature observed in the upland forest since the sensible heat fluxes are reduced over the flooded areas (Schedlbauer et al., 2011). This thermal gradient may intensify the river breeze circulation during the day. On the other hand, higher air temperature is expected over the floodplain region in the nighttime because the flooded forest stores more energy along the day. In this context, Dos Santos et al. (2014) showed that the nighttime surface temperature values are higher over the

Amazon and Solimões rivers vicinity compared with the *terra firme* forest. The authors also showed similar values when compared the temperature for rivers surrounding and water bodies region. The impact of the inundation on the surface temperature also was shown by Dadson et al. (2010) through numerical simulations for the Niger inland Delta region. However, the impact of flooding on the river breeze is still unknown.

The river breeze circulation in the central Amazon can also be affected by the roughness variation existent over the floodplain/upland forest interface region. This variation is a consequence of the forest height difference between *terra firme* and floodplain regions. According to measurements carried out by Simard et al. (2011) (Figure 3.1d) this height difference is about 11 m. The mentioned roughness variation may cause wind convergence/divergence affecting the river breeze propagation and the convection associated with the river breeze front. According to some authors (Pitman et al., 2004; Khanna and Medvigy, 2014; Khanna et al., 2017), strong roughness variation is capable of causing a spatial dipole of wind convergence and divergence and consequently the development of atmospheric vertical motion. The breeze intensity can also be affected by the thermodynamic response to the roughness variation (Lee et al., 2011).
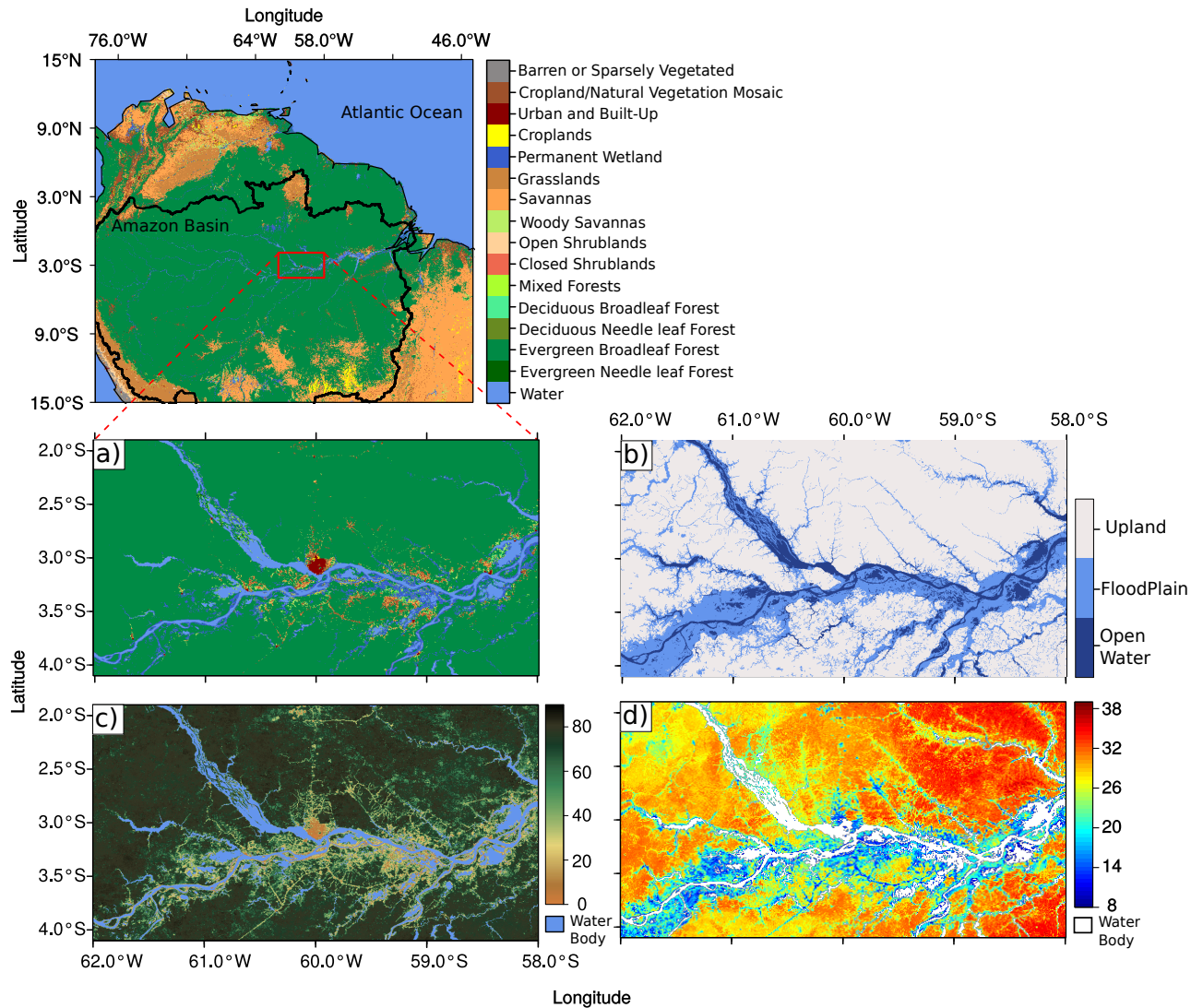
Figure 3.1: Environmental data for the central Amazon. (a) MODIS (Moderate Resolution Imaging Spectroradiometer) Land cover map (Product MCD12Q1), (b) Floodplain extent (Hess et al., 2003), (c) Maximum Green Vegetation Fraction (Broxton et al., 2014), and (d) Forest canopy height (Simard et al., 2011).

This papers aims to investigate the river breeze circulation in the central Amazon using numerical modeling (i.e., land surface-atmosphere plus river routing modeling) and specifically answer the following questions: (1) How are the river breezes triggered and how do they affect convection in the central Amazon region? (2) Does the seasonal flooding affect the river breeze intensity and its response to the local convection? (3) Does the roughness variation over the floodplain/upland forest interface alter the river breeze?

3.2   Methodology

3.2.1   Numerical Model description

We used the Catchment-Based Macro-scale Floodplain (CaMa-Flood) model and the Ocean-Land-Atmosphere Model (OLAM) to simulate a river breeze case study in the central Amazon and to investigate its response to seasonal flooding. The two models were run in sequence. First, CaMa-Flood was run to simulate flooding depth and extent. The outputs CaMa-Flood were used to force OLAM. There was no feedback from OLAM to CaMa-Flood.

The CaMa-Flood model, originally developed by Yamazaki et al. (2011), is a global river model that uses the continuity equation to prognose the water storage for unit catchments. Each unit catchment is composed of a river channel reservoir and a floodplain reservoir. Some parameters of these reservoirs (e.g., channel elevation, channel length, and drainage area) are calculated using high-resolution topographic data and a flow direction map (Yamazaki et al., 2009). The predicted total water storage along with the topographic parameters are used to derive the following diagnostic variables for the river and floodplain regions: river water depth, floodplain water storage, floodplain water depth, and flooded area. The rate of change of storage with time depends on the runoff (input variable) and net discharge. The discharge is calculated by a local inertial equation implemented by Yamazaki et al. (2013).

CaMa-Flood's ability to simulate discharge, water level, and flood extent for the Amazon region was evaluated by Yamazaki et al. (2011, 2012). The interannual variability of the simulated discharge agreed well with observations; the correlations between daily simulated and observed discharges was very strong – blue$r$ ranged from 0.8 to 0.87 over the different evaluated sites. The simulated flood extent was evaluated by comparing it with satellite estimates. The model underestimated the monthly flooded extent but the correlation between the simulated flood extent and the satellite data was strong ($r = 0.68$). One possible explanation for flooded extent underestimation is the limited quality of the satellites estimates used in the comparison. The CaMa-flood also reasonably simulated the seasonal cycle of the surface water level with correlation coefficients as high 0.91 (Yamazaki et al., 2012).

The OLAM model (Walko and Avissar, 2008a,b) is a non-hydrostatic global atmosphe-

ric model discretized in a global geodesic grid with a mesh refinement scheme (Walko and Avissar, 2011). The model simulates the atmospheric large scale circulation as well as the regional and local atmospheric phenomena for specified fine-resolution regions. The atmospheric primitive equations in OLAM are solved using the finite-volume method. Further, this model uses height vertical coordinates and a shaved-cell method to represent the topography. Thus, the model consider levels with constant height that intersects the terrain. The model has frequently been used in studies of Amazon hydroclimate (Medvigy et al., 2008; Khanna and Medvigy, 2014; Ramos da Silva et al., 2014), Amazon climate change (Ramos da Silva and Haas, 2016), and Amazon weather forest (Ramos da Silva et al., 2014).

3.2.2   Model input datasets

The runoff data used in our CaMa-Flood runs resulted from simulations was derived by the Treatment of Surface Interaction Runoff (MATSIRO) model. In the MATSIRO's simulations, the JRA-25 reanalysis and satellite-estimated precipitation were used as the forcing data (Kim et al., 2009). This approach for computing runoff was previously applied by Yamazaki et al. (2011, 2012, 2013).

The atmospheric and soil initial conditions used in the OLAM simulations originate from the operational analysis provided by the NCEP Climate Forecast System Version 2 (CFSV2) (Saha et al., 2014). The CFSV2 operational analysis here used have 37 atmospheric vertical levels, soil moisture and temperature information at 4 layers (0-0.1, 0.1-0.4, 0.4-1, 1-2 m), horizontal grid spacing of 0.5° and are available every 6 hours. These operational data also provided information regarding snow depth and ice concentration that are required in the global OLAM initialization. The other dataset used by the OLAM model (topography, land cover map, Normalized Difference Vegetation Index — NDVI , soil texture, and Water Table Depth) are available on the model's web page (https://sourceforge.net/projects/olam-model).

We modified the default topography, land cover, and water table maps for the central Amazon to improve the model performance in simulating the local circulation of this region. The updated topography has grid spacing of about 90 m and came from the Shuttle Radar Topography Mission (SRTM). The new land cover map was developed by combining the MODIS land cover map (Figure 3.1a) with the floodplain map produced by Hess et al.

(2003) — hess-floodplain map (Figure 3.1b). This combination allowed us to include a new surface type (floodplain-forest) on the land cover map (Figure 3.2a). The floodplain-forest was defined as the areas occupied by evergreen broad-leaf forest according to the MODIS land cover map and classified as floodplain region in the hess-floodplain map. Most of the floodplain-forest is located around the Amazon and Solimões rivers as shown in Figure 3.2a. This new land cover type was included because the main features of the evergreen broad-leaf forest over the floodplain region noticeably differs from the upland forest. The vegetation parameters of these two land cover types used in this study are shown in appendix A.1.
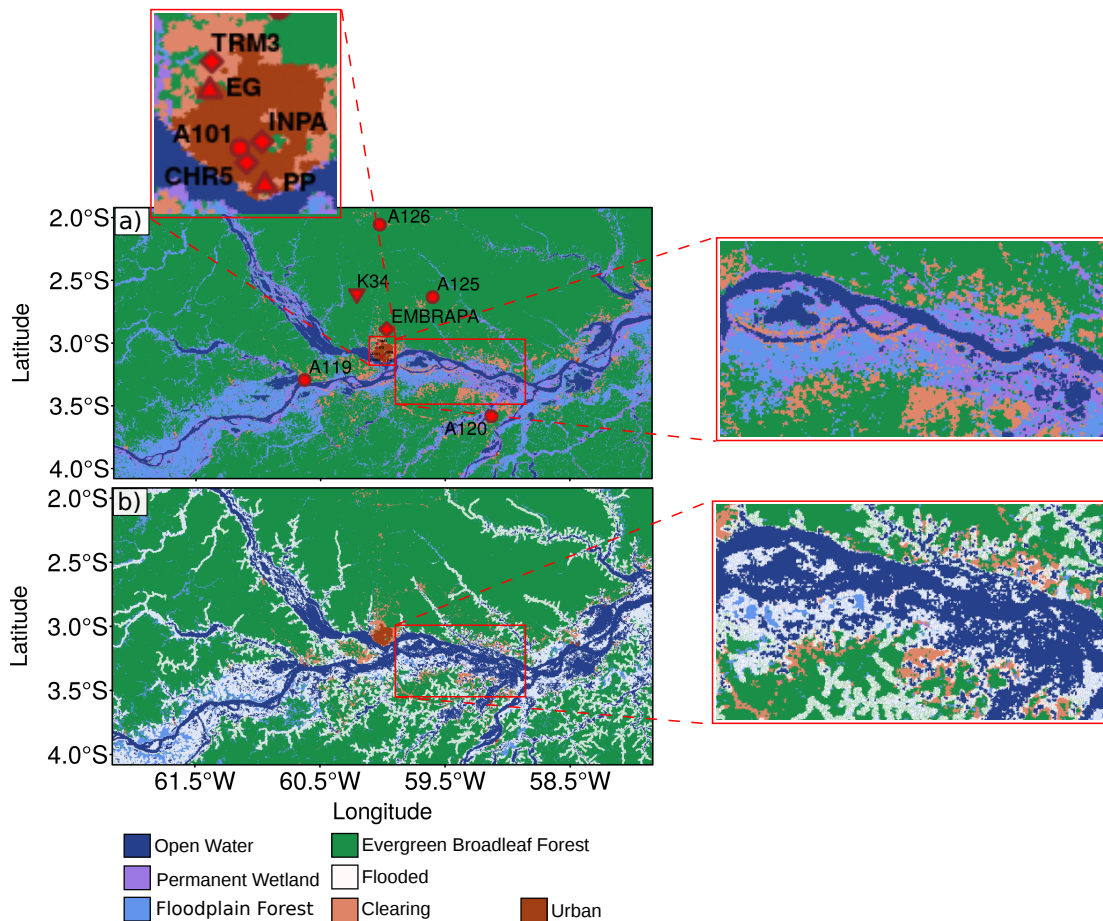
Figure 3.2: Land cover maps (showed only the predominant cover types of the central Amazon) used in the OLAM simulations. (a) Map resulted from the combination between the MODIS and the hess-floodplain map (Hess et al., 2003). The red points are the locations of the weather stations used in the OLAM model evaluation. (b) Same Land cover map showed in (a) but updated with the seasonal flooding simulation. The paches classified as flooded areas (in white) represents the areas inundated in July 2011, it is not a new surface type.

The Vegetation Fractional Coverage (VFC) in the original version of the LEAF parameterization is represented by fixed values attributed for each land cover type. These fixed values do not accurately represent the VFC over the Amazon region because the actual VFC has an annual variation (Doughty and Goulden, 2008; Malhado et al., 2009). Thus, we produced, and included in the simulations, month VFC for the central Amazon with grid spacing of about 500 m. The VFC computation was based on the following expression (Gutman and Ignatov, 1998):

$$VFC = \frac{NDVI - NDVI_0}{NDVI_\infty - NDVI_0} \tag{3.1}$$

Where $NDVI$ represents the monthly NVDI derived from the MOD13A2 MODIS product. $NDVI_0$ represents the NVDI value for the bare soil whereas $NDVI_\infty$ is the maximum NDVI for a determined time period. $NDVI_\infty$ values were those previous determined by Broxton et al. (2014) for each land cover type.

The original water table depth (WTD) data were replaced by typical values obtained from field campaigns for the central Amazon (Cuartas et al., 2012). The measurements spanned for environment regions (Landscapes) classified as waterlogged, ecotone, slope, and plateau. This classification was based on the following terrain parameters: slope and the Height Above the Nearest Drainage — HAND (Nobre et al., 2011; Cuartas et al., 2012). To include the WTD measurements in our simulations we built a class map to define the environment regions for the central Amazon. This map was based on the SRTM topography and the HAND data provided by Nobre et al. (2011), which is available on https://lpdaac.usgs.gov/data_access/data_pool. Finally, we applied the month typical values of measured WTD for each class resulting in a monthly spacial data of WTD.

The SST data over the continental water (e.g. rivers and lakes) were also updated because the original version of the OLAM model (like most atmospheric models) interpolates SST from distant marine regions to represent the inland Water Bodies Surface Temperature (WST). We used hourly-SST satellite estimates over the central Amazon with 6 km of spatial resolution, provided by NOAA/NESDIS (2014), as the WST. These satellite estimates have some limitations over the Amazon region because of cloud contamination and the data spatial resolution. Thus, the hourly-spatial values of WST were spatially averaged to produce unique time series for the main water bodies of the central Amazon (i.e., Negro, Solimões, and Amazon rivers and Camaçari and Cabaliana lakes). We then

computed median diurnal cycles based on these hourly-time series and characterized the median diurnal cycle by a polynomial fit. These computations were carried out for each month. Finally, the fitted diurnal cycles were used as the WST forcing data in our simulations. Figure 3.3 shows WST values of the Negro River, the median, and the fitted diurnal cycle for July 2011. The diurnal variation of the surface water temperature for the other rivers is similar to that shown in in Figure 3.3. The WST of the small lakes were assumed to have the same values of the nearest main rivers.
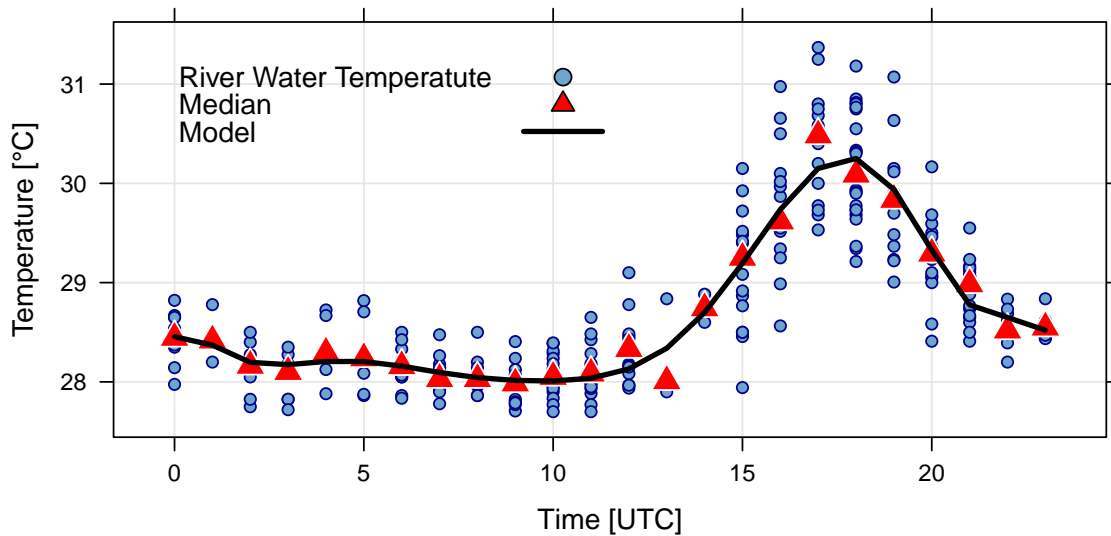
Figure 3.3: Water surface temperature of the Negro River for July 2011 based on NOAA/NESDIS satellite estimates.

3.2.3   Models Setup and Experiments Design

The numerical simulations in this study were carried out for July 2011. This period was chosen because in July the inundation in central Amazon is still significant (Sippel et al., 1994; Sorribas et al., 2016) and the river breeze occurrence is frequent (Dos Santos et al., 2014). The CaMa-Flood-Model was run for 01 January 2010 – 30 July 2011 and the first 18 months were discarded to allow for model spin-up. These simulations were performed for a spatial domain that covers the entire Amazon region (21°S – 6°N, 80° – 45°W) with 25 km spatial resolution. The output variables were downscaled to the DEM (Digital Elevation Model) resolution of about 500 m.

The land-atmosphere simulations are consisted of three numerical experiments (Exp-NonFlood, ExpFlood, and ExpRoughness). In all experiment the OLAM model was spun up for a period of 23 days (01 – 23 July 2011). This spin-up period was considered because

we previously ran the model for July 2011 and we decided to study the river breeze case occurred on 23 July. The soil variables and the surface water temperature resulted from the spin-up simulations were used as the soil and surface water initial conditions in new simulations of 48 hours (hereafter 48 h-simulations). However, the CFSV2 reanalysis was used for the atmospheric initial conditions because they are based on observational data and reasonably represent the large scale atmospheric phenomena. The 48 h-simulations also consisted the three experiments presented above. During both the spinup and the 48 h simulations, the model was nudged to the CFSV2 reanalysis data by using the Newtonian Nudging assimilation scheme.

OLAM was used as a variable resolution General Circulation Model (GCM) with 45 vertical levels. The innermost domain has grid spacing of about 780 m and was centered over the urban area of Manaus (3°S, 60 °N). This domain area is about 196,349 km^2 and extends over the main rivers (Amazon, Negro and Solimões) as well as over the Balbina Lake. Away from this region, the grid resolution gradually became coarser up to 200 km. The vertical resolution was 15 m near the surface, and gradually increased to 1500 m in the upper stratosphere. The physical processes in our simulations were represented by the Grell-Freitas cumulus parameterization (Grell and Freitas, 2013), the RRTMG radiation scheme (Iacono et al., 2008), the Smagorinsky-Lilly-Hill parameterization for the turbulent processes (Lilly, 1962; Smagorinsky, 1963; Hill, 1974), the microphysics scheme proposed by Walko et al. (1995) (parameters details in appendix A.2), and the LEAF parameterization (Walko et al., 2000) designed to represent the land-atmosphere surface fluxes. The cumulus parameterization was not activated in the domains with horizontal grid spacing lower than 3.12 km. In the LEAF scheme the soil was setup with 21 vertical levels and depth equal to 5 m. The soil vertical grid spacing was defined as 0.05 m near the surface and increased gradually to 0.5 m close to the soil bottom. To better compute the surface fluxes over the urban areas we implemented the Town Energy Budget (TEB) proposed by Masson (2000) in OLAM.

The experiment ExpFlood acted as our control. The seasonal flooding in this experiment was represented by the monthly average of the daily flood depth simulated by the CaMa-Flood model for July 2011. This simulated flood depth was used as initial condition in the LEAF parameterization to delimit the flooded areas, and to update the spatial extension of the areas occupied by water bodies on the land cover map. Regions where

the flood depth was higher than 100 mm and lower than vegetation height were defined as flooded vegetation regions. When flood depth was higher than the vegetation height the areas were treated as open water (i.e., lake or rivers). The land cover map updated with the simulated flood depth (Figure 3.2b) shows that the seasonal flooding increased the extent of open water. It occurred because the seasonal flooding covered the vegetation and the deforested areas that surrounding the rivers. Figure 3.2b also shows that the seasonal flooding simulated for July 2011 inundated a large area of vegetation mainly around the Amazon region. Over the flooded vegetation area, the soil was considered saturated and the low boundary condition of the total hydraulic head was set equal to the simulated surface water depth. In the ExpNonFlood the seasonal flooding information was not included. Neither the water body extent nor the soil moisture were altered. This experiment was compared with ExpFlood to understand the influence of seasonal flooding on the river breeze.

The ExpRoughness experiment was designed to assess the impact of the roughness difference (observed in the floodplain and upland forest interface region) on the river breeze circulation by comparing results with the control experiment. In this experiment the vegetation height of the floodplain region was defined equal to the height of the upland forest. In the control experiment the floodplain vegetation height is about 34 % lower than the upland forest height.

The temperature, humidity, and wind resulted from the control experiment were compared against observational weather station data to evaluate the model performance. This evaluation was carried out by computing the standard deviation of the predicted (σ_{pred}) and simulated variables (σ_{obs}), correlation coefficient — r, Mean Bias (MB), Root-Mean-Square Error — RMSE, and Root-Mean-Square Error with bias removal (RMSE$_{\mathrm{UB}}$). The equations used to compute these statistics are founded in Pielke Sr (2002) and Jolliffe and Stephenson (2003). Pielke Sr (2002) proposed that simulations have skills when the following criteria is established: $\sigma_{\mathrm{pred}} \simeq \sigma_{\mathrm{obs}}$, RMSE $< \sigma_{\mathrm{obs}}$, and RMSE$_{\mathrm{UB}} < \sigma_{\mathrm{obs}}$.

3.3 Results

3.3.1 Model Evaluation

GOES-12 satellite imagery reveals convective clouds along the margins of the Amazon rivers (Figure 3.4a). This cloud pattern is a signature of the river breeze that commonly develop in the morning during calm wind and clear sky conditions (Silva Dias et al., 2004). To qualitatively evaluate model performance, we compared this image to output from the ExpFlood simulation. We selected the vertically-integrated total condensate (r_{total}) as an indicator of clouds. Overall, the model simulated convective activity close to the margins and suppressed convection over water bodies, in accord with the observations (Figure 3.4b). However, the model underestimated the convection in some locations (e.g., eastern side of the Negro river) and did not simulate the convective clouds observed near the southern margin of the Amazon river.
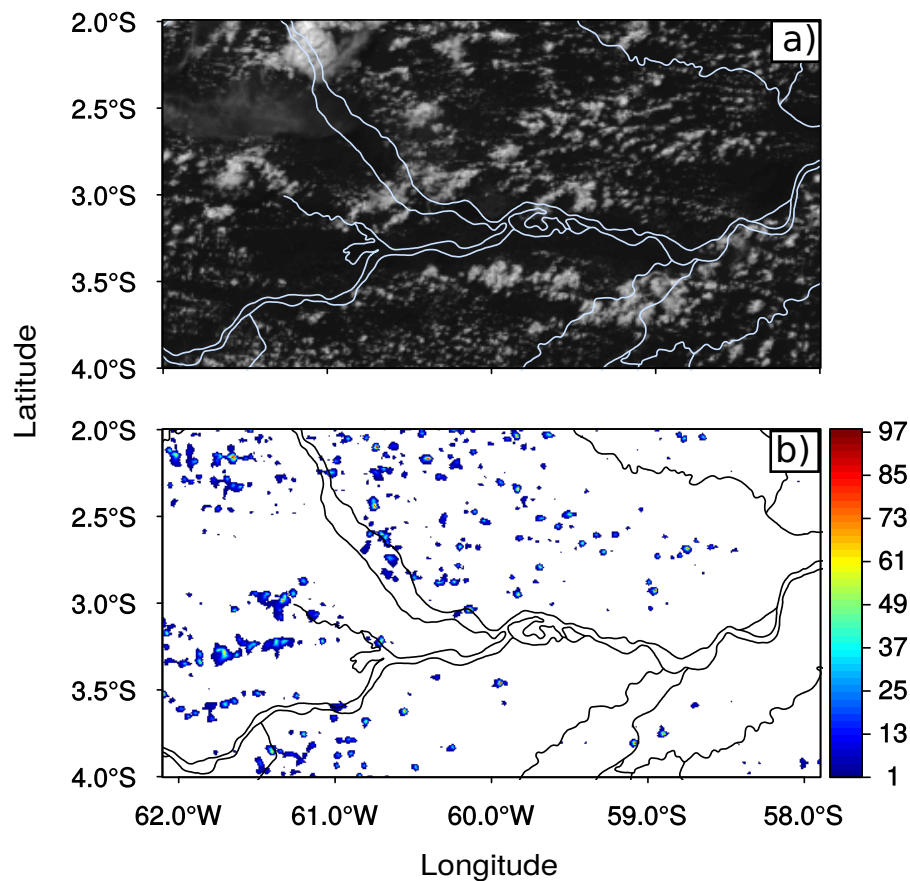
Figure 3.4: Simulated and observed fields for 23 July 2011. (a) Goes-12 satellite image (visible channel) at 17:45 UTC. (b) Hydrometers concentration vertically-integrated in g/kg (r_{total}) at 17:00 UTC

The predicted air temperature and wind speed were compared against observed data from meteorological weather station and field campaigns for the 24 h-period July 22 at 12 UTC to July 23 at 12. Station locations are presented in Figure 3.2. Figure 3.5 shows that the hourly air temperature was well simulated for the most locations. The correlation between the observed and simulated temperature is very strong (Table 3.1). However, the model has a bias in its prediction for the air temperature for stations A126 and TRM3. The predicted air temperature at TRM3 station was mostly below the observation with maximum differences. This bias probably occurred because the TRM3 is situated on the periphery of Manaus Urban Area (MUA) and the model considered this place as a forest clearing (Figure 3.2). The nighttime air temperature in clearings is commonly lower than in urban areas (Bastable et al., 1993; Gash and Nobre, 1997). The model simulates a smaller thermal amplitude than the observations at A126. This amplitude difference happened may be because the A126 Station is located in a small town (Presidente Figueiredo) and the TEB parameterization (the urban canopy scheme used in our simulations) was setup to compute the surface fluxes for the distinct features of the MUA.
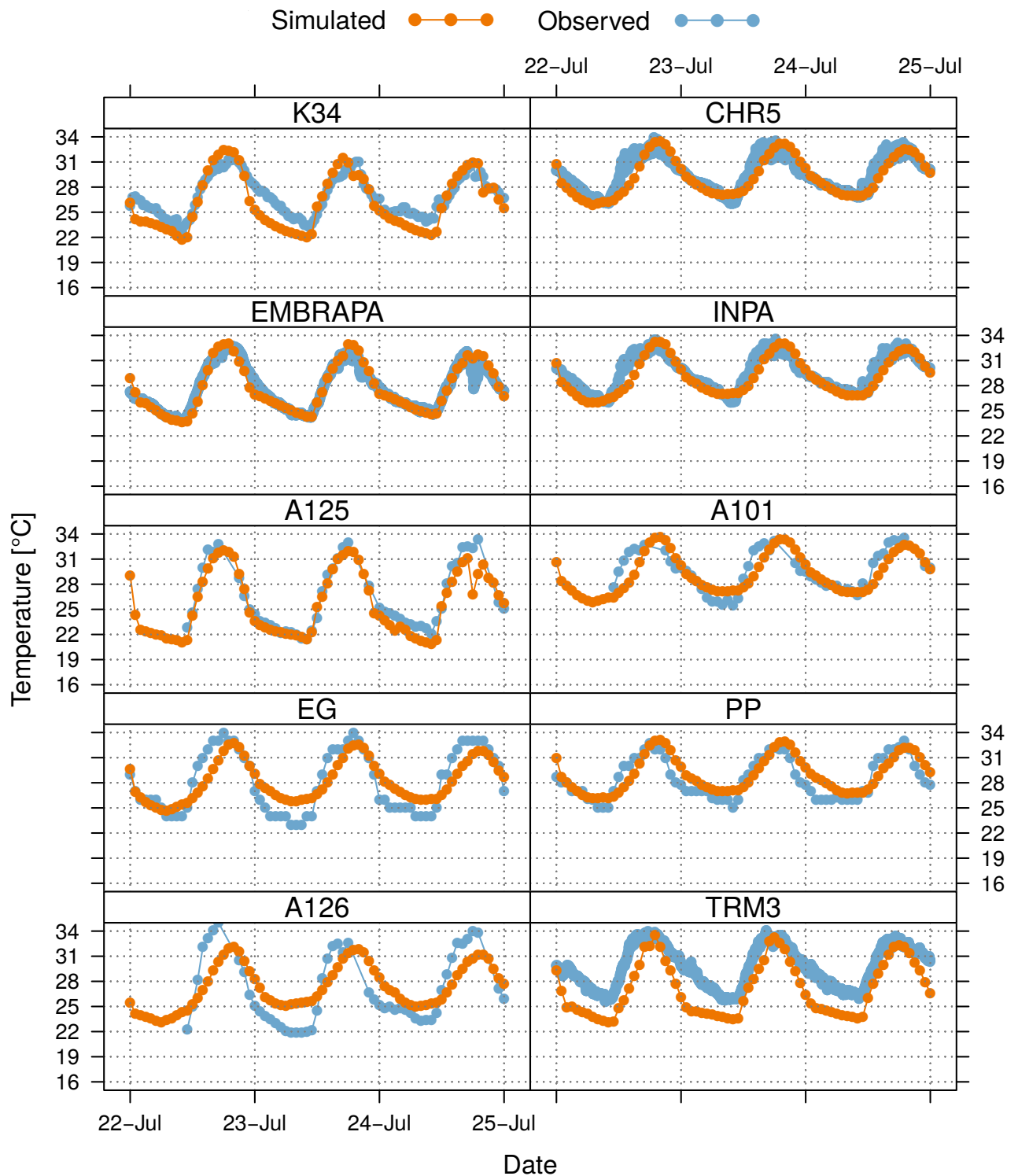
Figure 3.5: Simulated and observed air temperatures at 2m above the ground.

Figure 3.6 shows that the simulated wind speed was similar to observations at PP, A101, and A126 stations. The computed statistics for these stations (Table 3.1) confirm the model skill in simulate wind speed since the values of the observed standard deviation were lager than the root mean square errors (RMSE and RMSE$_{UB}$) and they also were

near the values of the simulated standard deviation. The strong correlations verified at A101 and A126 stations also confirm the model skill. The worst wind speed simulation was observed at the A125 station (Table 3.1).
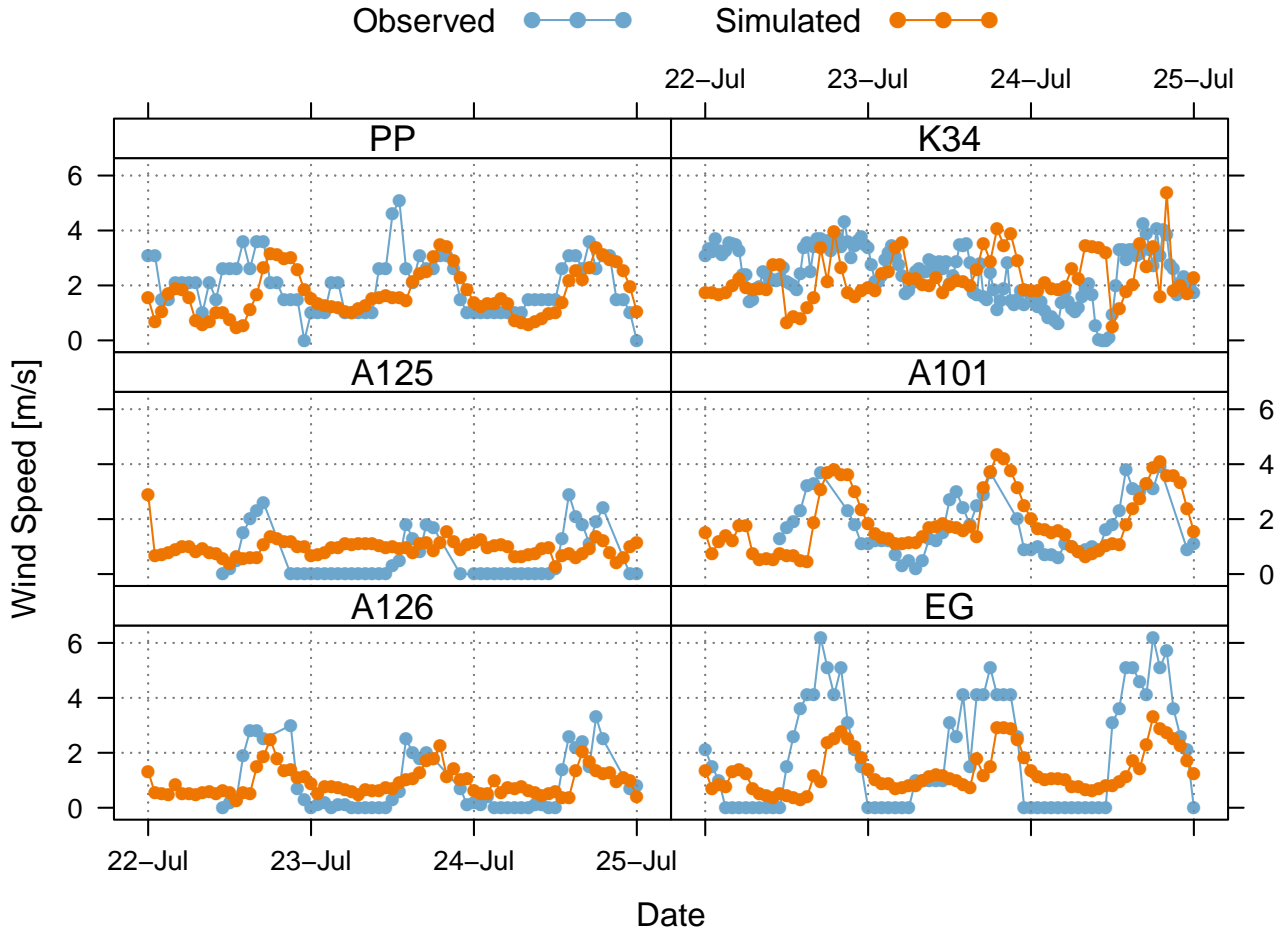
Figure 3.6: Simulated and observed air wind speed at 10 m above the ground.

Table 3.1 - Statistics for simulated and observed variables.

Station ID	Temperature						Wind Speed					
	obs	sim	Bias	RMSE	E_{UB}[1]	r	obs	sim	Bias	RMSE	E_{UB}[1]	r
k34	2.18	3.09	-0.96	1.74	1.46	0.29	0.61	0.70	0.20	1.12	1.11	-0.44
EMBRAPA	2.39	2.76	0.09	0.85	0.85	–	–	–	–	–	–	–
CHR5	1.94	2.14	-0.01	1.16	1.16	–	–	–	–	–	–	–
INPA	1.94	2.11	-0.14	1.09	1.08	–	–	–	–	–	–	–
TRM3	2.49	3.25	-2.50	2.81	1.28	–	–	–	–	–	–	–
PP	2.25	2.01	0.81	1.40	1.14	0.32	1.14	0.73	-0.27	1.09	1.06	0.41
EG	3.78	2.32	0.77	2.10	1.96	0.37	1.77	0.7	-0.41	1.55	1.5	0.55
A101	2.50	1.83	0.13	1.41	1.4	0.15	0.95	0.70	0.27	0.79	0.75	0.62
A125	3.68	3.49	-0.36	0.62	0.5	0.78	0.65	0.15	0.58	0.88	0.67	-0.02
A126	3.78	2.00	1.60	2.86	2.37	0.58	0.82	0.34	0.30	0.66	0.59	0.77

E_{UB} means $RMSE_{UB}$

3.3.2 Local circulations

We used the control experiment (ExpFlood) to study the physical processes involved in the formation, intensification and dissipation of the river breeze occurring on 23 July 2011. Figure 3.7 presents spatial fields of air temperature near the surface for the afternoon and early morning. In the afternoon, the lowest temperatures are found over and around water bodies (Figure 3.7a). The temperature contrast between flooded and upland areas was substantial, reaching 7 °C. In the western part of the Negro river, the simulated temperature shows a local horizontal variation that is a consequence of the cloud streets (Da Silva et al., 2011).In the early morning, opposite spatial pattern of temperature was simulated, with flooded areas being about 3 degrees warmer than upland areas (Figure 3.7b). Over some flooded areas the temperature in the nighttime was even higher than that found over the water bodies. The very highest early morning temperatuers occurred the MUA, characteristic of an Urban Heat Island (UHI) event.
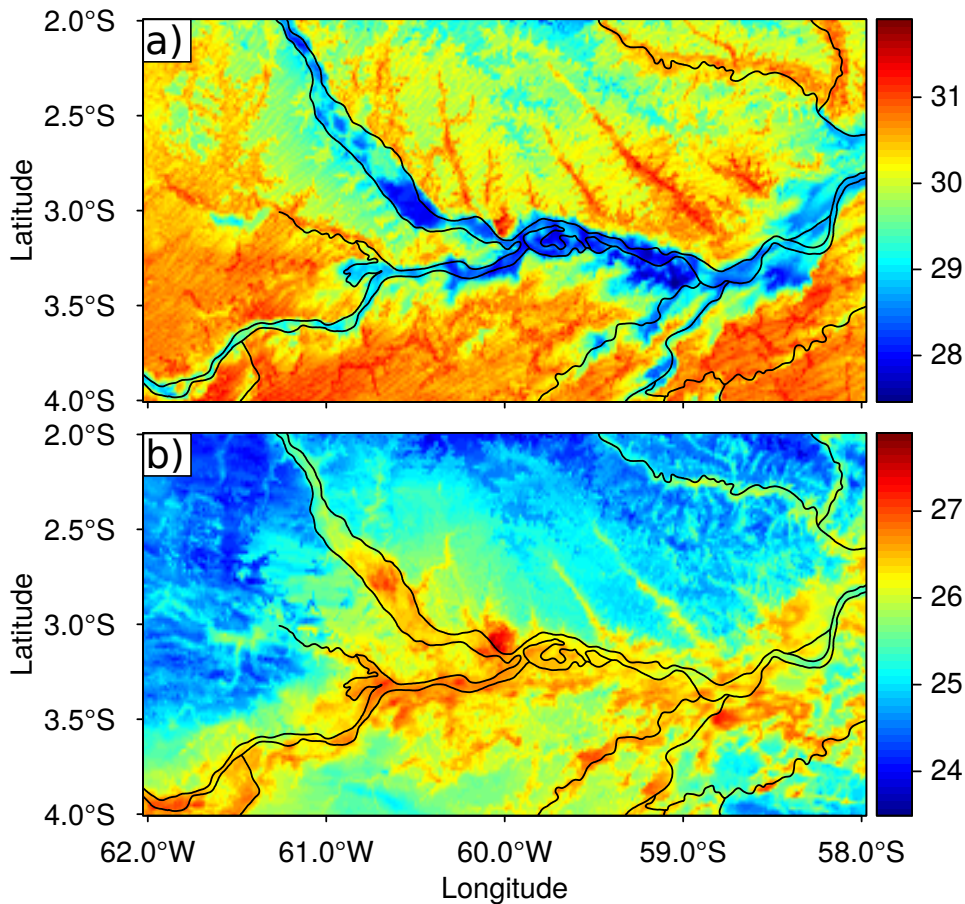
Figure 3.7: Near-surface air temperature (°C) simulated in the control experiment. (a) July 23 2011 at 16 UTC and (b) July 24 2011 at 12 UTC.

These spatial patterns can be understood in terms of the surface energy budget. Water surfaces store most part of net radiation during the daytime whereas a remarkable amount of the remaining energy is used to evaporate surface water. The sensible heat flux is comparatively small, and thus the Atmospheric Boundary Layer (ABL) warms slowly during the the daytime (Figure 3.8). In contrast, more energy is partitioned to sensible heat over the non-flooded area. This difference in energy partitioning leads to a more rapid rise in the air temperature over non-flooded land than over flooded land.
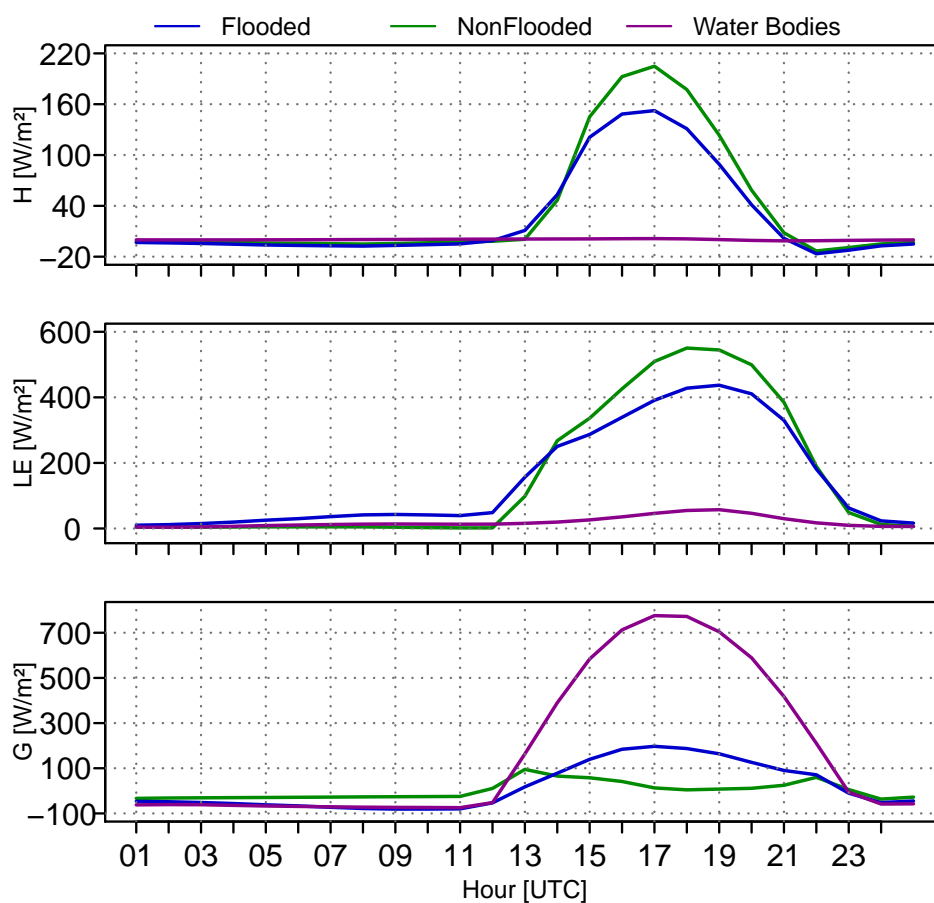
Figure 3.8: Surface fluxes simulated in the control experiment for July 23 2011.

Flooded and non-flooded areas also exhibit different surface energy balances at night. Figure 3.7b shows that in the early morning the air temperature is lower over the water bodies and flooded vegetation areas since the large quantity of energy stored in these surfaces along the day is used to maintain the air warmed. In the upland region the temperature decreasing is more rapidly owing to the smaller amount of solar energy stored in the daytime. This evident spatial variation of temperature was favored by the large-scale wind and cloudless condition as discussed above.

The strong spatial variability of the air temperature field (Figure 3.7) can trigger river breeze circulations. We analyzed these local circulations by plotting fields of wind perpendicular to river margins (Figure 3.9). Some remarkable perturbations in these fields (wind reversal highlighted by positive values) were simulated over and around the rivers in the midday and are consequences of the river breeze trigging. Smaller-scale perturbations on these wind fields are evidence of the cloud streets (Da Silva et al., 2011). The simulated cloud streets were clearly simulated on the western side of the Negro river where

it is perpendicular to the river. The river breezes on these perpendicular wind fields are characterized by wind reversal in the river side where the large-scale wind is onshore. In this side of the river, the front breeze is located along the offshore (local wind) and onshore (large-scale flow) wind convergences. In the opposite river side, the front breeze identification is difficult since local and large scale winds blow in the same direction.

Around 17:00 UTC (13:00 Local Time – LT), the river breeze fronts were nearly parallel to the rivers and far from coasts, except over some adjacent parts of the Negro River where the river width is smaller and the areas of flooded vegetation are larges (Figure 3.9). Over these areas, the front breeze propagation is slower in consequence of the weaker temperature gradient simulated between this part of the river and the upland region (Figure 3.5). Thus it indicates that the size of the water bodies in the central Amazon has a great influence on the temperature gradient and consequently on the front breeze propagation.

The temperature gradient supported river breeze front enhancement in the upland region throughout the afternoon period. At 19:00 UTC (15:00 LT), the distance between the river margins and front breezes of the main rivers reached values of about 16 km and the breeze circulation was very strong as indicated the elevated values of reversal perpendicular wind (4 $m.s^{-1}$) simulated near the front breeze. The breeze circulations weakened in the early evening (17:00 LT) but the breeze front remained evident and enhanced over the land until late evening (19:00 LT), when the front breeze of the Negro River was 45 km far from river margin (Figure 3.9).

In order to understand the vertical structure of the local circulations, we plotted vertical cross-sections of potential temperature and wind across the main rivers of the Central Amazon as shown in the Figure 3.10. Relatively cold air over rivers and flooded regions extended to upper level. This cold layer was deeper over the flooded vegetation where the turbulent fluxes are larger (compared with the open water) due to the higher temperature and roughness length. The temperature gradient established between rivers and upland region promoted local circulations, as previously discussed, that promoted vertical motion and consequently altered the vertical structure of the temperature.
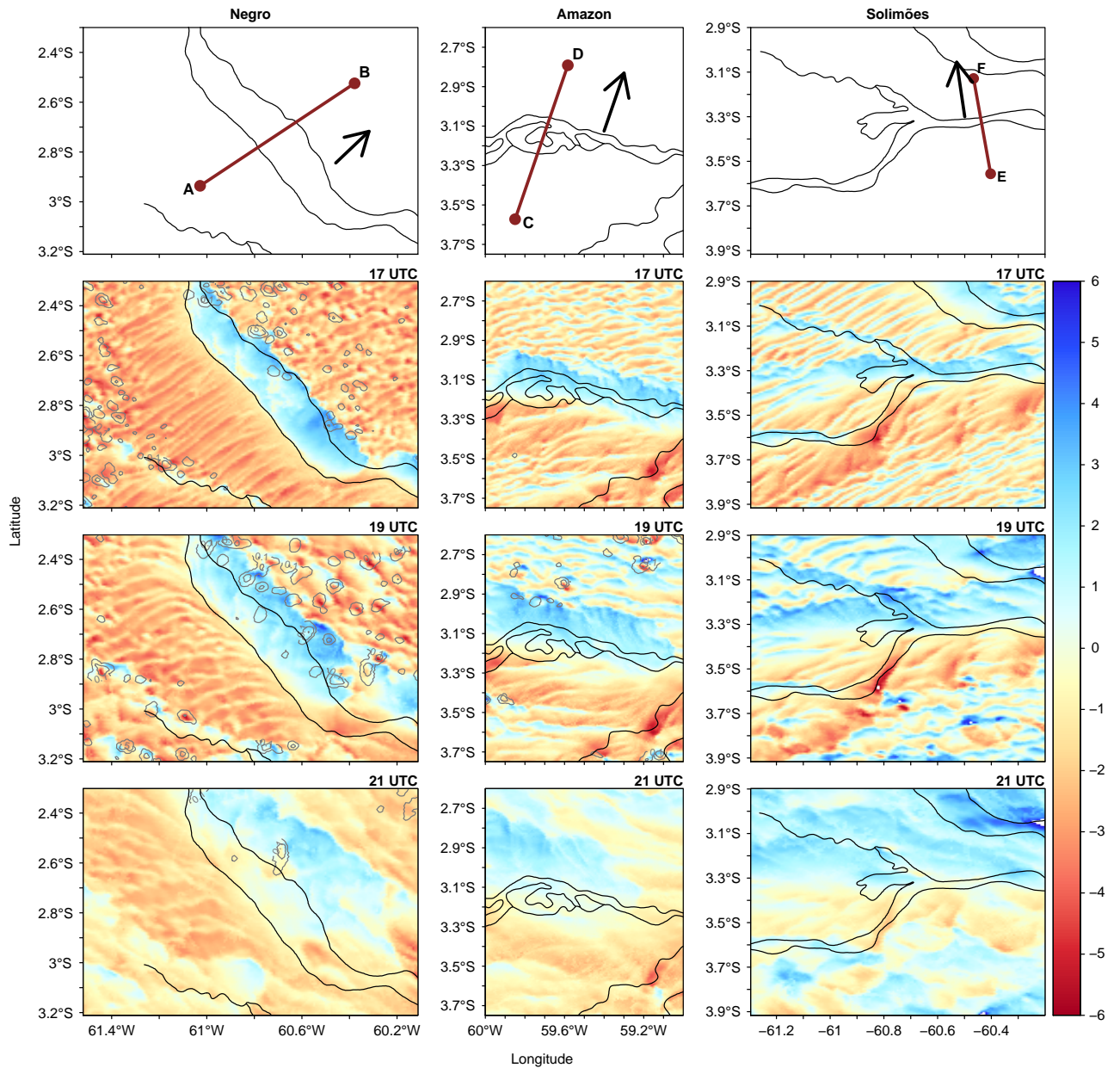
Figure 3.9: Wind perpendicular to the river margins in m/s (colors) and r_{total} in g/kg (contours) simulated in the control experiment. The black arrow is the wind across of reference.

Among all analyzed vertical cross-sections (Figure 3.10), the strongest river breeze circulation at 17 UTC was simulated over the Amazon river where the horizontal temperature gradient was very strong. The river breeze of this river was characterized by a remarkable offshore wind simulated over the margins (Figure 3.10b). This offshore wind converged with the weak scale-large circulation in the northern side of the Amazon river and promoted upward motion over the front breeze. The vertical motion transported colder air to upper atmospheric levels establishing an opposite temperature gradient. This opposite

gradient trigged the return flow located between 500 – 1200 m. The return flow was not evident over the flooded areas where the upper levels temperature gradient was not well established (Figure 3.10b).

Figure 3.10a shows the vertical cross-section of the temperature and the wind across the Negro River part composed of a large amount of flooded vegetation. The horizontal temperature gradient established between this part of the river and upland region was weaker than that simulated across the Amazon river. Although this gradient is weaker, the river breeze development was still evident and it caused convergence and consequently upward motion in the eastern margin of the Negro river. On the western side of this river, the downward motion was dominant. This subsidence was also responsible for the lack of convective clouds simulated near the western margin of the Negro river. Figure 3.10c shows that the local circulations developed across the Solimões river were evident, however it was not as well established as the local circulations simulated across the Amazon River (Figure 3.10a).

Although a temperature gradient was simulated in the early morning (Figure 3.7), no evidence of a land breeze was observed in the wind fields. Local circulations may have been impeded at this time because the horizontal thermal gradient was shallow and the background wind was strong than during the afternoon.
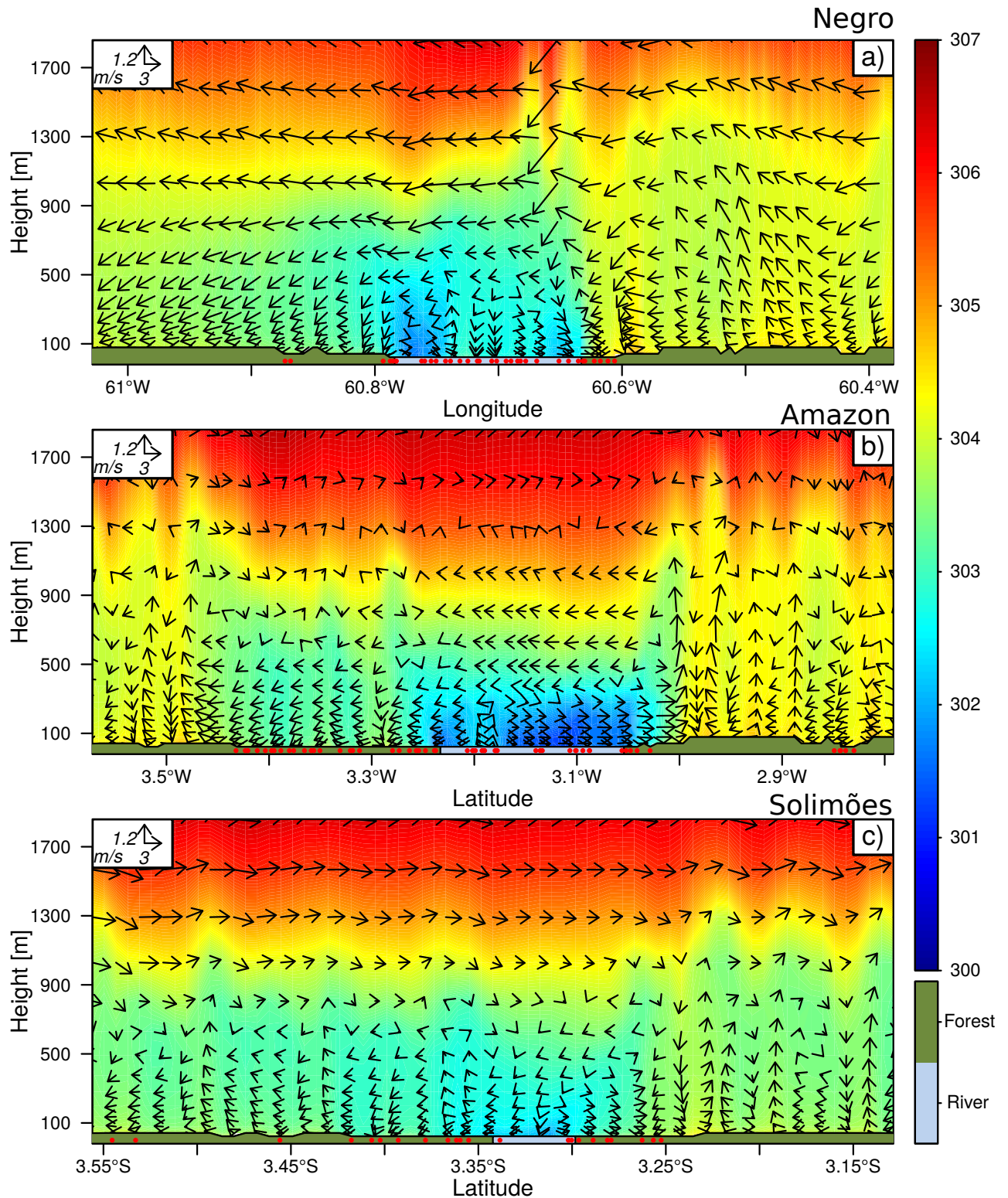
Figure 3.10: Vertical cross-sections of potential temperature in K (colors) and wind (perpendicular to the river margins and vertical components — arrows) at 17 UTC along the lines AB (a), CD (b) and EF (c) in Figure 3.9. The red dots represent the grid cell occupied by flooded vegetation.

3.3.3   Impact of the Seasonal Flooding on the River Breezes.

Section 3.3.2 shown that the breeze front displacement depends on the open water extent, suggesting that seasonal flooding can affect the river breeze in the central Amazon (Figure 3.2). Seasonal flooding may also affect the river breeze by inundating the vegetation since it alters the surface fluxes (Dadson et al., 2010; Schedlbauer et al., 2011) and consequently the air temperature. We investigate these hypotheses by comparing results from the ExpFlood and ExpNonFlood experiments.

Figure 3.11 shows that the temperature difference between ExpFlood and ExpNonFlood had a large magnitude over the regions where the seasonal flooding inundated the vegetation and enlarged the extent of open waters (Figure 3.2). This difference was negative in the daytime (reaching -3 °C — Figure 3.11a), indicating that the temperature was larger in the ExpNonFlood experiment. This result is consistent with the idea that seasonal flooding decreased air temperature due to a greater extent of open water. Figure 3.11a also indicates negative temperature differences near the river margin on the north side of the Amazon River. This difference is likely a consequence of the advection caused by the river breeze. At night, Figure 3.11b shows that the effect of seasonal flooding was an increase in air temperature.
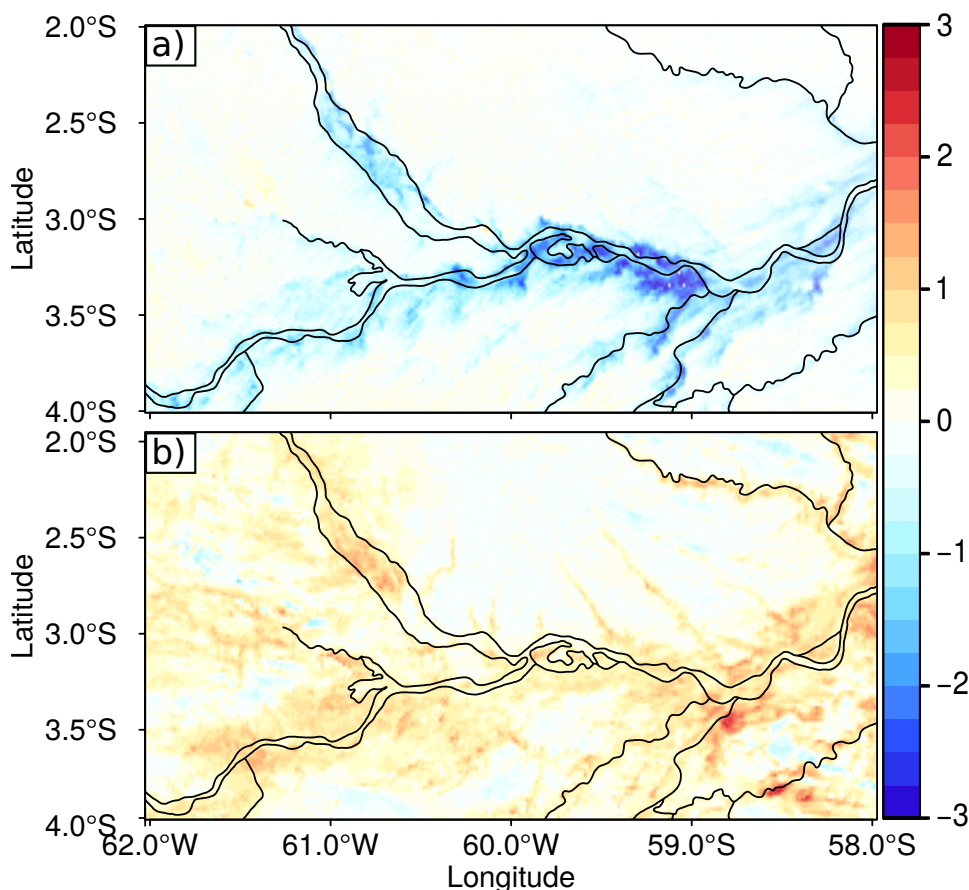
Figure 3.11: Difference between the near surface temperature (°C) simulated in ExpFlood and ExpNonFlood. (a) July 23 2011 at 16 UTC and (b) July 24 2011 at 12 UTC.

The temperature alteration caused by the flooding in July 2011 may affect the river breeze intensity in the central Amazon. Thus, we analyzed this possible consequence by plotting the wind perpendicular to river margins for the ExpNonFlood and comparing it with results from the ExpFlood. The wind fields along with the r_{total} are presented in Figure 3.12. Green lines that highlight the front breeze positions simulated in the ExpFlood are also plotted in this Figure. Thus, this Figure allows comparing the front breeze displacements since the reversal winds (positive values) point out the front breeze locations simulated in ExpNonFlood whereas the front breezes for the ExpFlood are highlighted by the green lines.

Results presented in Figure 3.12 show that in the early afternoon (13:00 LT) do not show wind reversal over the large floodplain areas of Negro river in the ExpNonFlood since these areas were not inundated on this numerical experiment. Nevertheless, wind reversal was simulated over the open water areas and some parts of the Negro river margins in consequence of the river breeze development. The river breeze was also triggered over the

Amazon and Solimões river margins as indicated by the positive values of the perpendicular wind simulated in these regions. However, the magnitude of these positive values was smaller than that simulated in the ExpFlood (Figure 3.9) indicating that seasonal flooding exerts a considerable influence on the river breeze intensity.

The triggered river breezes enhanced over the upland region in the afternoon period (Figure 3.12) as was also simulated in ExpFlood (Figure 3.9). However, the comparisons presented in Figure 3.12 shows that the front breezes propagated more slow in the ExpNonFlood. The distance between the front breezes simulated in the distinct experiments reached values of about 6 km. The results presented in Figure 3.12, when compared with Figure 3.9, also suggest that the river breeze duration was affected by the seasonal flooding. Figure 3.12 shows that the breeze of the Amazon River was still apparent at 21:00 UTC in ExpFlood whereas this river breeze in ExpNonFlood was practically undetectable this time.

The spatial variation of r_{total} simulated in the ExpNonFlood (Figure 3.12) was similar to that from ExpFlood (Figure 3.9). However, the convective clouds in ExpFlood were more spatially organized by the local circulations in the early afternoon. This better distribution of clouds seems to be a consequence of the stronger local circulations simulated in ExpFlood.
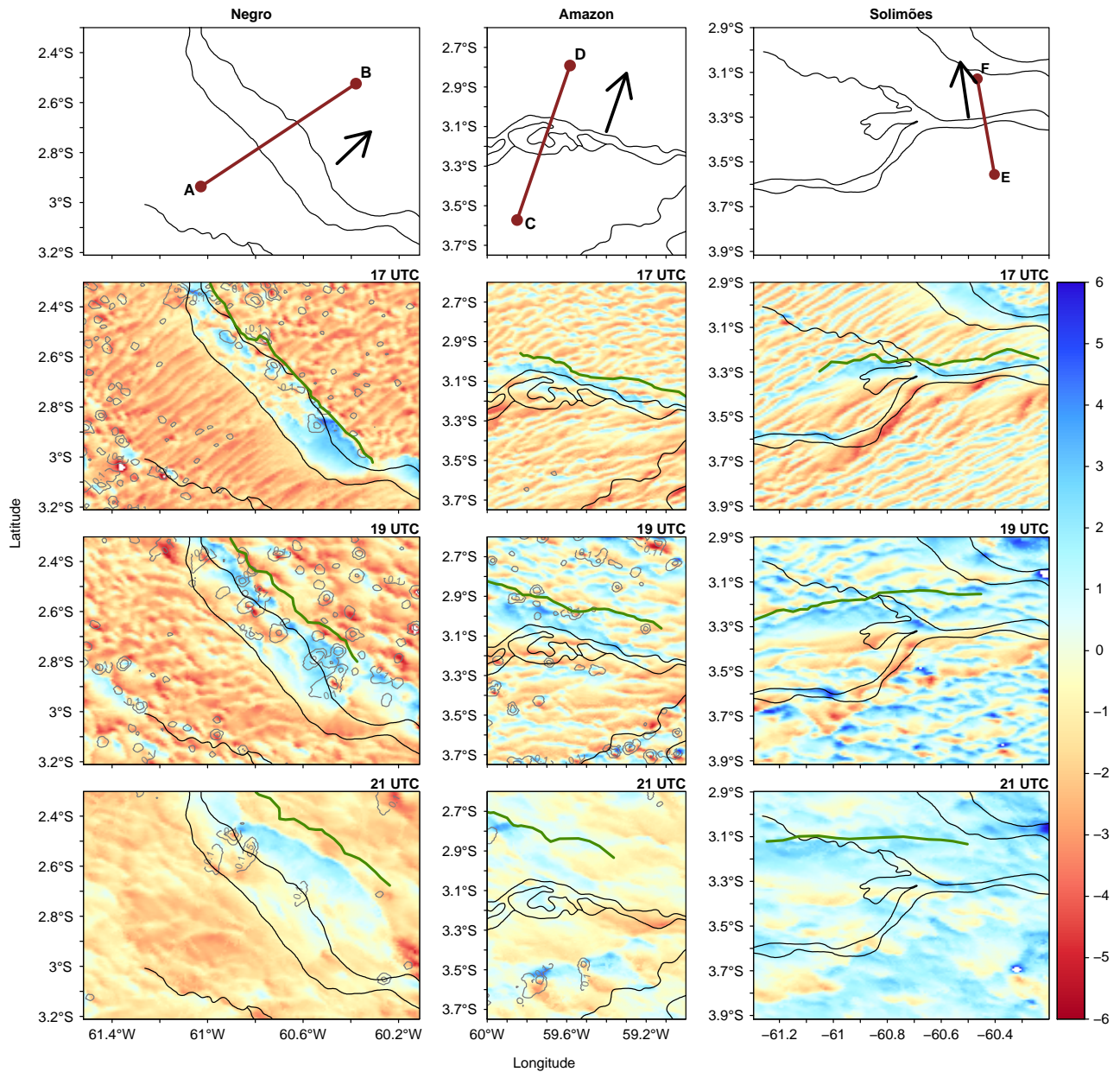
Figure 3.12: Wind perpendicular to the river margins in m/s (colors) and r_{total} in g/kg (contours) simulated in the ExpNonFlod. The green lines highlights the front breeze locations simulated in ExpFlood. The black arrow is the wind across of reference.

The effect of the seasonal flooding on the vertical structure of the atmosphere was analyzed by plotting vertical cross-sections of air temperature, moisture, and wind difference for the main rivers of the central Amazon (Figure 3.13 and 3.14). These differences were computed by subtracting the output values simulated in ExpFlood from those resulted from the ExpNonFlood. The vertical cross-sections for 13:00 LT (Figure 3.13) show that the temperature difference over the areas affected by the flooding is characterized by large negative values in the low levels and positive values in the upper levels. This pattern

is a consequence of the decreased sensible heat fluxes simulated over the inundated areas in ExpFlood that promoted colder air temperature near the surface and consequently reduced the turbulent fluxes. The reduced turbulent fluxes transfer colder air temperature to upper levels less efficiently over flooded areas, consequently, the upper air temperature in ExpFlood was warmer and explains the positive values presented in Figure 3.13. This Figure also shows that the vertical distribution of moisture is affected by seasonal flooding, with negative values of mixing ratio difference values simulated above the flooded areas at about 500 m of height. This negative difference is also a consequence of the reduced turbulent fluxes simulated in ExpFlood that transferred less moisture from surface to upper levels.

Figure 3.13 also shows stronger offshore winds in ExpFlood that advected lower temperature over the river margins. The consequence of these stronger winds and the transported colder air was the intensified convective activity simulated over the front breeze of the Negro and Amazon rivers in ExpFlood. This stronger convective activity is evidenced in Figure 3.13a and b by the strong upward vectors on the eastern and northern sides on the Negro and Amazon rivers respectively. Moreover, the positive values of mixing ratio difference and the negative temperature difference along the upward vectors in Figure 3.13b are also consequences of the stronger convection simulated in ExpFlood. The cross-section presented in Figure 3.13a also highlights upward vectors on the western side of the Negro river. However, these vectors indicates that the subsidence over this areas was stronger in ExpNonFlood.

The effect of the seasonal flooding on the vertical structure of the atmosphere was more remarkable in the late afternoon (16:00 LT) as shows Figure 3.14. This figure highlights that the most of the features previously discussed were also evident and even stronger in the late afternoon.
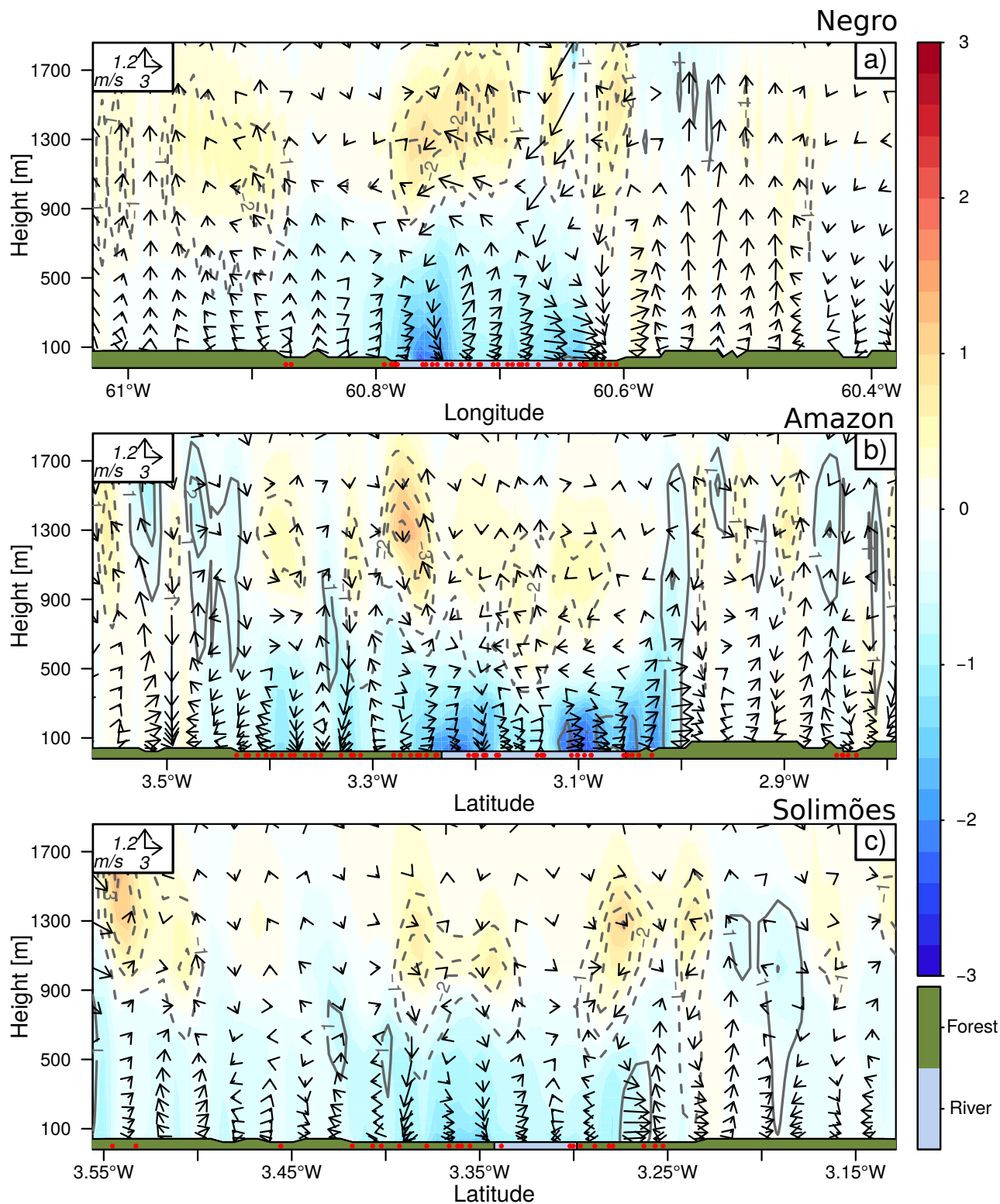
Figure 3.13: Difference between potential temperature in K (colors), wind (same components plotted in Figures 3.10 – arrows), and mixing ratio in g/kg (contours) simulated in ExpFlood and ExpNonFlood at 17 UTC, presented as vertical cross-sections along the lines AB (a), CD (b) and EF (c) in Figure 3.12. The red dots represent the areas affected by the seasonal inundation (open waters and flooded vegetation).
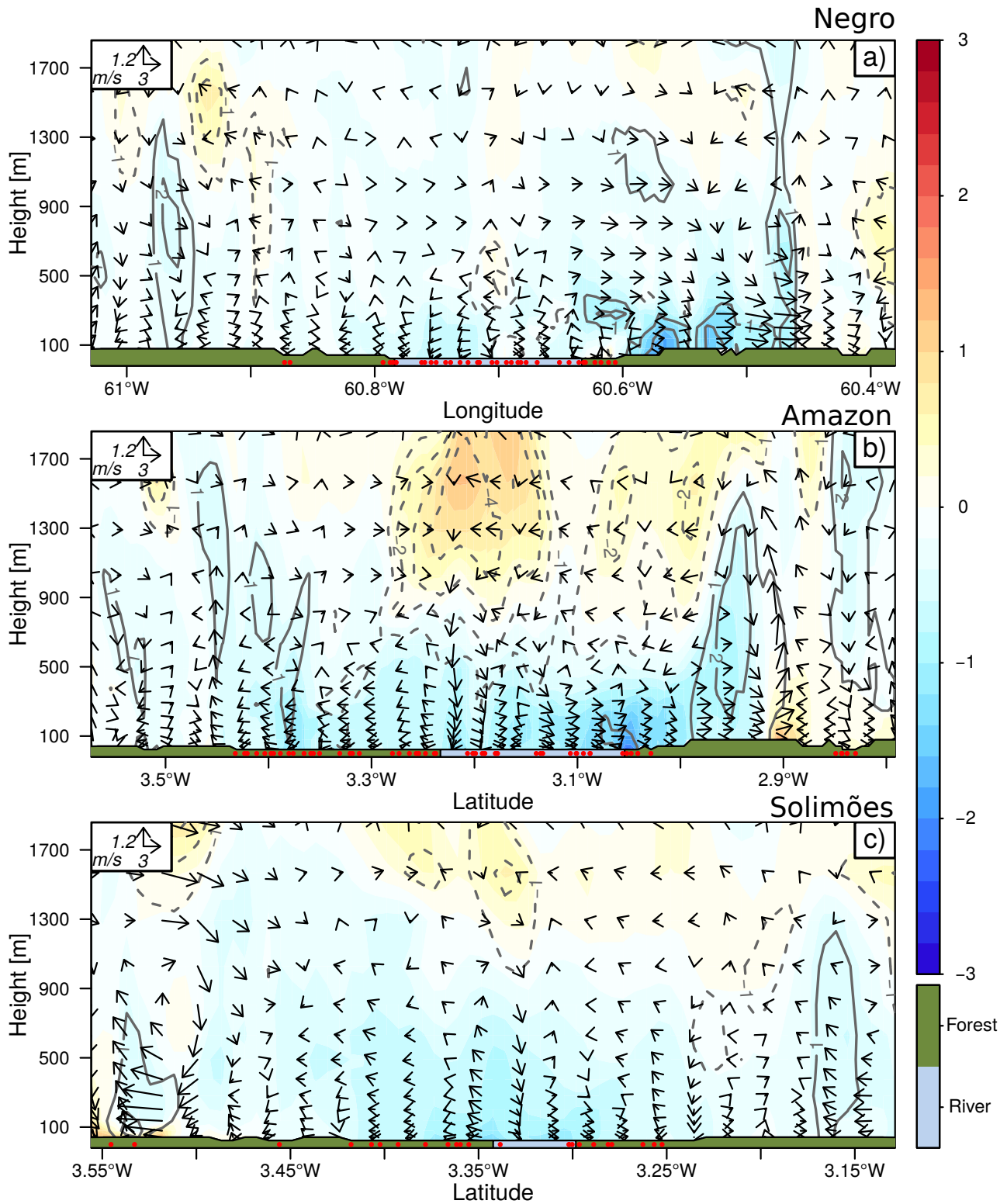
Figure 3.14: Same as Figure3.13 but for 21 UTC.

3.3.4   Impact of the roughness variation on the river breeze circulation.

The confrontation of these results was similar to that previously carried out in section

3.3.2; in other words, we plotted and analyzed spatial fields and vertical cross-sections of air temperature, mixing ratio, and wind difference.

Near-surface temperature difference (Figure 3.15) were larger in upland forests than in floodplain regions. This pattern of temperature difference was also observed throughout the vertical extent of the ABL (Figure 3.16). The negligible temperature difference over the floodplain areas (Figure 3.16) indicates that the smaller roughness length of the floodplain forest did not significantly affect the air temperature. This effect was not relevant because the sensible heat flux differences in the floodplain areas were similar to those of the upland forest (results not shown).
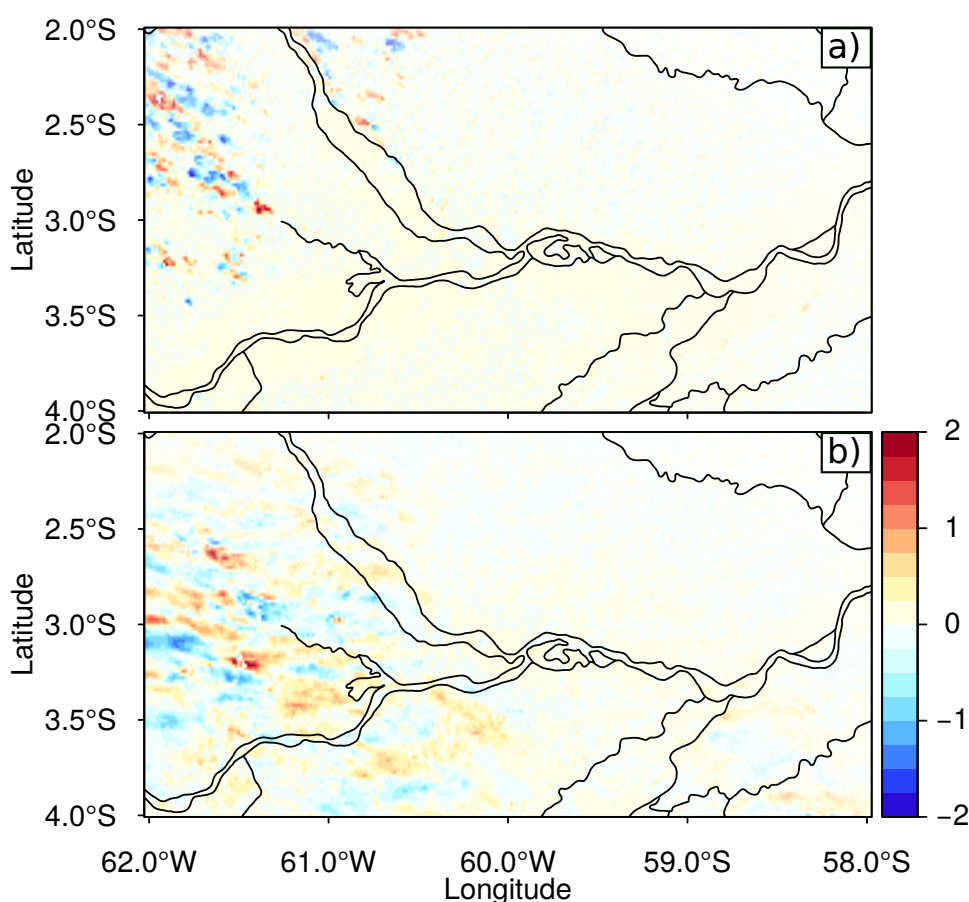
Figure 3.15: Difference between the near surface temperature (°C) simulated in ExpFlood and ExpRoughness. (a) July 23 2011 at 17 UTC and (b) July 24 2011 at 10 UTC.

Noticeable differences in temperature (-+1 K), winds, and mixing ratio were found in the upland region. This wind difference is a consequence of the distinct roughness length used in the numerical experiments (ExpFlood and ExRoughness). Thus, it indicates that the roughness variation affects the local wind and it consequently alters the vertical

structure of the air temperature and moisture. The effect of the roughness variation on the local winds seems to be mostly dynamical because the slight temperature difference over the floodplain areas (Figure 3.16) suggests that the thermal effect was negligible.
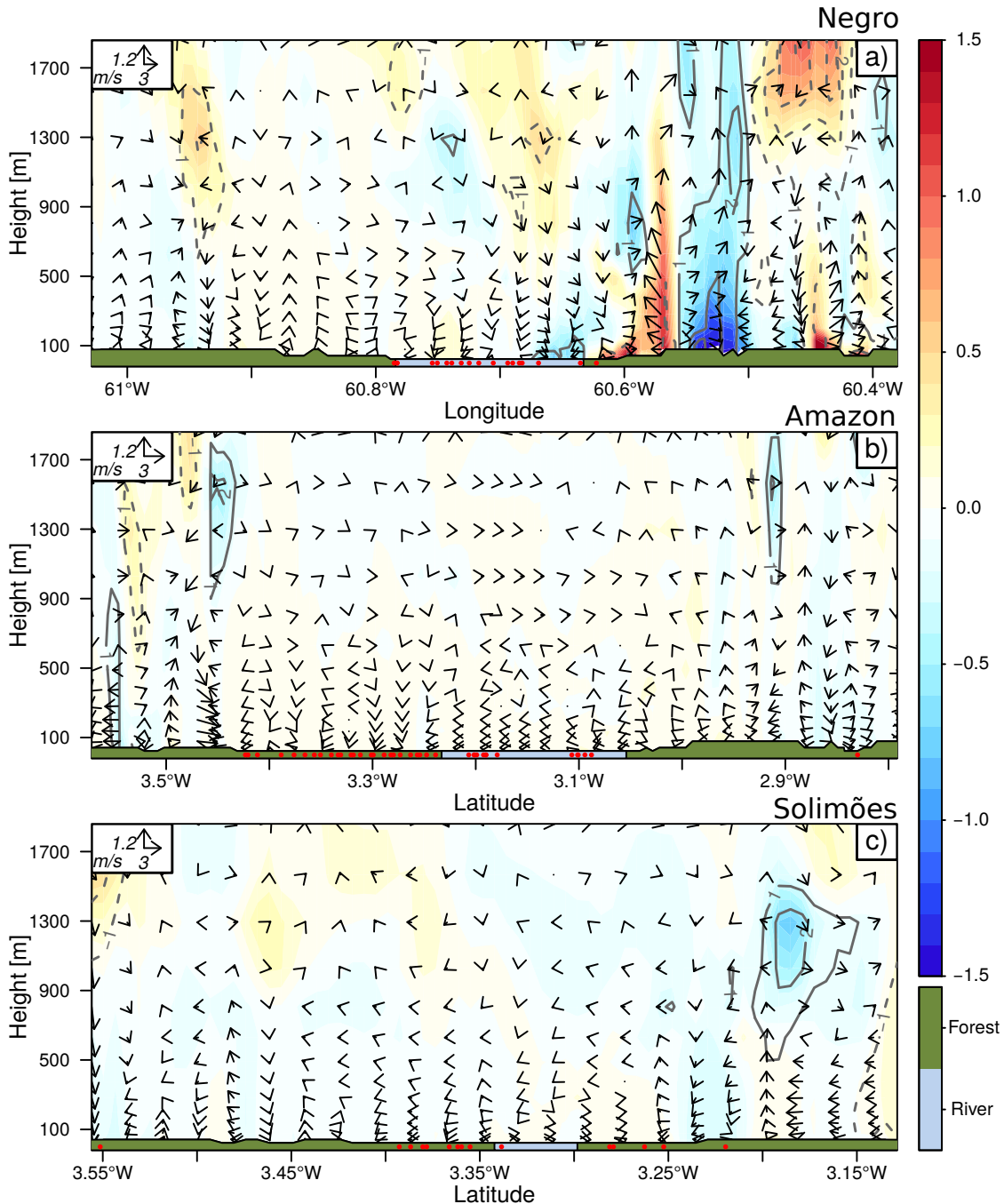
Figure 3.16: Same as Figure 3.13, however, the differences are between atmospherics variables simulated in ExpFlood and ExpRoughness. Moreover, the red dots represent the floodplain areas.

Despite the effect of the roughness length on the local winds, the displacement of the

breeze fronts were not remarkably affected (Figure 3.17). On the other hand, this Figure also reveals that the convection simulated in ExpRoughness considerably differed from that resulted in the control experiment. This convective difference was mostly noticeable in the early afternoon on the eastern side of the Negro River, where the convection simulated along the front breeze in ExpRoughness was more organized than that simulated in ExpFlood.
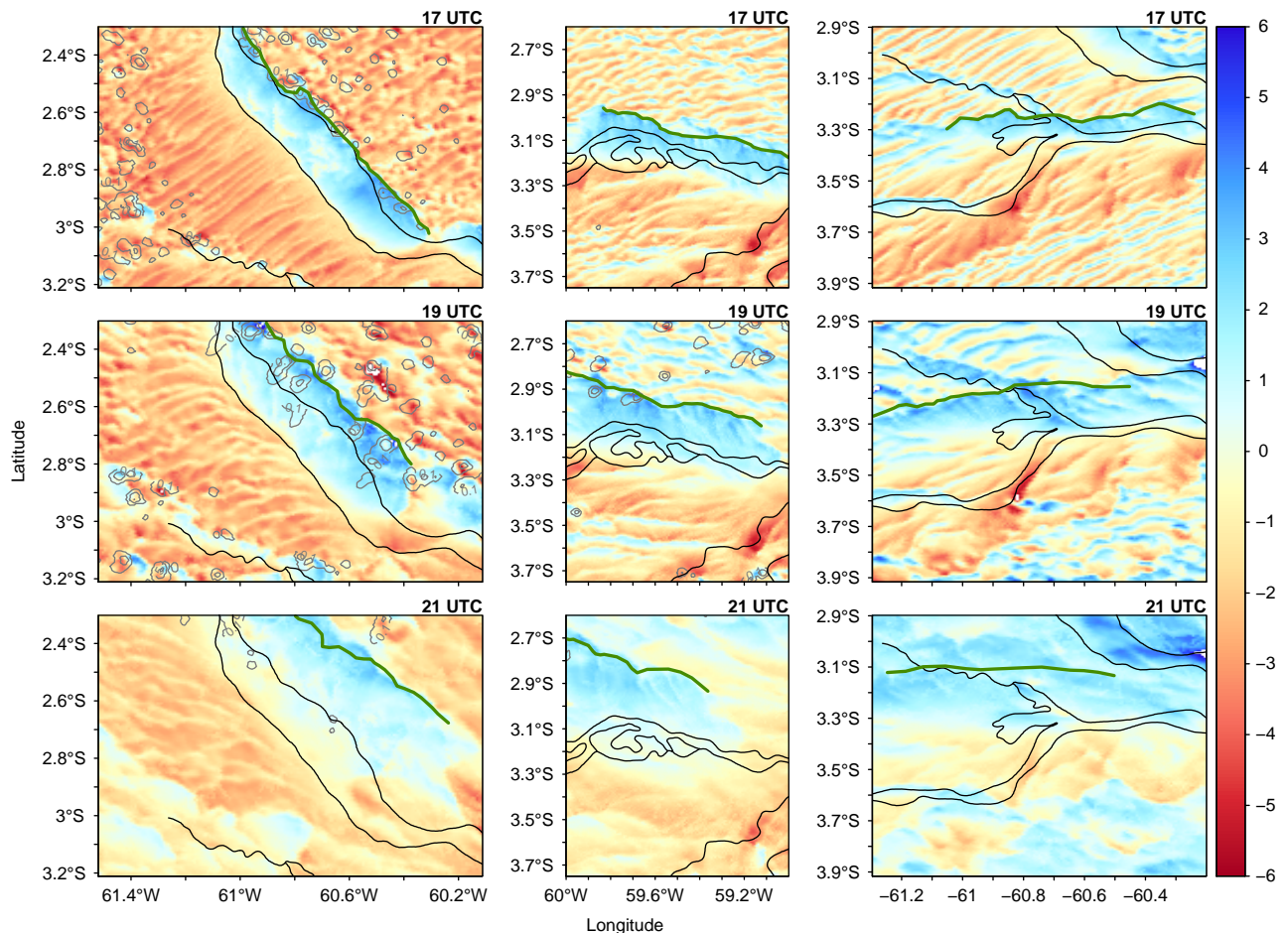
Figure 3.17: Wind perpendicular to the river margins in m/s (colors) and r_{total} in g/kg (contours) simulated in ExpRoughness. The green lines highlights the front breeze locations simulated in ExpFlood.

3.4 Conclusions

Observational studies have demonstrated evidences of river breeze and its importance to the local climate of central Amazon (Fitzjarrald et al., 2008; Paiva et al., 2011). In this region, the seasonal flooding is remarkable (Sippel et al., 1994; Hess et al., 2003; Prigent et al., 2007; Sorribas et al., 2016) and can affect the surface fluxes. Here we access the impact of the seasonal flooding on the river breeze by studying a case occurred in July

2011. We also detail the processes involved in the river breeze developments.

The different energy partitioning of the water and land surface leads to a horizontal thermal gradient that triggers the river breezes in the central Amazon. In the afternoon, the river breezes are intense (wind magnitude reaching 4 m/s) and remarkably propagates through the upland. The river breeze promotes vertical motion over the land altering the vertical structure of the moisture and temperature. At night and early morning, the local circulation triggering is not remarkable as happens in the afternoon.

The seasonal flooding alters the surface energy partitioning in central Amazon since it enlarges the water bodies and saturates the soil. This surface energy alteration promotes temperature decrease and intensification of the river breezes during daytime. The intensified rivers breezes propagate more rapidly through the upland region, take longer to dissipate, and promote stronger upward vertical motion altering the heat and mass transportation. The energy partitioning and the air temperature is also affected by the seasonal flooding at night. However, the temperature alteration at this time does not affect the local winds.

The roughness variation between the floodplain area and the upland region play an important role on the local wind and consequently on vertical transport of heat and mass. This effect is more noticeable on the eastern margin of the Negro River.

Studies have demonstrated that the seasonal flooding in the Amazonia has a remarkable interannual variability that depends on thermal oscillations of the Pacific and Atlantic oceans (Marengo, 2009; Marengo et al., 2012; Espinoza et al., 2013; Marengo et al., 2013; Satyamurty et al., 2013). Our findings suggest that this flooding variability plays an important role on the local climate since the seasonal inundation intensifies the river breezes in central Amazon. From now, we can infer that river breezes and its consequence to local climate are less (more) pronounced in drought (wet) years. These findings indicate that more studies about the seasonal flooding and river breeze interaction are still necessary, especially studies the that shows the importance of these phenomena to the hydroclimate of the central Amazon.

Chapter 4

The Amazon rivers impact on the Manaus-Brazil urban heat island

The figures and parts of the texts presented in this chapter will be submitted to the journal **Atmospheric Research**.

4.1 Introduction

Humans have modified the original Earth Planet landscape by deforestation, natural resource exploration, agriculture and urban development (Vitousek et al., 1997; Klein Goldewijk and Ramankutty, 2004). In the Amazon region, the conversion of tropical rainforest to pasture and crop fields has been the main human activity responsible for the landscape alteration (Margulis, 2004; Davidson et al., 2012; Ometto et al., 2011). In this context, Ramankutty et al. (2007) estimated that 68 % of the deforested area in the Amazon region have been occupied by pasture and crop fields. The consequence of this landscape degradation is a considerable local climate alteration as has been discussed in the literature (Shukla et al., 1990; Saad et al., 2010; Medvigy et al., 2011; Khanna et al., 2017). Such climate change occurs because the physical proprieties of the surface are considerably altered when the landscape is modified. The conversion of native vegetation to urban areas, for example, leads to a remarkable alteration of the thermal, radiative, hydraulic, and aerodynamic properties of the local surface that, consequently, affects the natural budget of energy and mass (Oke, 2002). Moreover, the energy balance in the urban centers is affected by anthropogenic sources, i.e., the energy released by the industrial activity, vehicles, air conditioners, etc (Oke, 2002; Rizwan et al., 2008). The consequence of the energy balance alteration caused by the urbanization processes is a local climate development known as

Urban Heat Island (UHI). This local climate is characterized by warmer air temperature compared with the surrounding region (Oke, 2002; Gartland, 2012).

In central Amazon, a remarkable area of tropical rainforest was replaced by low vegetation (i.e., grasslands, croplands, and savannas, herein referred as rural area) and the urban area of Manaus (Figure 4.1). This urban region has a effective area of approximately 173 km^2 as indicated by MODIS satellite estimates (product MCD12Q1 NASA (2014)) and a population of about 2,094,391 as suggests the last estimate carried out by the Brazilian Institute of Geography and Statistics (IBGE, 2010) in 2016. Thus, this urban area has caused an evident UHI as have been reported in the literature (Maitelli and Wright, 1996; de Souza and Alvalá, 2014). These previous studies have demonstrated that the temperature difference between the Manaus Urban area – MUA – and the surround region (i.e., the Urban Heat Island Intensity — UHII) is remarkable, mainly in the dry season (June – November) when this difference reaches 3.5 °C. These studies also pointed out that the intensity of the Manaus Urban Heat Island (MUHI) has a noticeable diurnal variation that depends on the landscape of the surrounding region. In other words, the authors observed that the diurnal cycles of the UHII are highlighted by maximum values in the daytime when this index is defined as the hourly temperature difference between the metropolitan area of Manaus and the forest region. On the other hand, when the UHII was computed with the air temperature of the rural area the maximum values occurred in the nighttime.

The consequence of the UHI of the Manaus city to the local circulations was investigated in a numerical study presented by De Souza et al. (2016). According to these authors, the thermal contrast established between the urban area and its surrounding triggers an Urban Heat Island Circulation (UHIC) that is more intense on the urban area side that encloses the rivers. Thus, this UHIC may probably interact with the breeze circulation of the rivers that surround the urban area. In this context, some studies have demonstrated that the UHIC affects the conventional local circulations (e.g., sea and lake breeze) when the urban area is placed near the coast (Freitas et al., 2007; Chen et al., 2011; Sharma et al., 2017). Freitas et al. (2007), for example, showed that the local winds generated by the UHI of São Paulo metropolitan area accelerate the sea breeze front when it approaches the city, intensify the convection of the breeze front when it is over the urban area, and retard the propagation of the breeze front when it leaves the city. The river breezes may affect the intensity of the UHI of Manaus by advecting cooler air temperature from the river into the

city. In this sense, Chemel and Sokhi (2012) showed that the sea breeze transports cooler marine air into the London urban area and causes weakening and horizontal displacement of the UHI. Thus, it is expected that the river breeze affets UHI of the Manaus but studies about this subject are still missing.
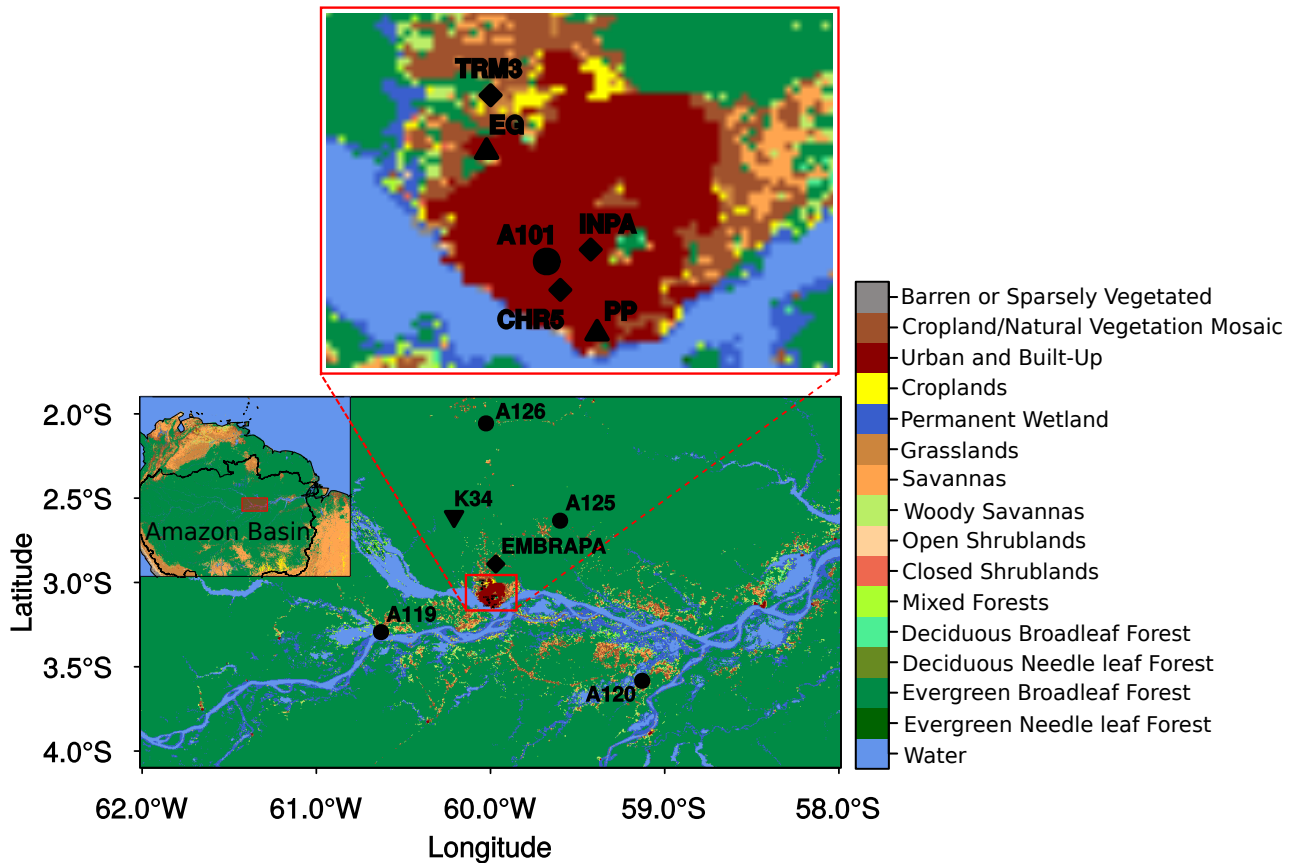
Figure 4.1: Land cover map for the Amazon region (MODIS-MCD12Q1 NASA (2014)) plus locations of the weather stations (black triangles and circles) and the field campaigns measurements (black diamonds).

The river breeze of the central Amazon has been evidenced in the observational studies carried out in the Manaus region (Oliveira and Fitzjarrald, 1993; Dos Santos et al., 2014). These authors pointed out that the onshore and offshore winds observed in the day and nighttime respectively are caused by the river breeze action. According to Dos Santos et al. (2014), this local phenomenon occurs more frequently in the dry season since the reduced cloud cover observed in this period (Machado et al., 2004) allows large incidence of solar radiation at the surface that, consequently, supports strong thermal gradient between the river and upland region. The seasonal flooding of the central Amazon is also a remarkable natural phenomena that affects the river breeze as reveals the recent study performed by

Dos Santos et al. (2017). These authors showed that the seasonal flooding decreases the air temperature over the rivers in the daytime causing an intensification of the thermal gradient that consequently enhances the river breeze circulation. Therefore, it suggests that the seasonal flooding may affect the UHI of the Manaus by altering the river breeze intensity and consequently the advection of temperature into the city. However, this hypothesis has never been addressed yet.

The above paragraphs highlighted the role of the landscape in the development of the river breezes in the central Amazon and the urban heat island of Manaus. The main features of these phenomena and its importance to the local climate have been considerably studied as shows the literature (Oliveira and Fitzjarrald, 1993; Maitelli and Wright, 1996; de Souza and Alvalá, 2014; Dos Santos et al., 2014; De Souza et al., 2016; Dos Santos et al., 2017). However, studies that illustrate the interaction between them are still scarce. Thus, we present here an ensemble of numerical simulations over the central Amazon to answer the following questions: What are the rivers impact on the UHI of Manaus? Does the seasonal flooding affect the UHI of Manaus?

4.2   Models Description

The local climate of the central Amazon is here simulated by the Ocean Land Atmospheric Model – OLAM (Walko and Avissar, 2008a,b) coupled with land surface models (i.e., the Land Ecosystem-Atmosphere Feedback model V4 — LEAF4 and the Town Energy Balance — TEB). The OLAM is a GCM (General Circulation Model) that allows horizontal grid refinement. Thus, this model can simulate atmospheric phenomena of large and small scales with the same timestep. The atmosphere primitive equations in OLAM are solved in an unstructured grid using the finite volume method, which is more conservative than the more used finite difference method.

The LEAF scheme (Walko et al., 2000) is coupled in OLAM to simulate land-atmosphere fluxes for fractional areas of atmospheric grids named as patches. In each patch, the LEAF parameterization computes the fluxes and solves the prognostic equations of energy and mass for the canopy, vegetation, and layers of the soil and surface water. Thus, the LEAF scheme is not adequated to simulate the surface fluxes in the urban patches since there are no specific equations and fluxes computation for the urban canopy as well as the anthro-

pogenic sources of energy is not take into account in this parameterization. However, in practice, LEAF estimates the surface fluxes in the urban patches by attributing the soil and biophysical parameters based on the physical features of the urban canopy. In this context, some studies have shown reasonable air temperature simulated over the urban area using this approach. Nevertheless, better results have been shown when simulations are carried out with an urban canopy parameterization (Freitas et al., 2007; Cantelli et al., 2008; Zhang et al., 2008).

Therefore, we implemented a urban parameterization (TEB) in the LEAF to simulate the fluxes in the urban patches. The TEB scheme (Masson, 2000) considers that the soil in the urban areas is occupied by identical buildings and roads that can assume any orientation. The surface fluxes in TEB are computed for three distinct surface types (i.e., roof, wall and road) and the prognostic equation of temperature is solved for several surface levels. The anthropogenic sources of heat in TEB are defined according to the population size, the quantity of fuel consumed by the vehicles and the amount of electricity expended in the industries and houses (Freitas et al., 2007; De Souza et al., 2016). The industrial sources in TEB are constant whereas the sensible and latent heat released by the traffic is variable along the day with maximum values in the rush time (Freitas et al., 2007).

The Catchment-based Macro-scale Floodplain (CaMa-flood) (Yamazaki et al., 2009) model is used to simulate the seasonal flooding of the central Amazon. This model prognosis the water storage for the unit catchments (as the grid points are considered) by solving the continuity equation. The diagnose variables (i.e., river water depth, floodplain water storage, floodplain water depth, flooded area) are derived from the predicted water storage and topographic parameters. In the continuity equation, the runoff is the forcing data and they are from land surface simulations.

4.3 Models Setup and Input Data

The OLAM was used here as a global model with a local grid refinement centered in the urban area of Manaus. The coarse grid was defined with a horizontal resolution of about 200 km whereas the resolution of the refined grids increases gradually until reaching about 780 m in the innermost domain. The vertical grid was also defined with a variable resolution and with 45 levels in total. Most of this levels are located near the surface where

the vertical resolution is 15 m. The vertical grid spacing in the upper levels increases gradually and reaches 1500 m in the stratosphere. The land-atmosphere processes in the OLAM simulations were here represented by the LEAF and TEB schemes as described above. The others physical processes were represented by the parameterizations presented in Table 4.1. The physical parameters of the Manaus city along with the anthropogenic sources of heat set up in the TEB were derived from the previous studies (Masson, 2000; De Souza et al., 2016) and are presented in Table 4.2.

Table 4.1 - Physical schemes used in the OLAM simulations.

Physical process	Chosen Scheme
Cumulus	Grell-Freitas Grell and Freitas (2013)[a]
Radiation	RRTMG scheme Iacono et al. (2008)
Turbulent Processes	Smagorinsky-Lilly-Hill Lilly (1962); Smagorinsky (1963); Hill (1974)
Microphysics	CSU-RAMS microphysics Walko et al. (1995)

[a] This scheme was turned off when the grid spacing was lower than 3.12 km

Table 4.2 - TEB Parameters values defined for all OLAM simulations.

Parameters	Values
Urban roughness length	2.0 m
Building Height	10.0 m
Fraction occupied by buildings	0.8
Sensible heat released by traffic (HTRAF)	2.95 $W.m^{-2}$
sensible heat released by industry (HINDU)	20.0 $W.m^{-2}$
Latent heat released by traffic (LETRAF)	0.17 $W.m^{-2}$
Latent heat released by industry (LEINDU)	40.0 $W.m^{-2}$

The initial conditions used in the OLAM simulations are the operational data provided by the NCEP Climate Forecast System Version 2 (CFSV2) (Saha et al., 2014). These data have atmospheric information with 37 vertical levels and the soil temperature and moisture in 4 soil layers (0-0.1, 0.1-0.4, 0.4-1, 1-2 m) with horizontal grid spacing of 0.5 °. The Sea Surface Temperature (SST) and ice cover information were also provided by the CFSV2 operational data. The others surface data required by the LEAF package (i.e., topography, land cover map, Normalized Difference Vegetation Index — NDVI, soil texture, and water table depth) were provided by different research agencies and are available in the OLAM's official web page (https://sourceforge.net/projects/olam-model).

Some of the original surface data (i.e., topography, land cover map, and water table depth – WTD) were updated over central Amazon to improve the numerical simulations over this region. The original topography data were replaced to the digital elevetaion model provided by the STRM (Shuttle Radar Topography Mission) that has grid spacing of about 90 m. The land cover map was substituted by the digital map produced by Dos Santos et al. (2017) wich is based on the MODIS's Land Cover Map (product MCD12Q1) and the seasonal floodplain map provided by Hess et al. (2003). This new land cover map has a higher horizontal resolution (grid spacing of about 500 m) and a new land cover class – floodplain forest. The novel land cover type, which represents the evergreen broadleaf forest of the floodplain region, was defined because the vegetation features in the floodplain area differ from those located in the upland region. In other words, the vegetation fraction and forest canopy height are higher in the upland region (Dos Santos et al., 2017). The WTD and the green vegetation fraction (GVF) data for the central Amazon were also provided by Dos Santos et al. (2017). These authors elaborated spatial data of WTD and GVF based on observational measurement and satellite estimates.

The surface temperature information for the main rivers of the central Amazon is based on satellites estimate provided by NOAA/NESDIS (2014). These estimates have some limitations regarding horizontal resolution (about 6 km) and cloud contamination. Thus, some statistical procedures were carried out by Dos Santos et al. (2017) to reduce the errors and consequently produce hourly-diurnal cycles of surface temperature for the main rivers. These diurnal cycles of temperature (computed for each month) were also used to represent the surface temperature of the lakes and small rivers located near the main rivers (Dos Santos et al., 2017).

The flooding information included in the OLAM simulation came from numerical simulations driven by the CaMa-flood model. These simulations were performed for a regional domain that extend most part of Amazon region (21°S – 6°N, 80° – 45°W) with a horizontal resolution of 25 km and an adaptive time-step (Yamazaki et al., 2013) of 24 hours. The output variables resulting from these simulations were downscaled to the digital elevation model resolution (about 500 km). In the CaMa-flood's simulations, the model was forced with runoff data provided by numerical simulations carried out with the Treatment of Surface Interaction Runoff (MATSIRO). The input data for the MATSIRO's simulations were provided by the JRA reanalysis and Global Precipitation Climatology Project – GPCP. A

complete description about the coupling of these models is available in Dos Santos et al. (2017)

4.4   Experimental Design

Herein, a group of numerical simulation is carried out to study the impact of the rivers and the seasonal flooding on the UHII of Manaus. All of these simulations were carried out for July 2011 since the urban heat island and the river breeze are remarkable in this period (Dos Santos et al., 2014; de Souza and Alvalá, 2014). In these simulations, the OLAM integration started at 00 UTC of July 2011 and ran for 31 days with a time-step of 10 seconds. The first 14 days of integration were here considered as the model spinup.

In order to separate the factors that impact the UHII of Manaus, we set up three numerical experiments (CTL, NonRiver, NonFlood) with different landscape features. In the control experiment (CTL) the simulations were carried out with the land cover map produced by Dos Santos et al. (2017) that represents the real landscape of the central Amazon in 2011. The seasonal flooding information is included in this experiment by updating the water body extent in the land cover map and altering the soil parameters according to the flood depth simulated by the CaMa-Flood. In other words, the areas with vegetation height below the mean flood depth of July 2011 (previously simulated by the CaMa-Flood) are considered as water bodies (Figure 4.2a). On the other hands, areas, where the flood depth is below the canopy of the plants, are defined as areas of flooded vegetation. In these flooded areas, the soil is considered saturated and the low boundary condition of the total hydraulic head is equivalent to the flood depth simulated by the CaMa-Flood.

In the NonRiver experiment, the water body areas are replaced by evergreen broadleaf forest (Figure 4.2b) and the seasonal flooding is not taken into account. Thus, this experiment simulates the urban climate of Manaus without the influence of the river breeze intensified by the seasonal flooding. However, the isolation of this effect is carried out by subtracting the results produced in the NonRiver from the CTL experiment (CTL-NonRiver). The effect of the seasonal flooding itself on the urban climate of Manaus is here analized by setting up the NonFlood experimet and subtracting its results from the CTL experiment (CTL-NonFlood). In the NonFlood experiment the land cover map produced

by Dos Santos et al. (2017) is not altered by the seasonal flooding and the inundation of the vegetation is not considered (Figure 4.2c).
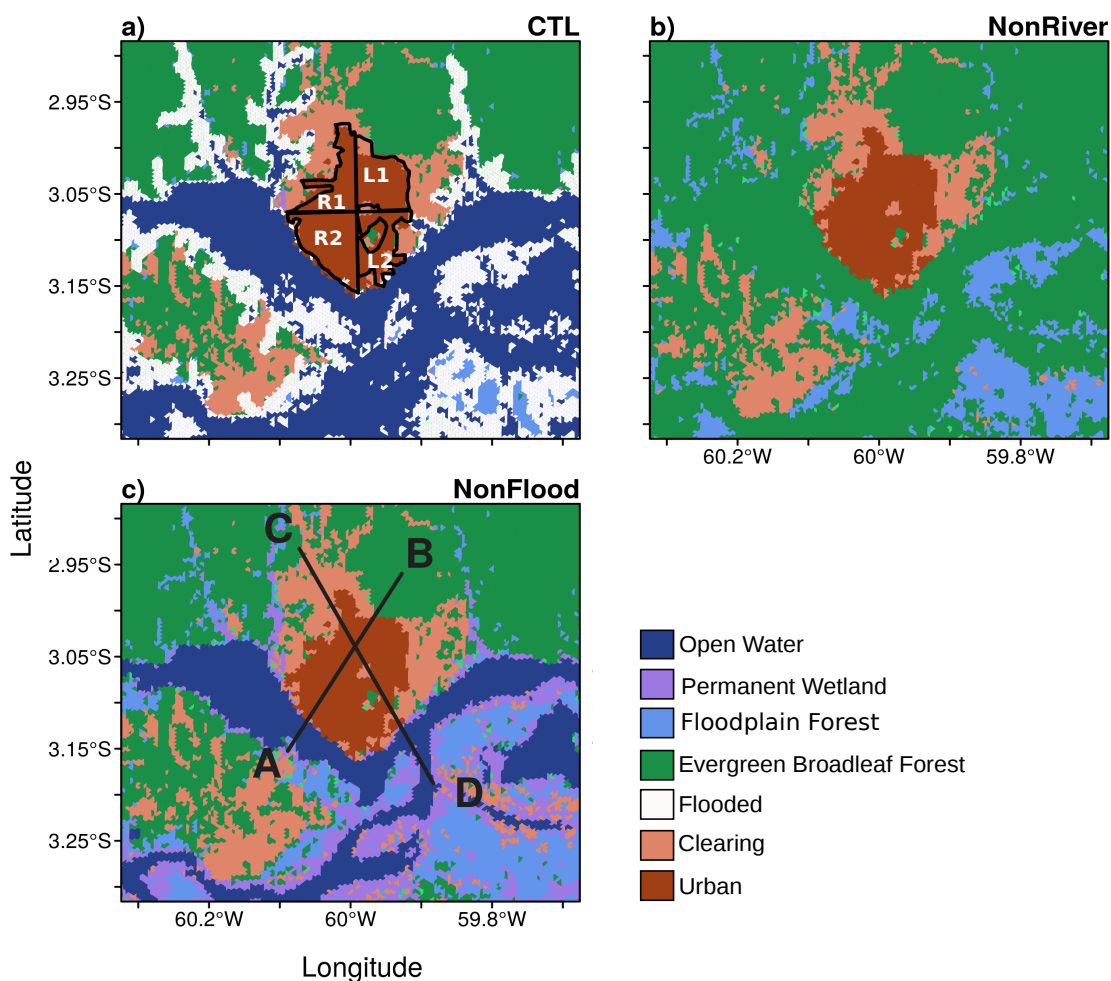
Figure 4.2: Land cover maps used in the different experiments.

4.5   Model Evaluation

The ability of the OLAM model in simulating the local climate over the central Amazon is herein evaluated by comparing the simulated temperature, moisture, and wind with observational data from meteorological weather stations and fields campaigns carried out over the central Amazon. The simulated variables evaluated in this comparison are those simulated in the CTL experiment. An objective analysis of the OLAM simulations (CTL experiment) is also performed by computing the following statistics parameters: standard deviation of the predicted (σ_{pred}) and simulated (σ_{obs}) values, correlation coefficient — r, Mean Bias (MB), Root-Mean-Square Error — RMSE, and Root-Mean-Square Error

with bias removal (RMSE$_{UB}$). Pielke Sr (2002) suggests that a good model simulation establishes the following criteria: $\sigma_{pred} \simeq \sigma_{obs}$, RMSE $<\sigma_{obs}$, and RMSE$_{UB}$ $<\sigma_{obs}$.

Figure 4.3 shows that the diurnal cycle of temperature was well simulated by the OLAM in the most weather locations. This good performance is also confirmed by the statistics values presented in Table 4.3. The errors presented in this Table are small, except for the EG and TRM3 sites. Over these two stations, the criteria suggested by Pielke Sr (2002) is not verified since the standard deviation of the simulated temperature is far from observation. In the EG station, the model overestimated the air temperature in the nighttime causing a significative systematic error (bias = 1.0 °C). Over the TRM3 station, the model underestimated the diurnal cycle of temperature, mainly during the early night where the difference reached 3.0 °C. Although the systematic errors occurred over some sites, the simulated temperature agrees with observation as indicates the strong correlation (r $\geq$ 0.9) shown in Table 4.3.

A comparison of the simulated and observed Dew Point Temperature (Td) are also presented in Figure 4.3. This Figure shows that Td was properly estimated over EG, PP, and A125 stations. Over these locations, the simulated diurnal cycle of Td is in agreement with observation hence the computed errors for these sites are considerably small and the Pearson's correlation values are elevated (Table 4.3). On the other hands, the model fails to reproduce the Td diurnal cycles for PP and K34 stations as suggest Figure 4.3 and the remarkable errors shown in Table 4.3. In PP station, the model underestimated Td (bias=-2.89 °C) in the entire period whereas over K34 site the diurnal cycle of Td was overestimated (bias=1.91 °C), mainly in the afternoon and early night. In spite of the considerable errors over PP station, the correlation between the observed and simulated Td is strong (r=0.75), indicating that the diurnal variation of Td agrees with observation over this site.
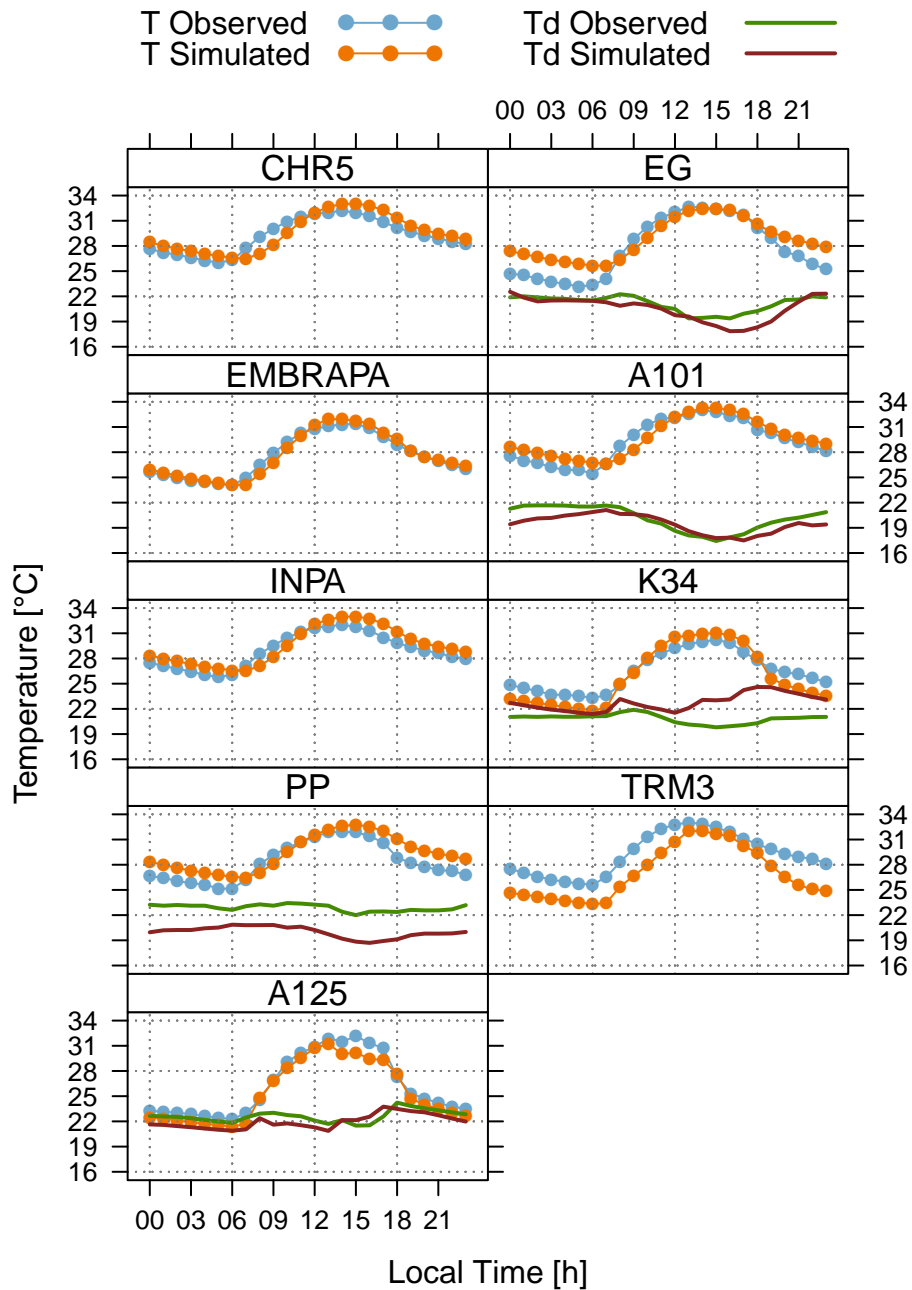
Figure 4.3: Diurnal cycles of the simulated and observed air temperature (T) and moisture (dew point temperature – T_d) for July 15 to 31 of 2011.

Figure 4.4 compares the diurnal cycles of the simulated wind magnitude against observations values measured of the central Amazon. This comparison reveals that the simulated cycles are shifted over stations located near the rivers (EG, A101, and PP). However, the model captured well the amplitude of the cycles over the PP site in the most period of the day. Thus, the computed errors for this station are small as shown in Table 4.3. The diurnal cycle amplitude also was well predicted over the K34 weather station, which is located

far from the rivers. The computed errors for this station are small as shows Table 4.3. The model performance for the two stations located far from the rivers (K34 and A125) was distinct. Over the K34 station, the simulated wind is close to observation (Figure 4.4) resulting in small computed errors (Table 4.3) that satisfy the criteria suggested by Pielke Sr (2002). On the other hand, the errors presented for the A125 station is remarkable since the model fails in reproducing the diurnal cycle amplitude over this point.
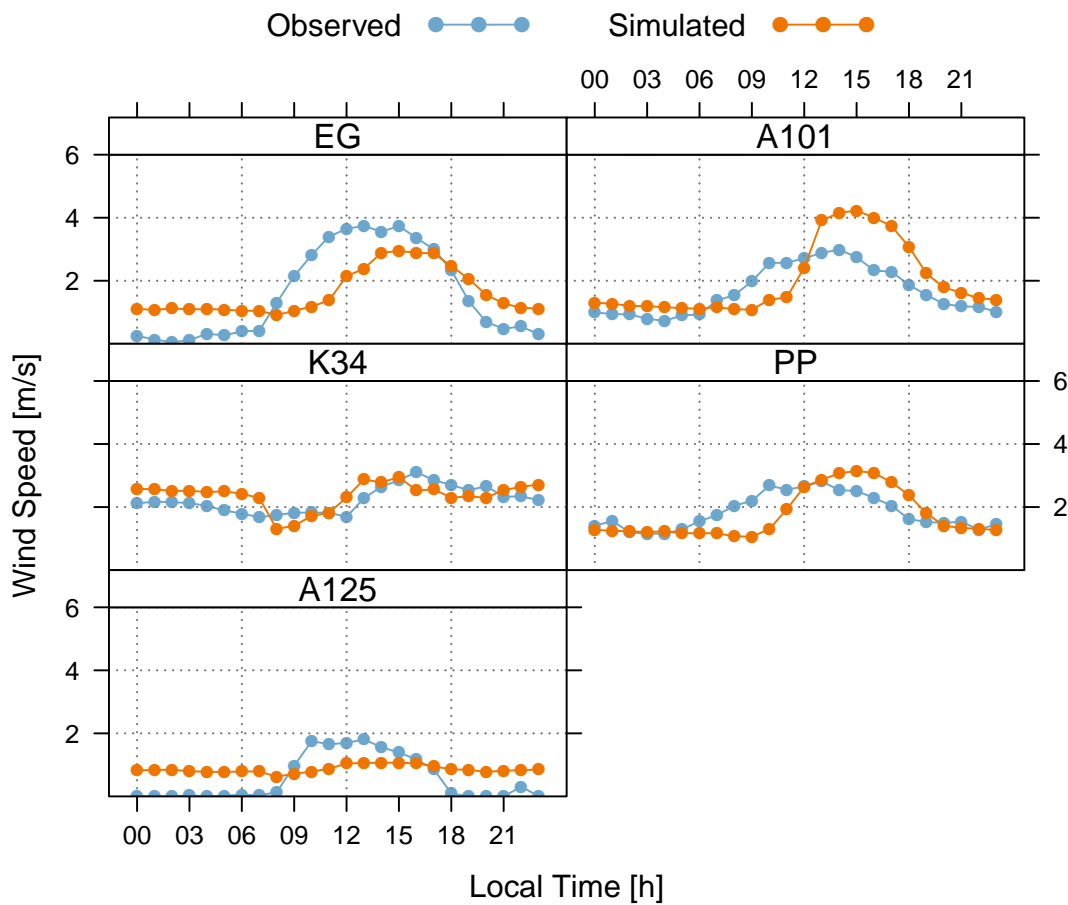
Figure 4.4: Diurnal cycles of the simulated and observed wind magnitude for July 15 to 31 of 2011.

4.6   Results and Discussion

Herein a series of three numerical simulations (CTL, NoRiver, and NonFlood) are analyzed so as to understand the how the Amazon rivers affect the local climate of Manaus city. The isolated impact of the seasonal flooding on the UHI of Manaus is also assessed here. These numerical simulations herein analyzed were driven by the OLAM model coupled

Table 4.3 - Statistics computed with simulated and observed values.

Station ID	Temperature						Dew point Temperature						Wind Speed					
	obs	sim	Bias	RMSE	E_{UB}[a]	r	obs	sim	Bias	RMSE	E_{UB}[a]	r	obs	sim	Bias	RMSE	E_{UB}[a]	r
K34	2.32	3.37	-0.48	1.25	1.16	0.98	0.54	0.97	1.91	2.28	1.24	-0.28	0.41	0.41	0.14	0.42	0.39	0.53
EMBRAPA	2.49	2.69	0.079	0.53	0.53	0.98	—	—	—	—	—	—	—	—	—	—	—	—
CHR5	2.03	2.2	0.31	1.00	0.96	0.90	—	—	—	—	—	—	—	—	—	—	—	—
INPA	2.02	2.18	0.56	1.00	0.83	0.92	—	—	—	—	—	—	—	—	—	—	—	—
TRM3	2.47	3.03	-2.27	2.45	0.94	0.96	—	—	—	—	—	—	—	—	—	—	—	—
PP	2.29	2.07	1.03	1.38	0.93	0.91	0.39	0.65	-2.89	2.92	0.44	0.75	0.54	0.74	-0.09	0.56	0.56	—
EG	3.44	2.33	1.00	1.75	1.45	0.94	0.95	1.42	-0.59	0.94	0.74	0.87	1.41	0.72	0.02	0.96	0.96	0.77
A101	2.48	2.22	0.36	0.97	0.91	0.93	1.43	1.07	-0.64	1.01	0.78	0.84	0.75	1.12	0.34	0.83	0.75	0.74
A125	3.56	3.47	-0.81	0.97	0.54	0.98	0.68	0.82	-0.64	0.92	0.67	0.61	0.70	0.12	0.29	0.70	0.63	0.65

[a] E_{UB} is an abbreviation of $RMSE_{UB}$

with land surface parameterizations as described in above sections.

4.6.1 Simulated Local Climate of the Central Amazon

In this section, we present a brief analysis of the UHI of Manaus and the local circulations triggered in June 2011. This analysis is essential to better understand how the rivers and the seasonal flooding influence the UHI of Manaus in the subsequent sections.

Figure4.5 presents spatial fields of temperature and winds for the rivers confluence region of the central Amazon. This region has a remarkable horizontal variation of temperature as a consequence of its inhomogeneous land cover type (Figure 4.1). This pattern of temperature variation considerably changes along the day. In other words, in the daytime, the air temperature fields present low values in the river regions and maximum over the land, especially over the urban area. In the night, the highest values of temperature are also established over the Manaus city. However, the air temperature over rivers is higher than that observed in the vegetated surfaces. The evident larger temperature in the urban area along the day characterizes the heat island of Manaus. This heat island is more intense and spatially uniform in the nighttime when the horizontal wind is calm.

This remarkable horizontal variation of temperature in the central Amazon triggers river breezes 4.5 that play an important role to local circulations and horizontal transportation of the heat and mass. In this context, Figure 4.5 shows that in the midday, when the river breeze is well established, the air temperature in the periphery is lower than the urban center. Thus, it suggests that the colder air from the rivers and the forested region is transported into the city by the local winds. This effect is more evident in Figure 4.6 that shows the vertical cross-sections of potential temperature and wind along the urban area and rivers for the noontime (16 UTC). At this time, the river breeze fronts have penetrated the southern edge of the urban area causing temperature reduction and a significant upward transportation of the warmer air. The vertical motion simulated in frontal areas occurs because the river breeze (onshore wind) converges with the offshore wind triggered due to the thermal difference of the urban and vegetated region. The river breezes also transport moisture from the rivers into the urban areas as shows Figure 4.7. Part of this moisture is carried to upper levels by the breeze front convection.
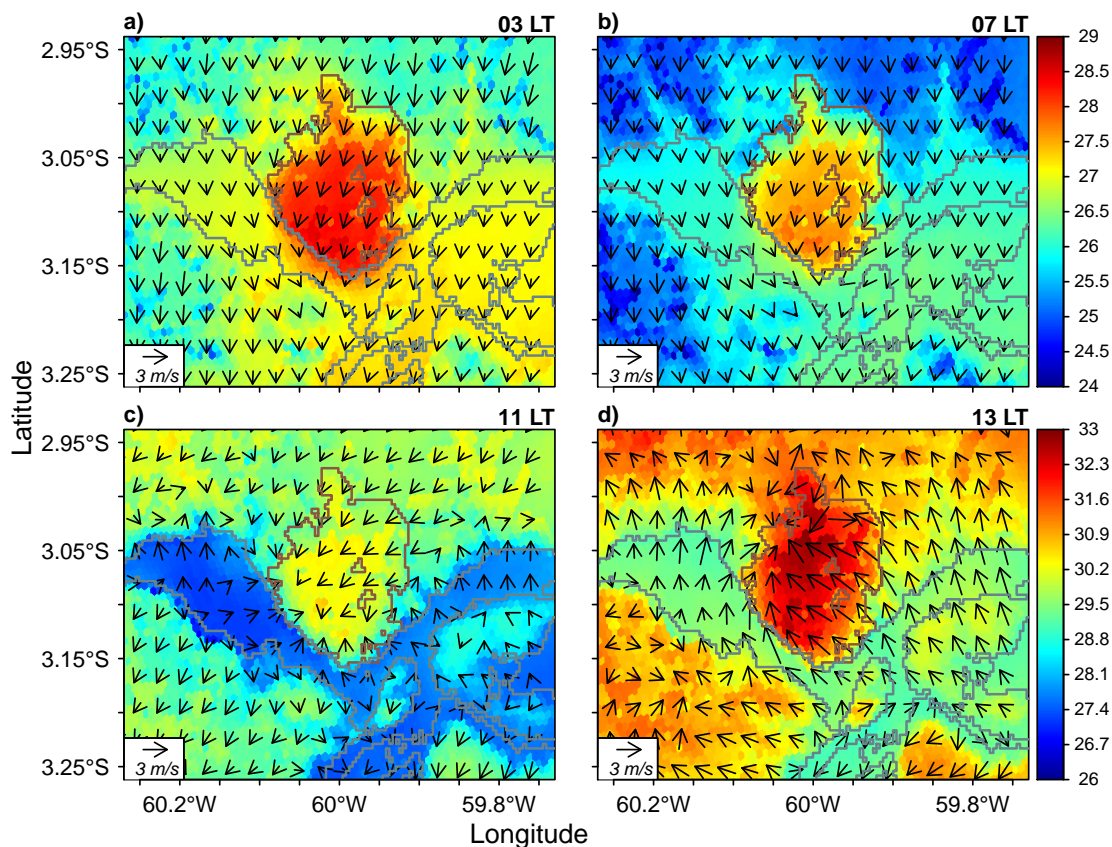
Figure 4.5: Spatial fields of the mean temperature in °C (colors) and the mean horizontal wind (arrows) for the CTL experiment.
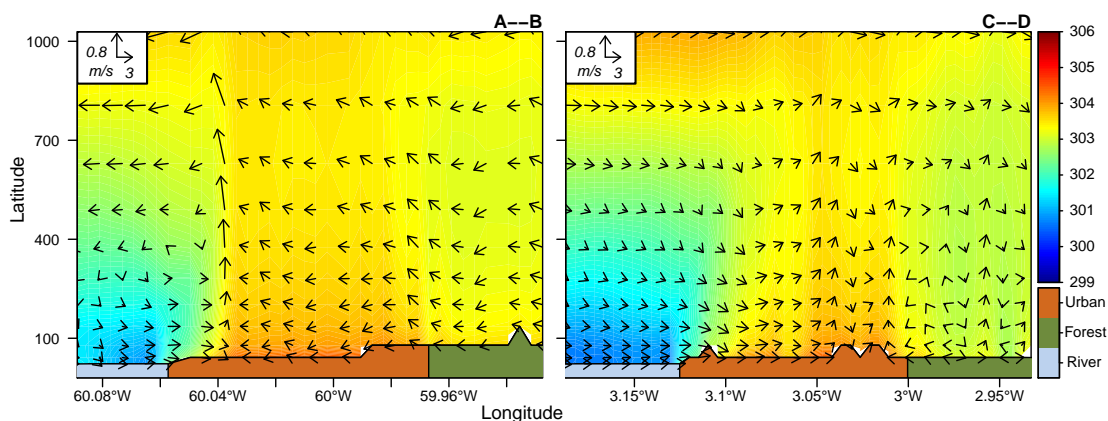
Figure 4.6: Vertical cross-sections of averaged potential temperature in K (colors) and averaged wind (component perpendicular to the coast plus vertical component – arrows) along the lines defined in Figure 4.2 at 16 UTC.
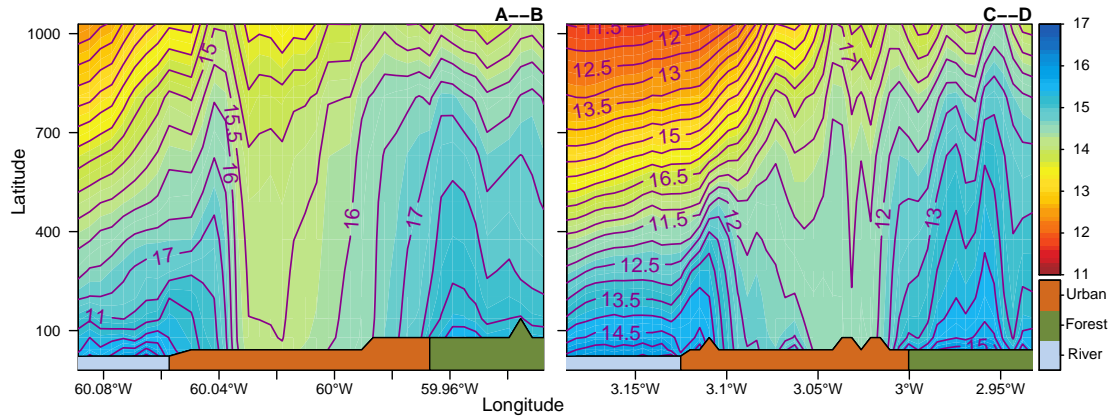
Figure 4.7: Vertical cross-sections of mean mixing ratio (g/kg) along the lines defined in Figure 4.2 at 16 UTC.

4.6.2   The impact of the Amazon Rivers on the UHI of Manaus

Although the above convincing evidence that the rivers influence the UHI of Manaus, an investigation that allows quantifying and better understand this effect is necessary. Thus, we compare herein results from CTL experiment with those simulated in the NonRiver. This comparison permits isolating the effect of the rivers on the urban climate of Manaus.

Figure 4.8 shows the spatial fields of the mean temperature difference (CTL-NonRiver) for the diurnal and nocturnal period. In the daytime, the temperature difference over the rivers reaches -3.0 °C, indicating that these water bodies are responsible for triggering a remarkable gradient in this period. The consequence of this temperature gradient is the river breeze development as discussed in the previous sections and represented by the remarkable mean wind difference simulated over the river margins at 13 LT (Local Time). These mean winds converge in the urban area center since the coastline is convex in the rivers confluence region and the breezes penetrates nearly perpendicular to the coast. The cold temperature advected by the river breeze is also evidente in Figure 4.8. This figure points out that the temperature difference is remarkable in the urban area edges when the mean wind difference penetrates on the city.

In the nighttime, especially at dawn, the effect of the rivers on the local temperature is also noticeable as indicates the large positive difference (values around 2.5 °C) of the mean temperature simulated over the rivers (Figure 4.8). However, the thermal gradient triggered by the rivers is not capable of promoting a remarkable local circulation as happens in the daytime. At 03 LT (Figure 4.8a) the mean wind difference over the urban area is

only relevant in the extreme coastal part of the city. Near the sunrise (07 LT), the mean wind difference is relevant (magnitude of about 0.3 m/s) over the entire urban area. At this time, the mean temperature difference simulated over the urban area is positive and indicates that the urban heat island is more intense when the rivers are taken into account in the numerical simulations. This mean temperature difference is a consequence of the wind and the atmospheric diffusive process that is more intense in the CTL experiment. The stronger diffusion in the CTL experiment occurs because the rivers cause a more intense thermal gradient in the city edge.
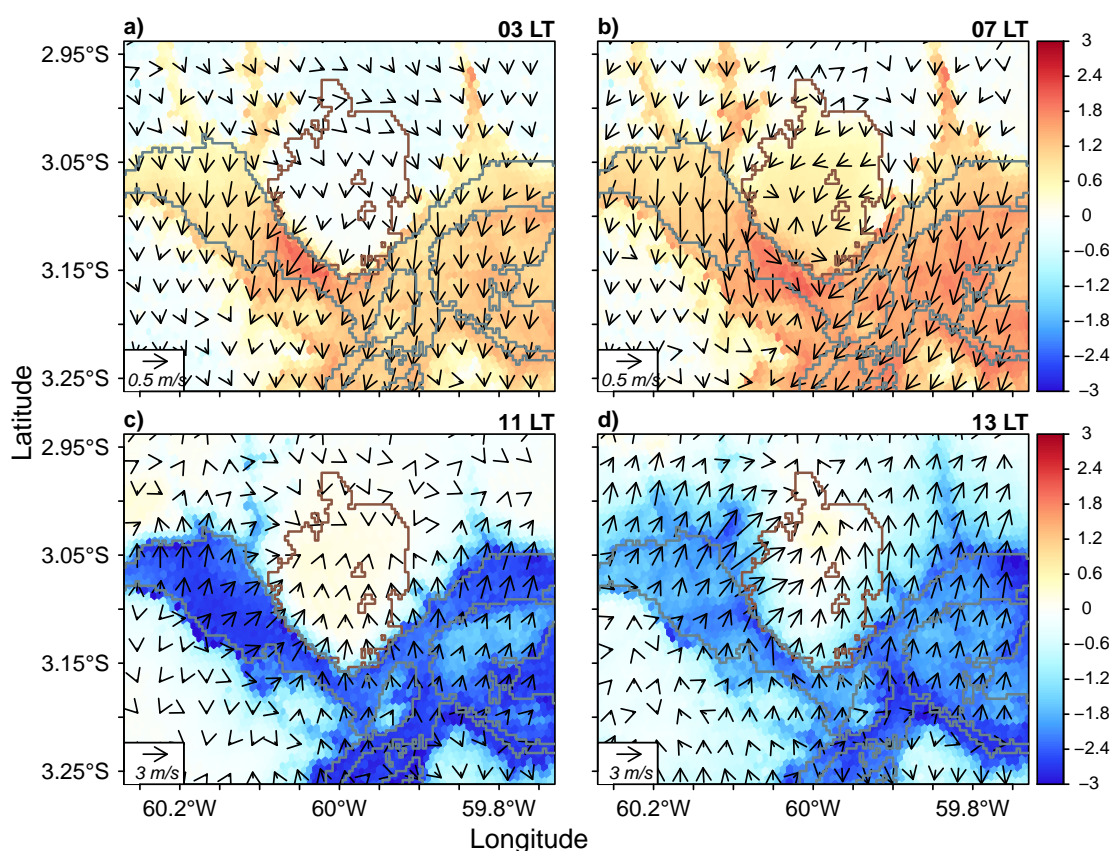
Figure 4.8: Spatial fields of the mean temperature in °C (colors) and the mean horizontal wind (arrows) difference between CTL and NonRiver experiments.

Figures 4.9 shows the diurnal cycles of the atmospheric variables for four parts of Manaus. These diurnal cycles were established considering spatial averages over the areas defined in Figure 4.2. This approach is essential to quantify the effect of the river on the different parts of the urban area. Figure 4.9a shows that the diurnal cycles of the mean temperature difference (CTL-NonRiver) are highlighted by maximum values about 07 LT and minimum around 13 LT. These negatives and positives peaks are more obvious in

Figure 4.10. The diurnal cycles of temperature plotted in this Figure were computed by considering percentiles 10 and 90 over the area instead of the mean average. Thus, the more evident peaks of this Figure reveal the clear difference existent between the diurnal cycle amplitude of the regions located near (R2 and L2) to those situated far from the rivers (R1 and L1). This Figure also shows that the rivers promote a temperature larger than 1.0 °C in the nighttime and a decreasing inferior to -1.5 °C in the day time.

The negative peaks of the mean temperature difference (Figure 4.10) coincide with the maximum positive values of the wind and mixing ratio presented in Figure 4.9b, c, and d. Thus, it indicates that the rivers cause remarkable local circulations (mean positive difference of the zonal and meridional wind around noon – Figure 4.9c and d) that advect colder and moister air into the urban area decreasing the temperature and increasing the humidity. Figure 4.9a and b also shows that the maximum values of the zonal wind difference occurs earlier and are more intense in the regions located near the rivers. This remarkable discrepancy in the diurnal cycles of the mean wind difference explains the distinct magnitude of the temperature decrease presented in Figure 4.9a and Figure 4.10.
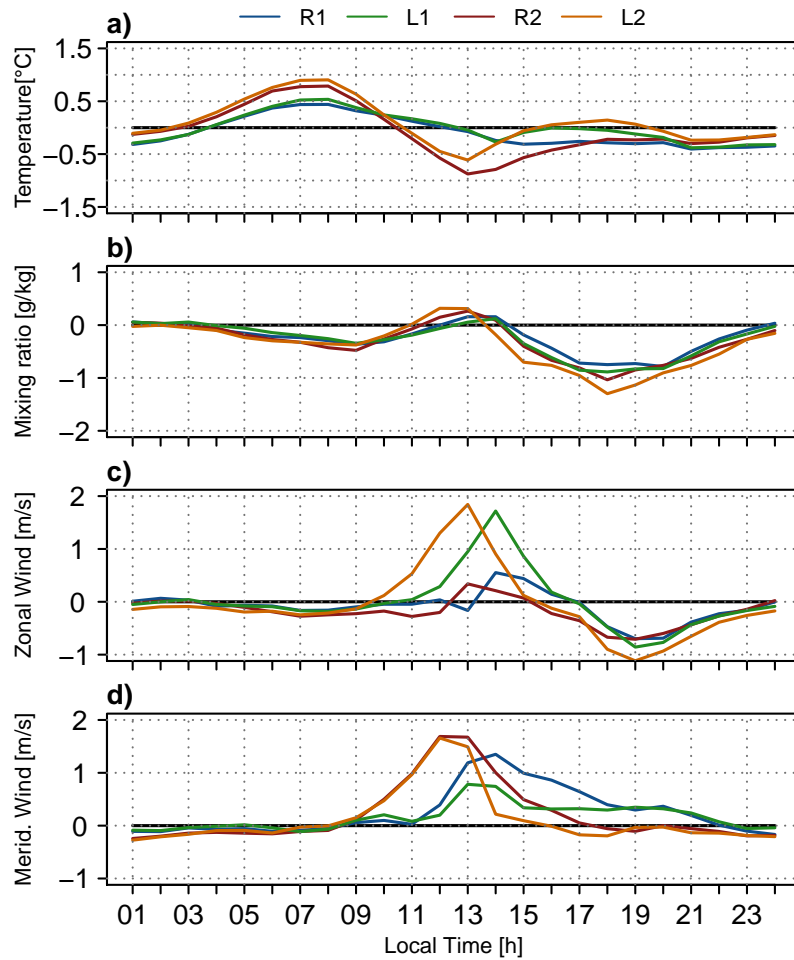
Figure 4.9: Diurnal cycles of the temperature, moisture and wind difference between CTL and NonRiver experiments for four regions of the Manaus city (L1, L2 ,R1, R2 – see Figure 3.2)
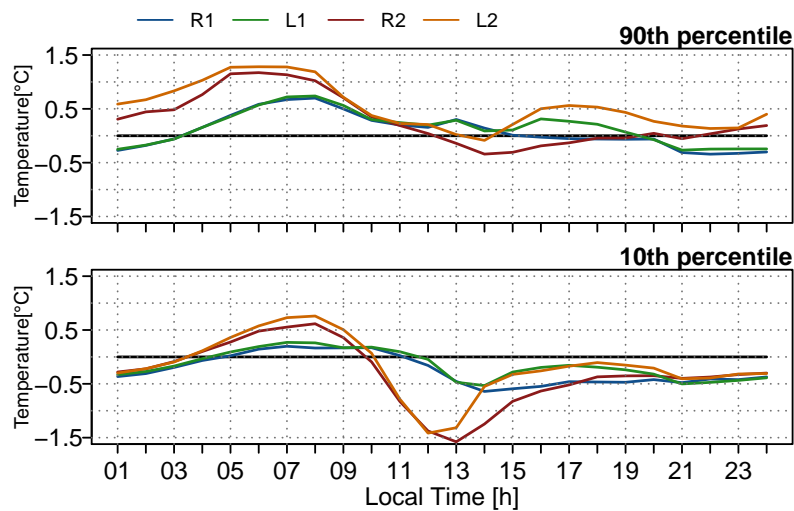
Figure 4.10: Same as Figure 4.9 but consireing the percentils 90 and 10 over the areas instead of the average.

In order to quantify the river breeze effect on the vertical structure of the atmosphere, we present vertical cross-sections of the mean wind difference, temperature, and moisture in Figure 4.11. This figure points out that the mean difference of the perpendicular wind towards the city in the low levels and reaches a magnitude of about 3 m/s. Near the urban center, this perpendicular wind is weak whereas the vertical component of the mean wind difference reaches 0.8 m/s. This well seen local circulation is a consequence of the river breezes triggered in the CTL experiment that affect the horizontal and vertical transport of heat and mass as indicates the significative temperature and moisture difference presented in Figure 4.11. The vertical transport alteration is another factor that justifies the warmer temperature simulated in the CTL experiment in the nighttime. In other words, the vertical transport modified by the river breezes alters the surface fluxes (i.e., it increases the heat and reduce the latent fluxes — appendix B.1), especially in the daytime, causing a significant temperature increase as previously shown.
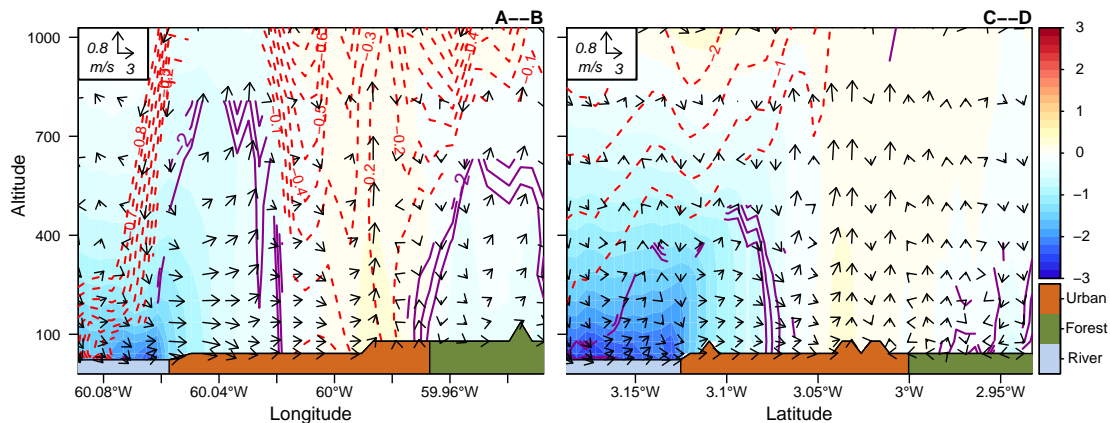
Figure 4.11: Vertical cross-sections of mean potential temperature in K (colors), mean wind (component perpendicular to the coast plus vertical component represented – arrows), and mean mixing ratio of vapor (contours) difference between CTL and NonRiver experiments along the lines defined in Figure 4.2) at 17 UTC.

4.6.3   The Impact of Seasonal Flooding on the UHI of Manaus.

In order to verify the effect of the seasonal flooding on the UHI of Manaus, we compared in this section results produced in the CTL experiment with those resulted in the NonFlood. In this context, Figure 4.12 shows the mean temperature and the horizontal wind difference (CTL-NonFlood) for the central Amazon. In this Figure, the effect of the seasonal flooding on the air temperature is characterized by the positive values simulated in the nighttime

and negatives in the daytime over the river region. The lower temperature simulated over the floodplain region in the CTL experiment intensify the winds over the urban region in the daytime as observed in Figure 4.12 . The consequence of this local wind intensification is the temperature reduction over the urban area as shows (Figure 4.12). In words, the more intense local winds in the CTL experiment transport cooler air more efficiently into the urban area.

In the nighttime, the seasonal flooding causes temperature increase over the floodplain and in the urban area as shown in Figure 4.12. The wind difference over the floodplain region in this Figure is also relevant (maximum difference reaches 1.0 m/s), indicating the seasonal flooding affects considerably the local winds. In the urban area, the wind alteration is slight with the magnitude difference about 0.2 m/s.
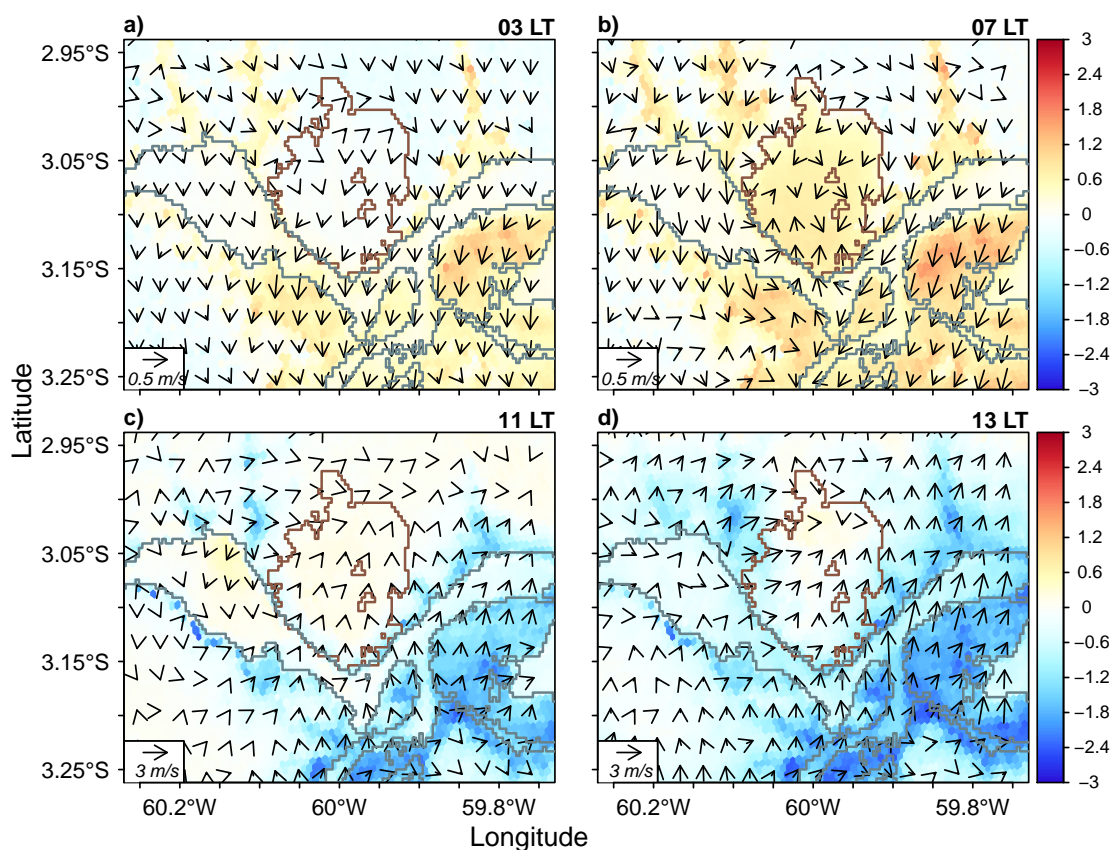
Figure 4.12: Same as Figure 4.8 but the difference is calculated between the CTL and NonFlood experiments.

Figure 4.13 quantify better the effect of the seasonal flooding on the UHI of Manaus. This Figure points out that the temperature increase caused by the seasonal inundation reach values of about 0.5 °C at dawn whereas the reduction in the afternoon reaches -1 °C.

Moreover, this Figure also illustrates that the temperature reduction in the afternoon is more significant in the regions located near the rivers, spatially in the region R2. Figure 4.14 shows that the reduction of the mean temperature difference in the afternoon coincides with the increasing of the mean wind difference. Thus, it confirms that the seasonal flooding increases the local wind and it promotes temperature reduction in the daytime.
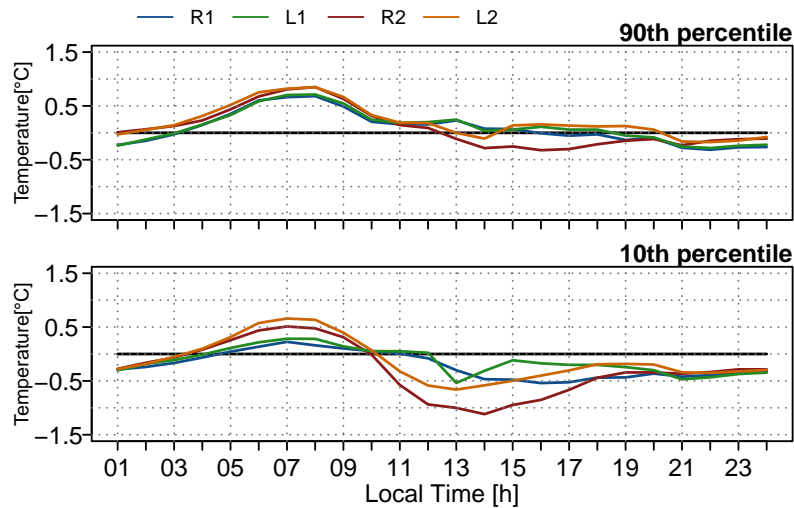
Figure 4.13: Same as Figure 4.10 but the difference is calculated between the CTL and NonFlood experiments.
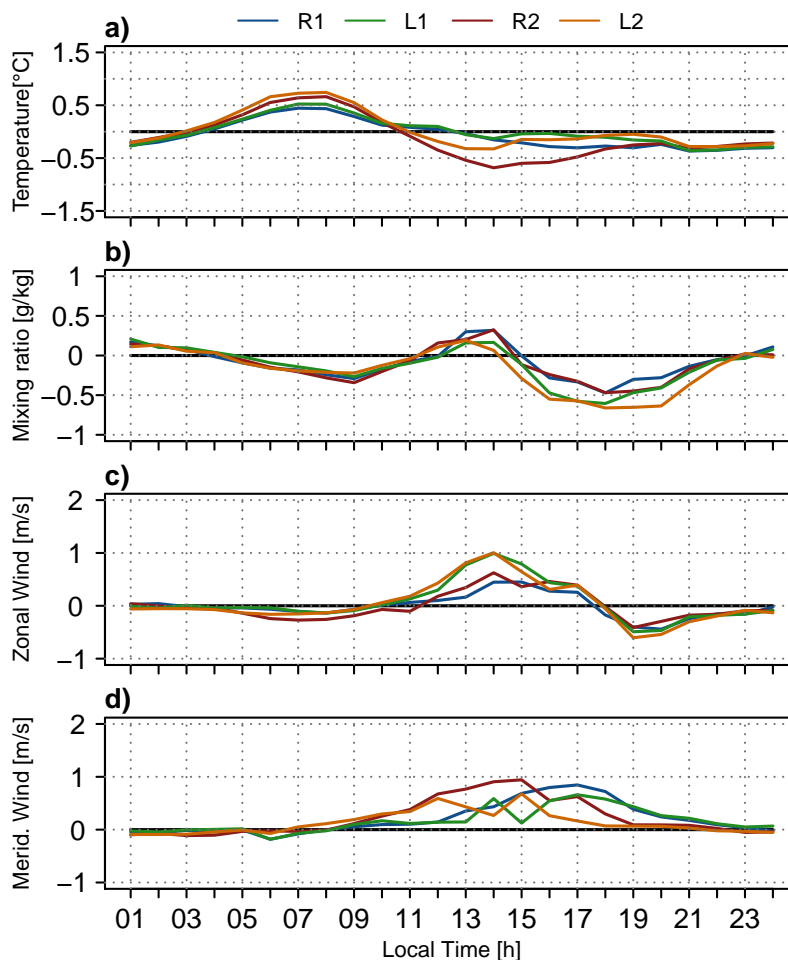
Figure 4.14: Same as Figure 4.9 but the difference is calculated between the CTL and NonFlood experiments.

The effect of the seasonal flooding on the vertical structure of the atmosphere is shown in Figure 4.15. This figure points that the stronger onshore wind simulated in the CTL experiment causes a remarkable alteration of the vertical motion over the urban area. This effect is evident in Figure 4.15a where the positive difference of the vertical wind values is larger than 1 m/s near the Negro River. The vertical wind difference is remarkable over this area because the intensity and position of the breeze front were different in the numerical experiments. In the other parts of the urban area, the intensity of the vertical motion was also differently simulated in the numerical experiments as shows the considerable wind difference. Thus, the vertical structure of temperature and moisture in these experiments are considerably different as indicates the negatives and positives values of the mean temperature and mixing ratio difference presented in Figure 4.15. The vertical wind affects the vertical structure of the atmosphere by two different ways: i)

the direct transportation of heat and mass thought the vertical levels and ii) The vertical motion alters the turbulent and surface fluxes and it, consequently, modifies the vertical structure of temperature and moisture. These fluxes alteration (appendix B.3) is the possible explanation for the larger temperature simulated over the urban area in the CTL experiment shown in Figure 4.13 and 4.14.
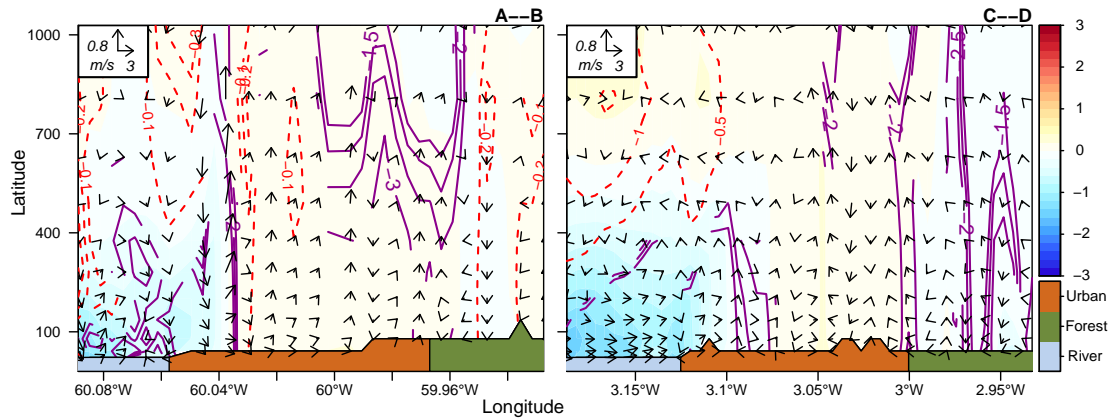
Figure 4.15: Same as Figure 4.11 but the difference is calculated between the CTL and NonFlood experiments.

4.7　Conclusions

The landscape of the Amazon region plays an important role on the local climate as have been discussed in the literature (Fitzjarrald et al., 2008; Saad et al., 2010; Tanaka et al., 2014; Dos Santos et al., 2014; Burleyson et al., 2016). In the Amazon and Solimões confluence region, the water bodies trigger local circulations that affect the spatial distribution of clouds and rainfall (Tanaka et al., 2014; Dos Santos et al., 2014; Burleyson et al., 2016) whereas the Manaus metropolitan area develops an evident UHI (Maitelli and Wright, 1996; de Souza and Alvalá, 2014). These phenomena can interact each other as have been observed around the world Freitas et al. (2007); Chen et al. (2011); Chemel and Sokhi (2012); Sharma et al. (2017). Thus, we investigated here the effect of the rivers on the local climate of Manaus. Moreover, we investigated the impact of the seasonal flooding on the UHI of Manaus since the inundation affect the river breeze intensity (Dos Santos et al., 2017). The main conclusions of these investigations are presented below.

The water bodies in the central Amazon causes remarkable horizontal gradients of temperature that is more intense around noon and at dawn. The mean temperature

difference between water bodies and the Amazon forest is near to 3 °C. The temperature gradient established between rivers and land develops river breezes that propagate over the urban area of Manaus. The velocity of these local circulations is larger than 3.0 m/s. The river breezes transport cooler air from the rivers into the Manaus city causing decreasing of the UHI intensity in the afternoon. This effect is strongly evident near the rivers. The river breeze also affects the UHI of Manaus by altering the vertical structure of the atmosphere and hence the turbulent and surface fluxes. However, these fluxes alteration along with the large temperature gradient caused by the rivers contributes to increases the air temperature over the Manaus city in the nighttime.

The seasonal flooding causes a considerable mean temperature alteration over the floodplain area. In the daytime, this phenomenon promotes a mean temperature decreasing of about 2.5 °C that hence intensifies the river breezes. The intensified river breezes, in turn, transports colder air from the rivers into the urban area more efficiently causing an evident disidentification of the UHI of Manaus in the afternoon. The seasonal flooding also alters the vertical structure of the atmosphere over the urban area causing a remarkable alteration of the surface fluxes. The flux changes contribute to intensifying the UHI of Manaus in the nighttime.

The seasonal flooding in the Amazon is greatly affected by the interannual variability of rainfall as shows the literature Marengo (2009); Marengo et al. (2012); Espinoza et al. (2013); Marengo et al. (2013). Our findings show that one way that regional rainfall variability, over the Andes region for example, may impact the local climate in Manaus by altering the seasonal inundation extent and hence the intensity of the local circulations.

The effect of the rivers and the seasonal flooding on local urban climate is expected to occur in the others cities of the Amazon region that are located close to water bodies. However, studies are necessary to quantify this effect.

Chapter 5

Main Conclusions and Future Works

5.1 Conclusions

This research was organized in three parts. Firstly, we analyzed long-term data set to verify the local wind patterns and its influence on the moisture and precipitation. Secondly, we carried out numerical experiments for a river breeze case to address the role of the seasonal flooding on the river breeze intensity. Finally, numerical simulations for the dry season allowed to establish the impact of the rivers and seasonal flooding on the urban climate of Manaus.

The observational analyses of the local circulations and its role on the moisture transport (chapter 3) were carried out with wind direction and dew point temperature data provided by airport weather stations. The diurnal cycle of precipitation in the central Amazon was analyzed using satellite estimates (TRMM and CMORPH). These investigations allowed to establish the following conclusions:

1. In the daytime, onshore winds commonly observed in the airport weather stations are likely excited by the river breezes;

2. The water vapor pressure during the day is higher when winds are onshore. It suggests that onshore winds (which includes the river breezes) transport moisture air from the river to the Manaus City;

3. Evidence of land breezes at Ponta Pelada Airport are clear as suggests the offshore winds usually verified at night. In offshore wind conditions, drier air from Manaus City is transported to the river regions;

4. The river breeze activity is more evident in the dry season (June – November);

5. The diurnal cycle of precipitation in the central Amazon depends on the river distance. Near and over the rivers, maximum of precipitation happens at dawn and in the early morning. In the region located far from the rivers, maximum of rainfall occurs in the afternoon;

6. The influence of the rivers on the rainfall daily cycle is much more evident in the rainiest quarter (March – May).

In the case study presented in chapter 3, we set up numerical experiments with and without seasonal flooding information and an additional experiment that considered the height of the floodplain forest equal to upland forest. By comparing results provided by these experiments we obtained the following conclusions:

1. The river breezes in the central Amazon are triggered in consequence of the different energy partitioning over the water and land surfaces;

2. The river breezes promote vertical motion over the land altering the vertical structure of the moisture and temperature;

3. The seasonal flooding promotes temperature decrease in the daytime and hence intensification of the river breezes. The intensified rivers breezes propagate more rapidly through the upland region, take longer to dissipate, and promote stronger upward vertical motion;

4. The roughness variation between the floodplain area and the upland region promotes a considerable alteration on the local wind patterns and hence on vertical transport of heat and mass.

The analyses in chapter 4 separated rivers and seasonal flooding influence on the Manaus urban climate. This isolation was carried out by comparing the control with numerical experiments that did not consider the rivers and seasonal flooding effects. The main conclusions of these analyses are presented below:

1. The rivers in the central Amazon promotes development of river breezes that propagate over the urban area of Manaus;

2. The river breezes weaken the UHI in the afternoon by transporting cooler air from the rivers into the Manaus city;

3. The influence of the rivers on the UHI of Manaus is more evident near the rivers;

4. The river breeze also alters the vertical structure of the atmosphere and hence the turbulent and surface fluxes;

5. The seasonal flooding intensifies the river breezes in the afternoon and it, in turns, advects colder air from the rivers into city reducing the UHI magnitude.

The observational analyses presented in chapter 2 evidenced a diurnal pattern of the wind that is likely explained by the river breezes. The numerical simulations presented in chapter 3 and 4 show that the rivers promote a remarkable development of the river breezes in the afternoon. The river breezes are intensified by the seasonal flooding as demonstrated in chapter 3. The local circulations triggered by the rivers also affect the UHI intensity as illustrated in chapter chapter 4. In the afternoon the river breezes advect colder air from the rivers into the Manaus city weakening the UHI magnitude. This effect is more evident when the seasonal flooding is present since it intensifies the river breezes.

This study is the first that shows the flooding influence the local circulation development and on urban heat island intensity. These findings can be applied to studies about urban thermal comfort and regarding local circulations. It also allows us to suggest that the seasonal flooding effect has to be taken into account by the GCMs for an appropriated prediction of the local temperature and precipitation in the weather, climate and climate change simulations. The numerical analyses carried out here also allowed to understand the physical processes involved in the river breeze development and its influence on the local convection of the central Amazon, which has never been done before with the detail and advanced modeling tools presented here. The results concerning the local circulations and diurnal variation of the spatial patterns of precipitation are useful for the agricultural management, waterway transport, Amazon conservation, and the renewable energy studies.

5.2   Future Works

In spite of the conclusions presented in this thesis, more studies are still necessary to fully understand the local climate of the central Amazon. Thus, we plan to contribute

more to the understanding of the Amazon local climate by doing the following analysis:

- Investigation of the rivers and the Manaus urban area influence on the hydroclimate of the central Amazon;

- Evaluation of the interannual variability of river breeze occurrence and its relation with the surface water extent;

- Implementation of new numerical schemes in the OLAM model to predict the surface temperature of the rivers and hence verification of its impact on the river breeze intensity;

- Investigation of the contemporary and predicted deforestation influence on the river breeze;

- Analysis of the deforestation influence on the UHI of Manaus urban.

Bibliography

Artaxo P., Rizzo L. V., Brito J. F., Barbosa H. M. J., Arana A., Sena E. T., Cirino G. G., Bastos W., Martin S. T., Andreae M. O., Atmospheric aerosols in Amazonia and land use change: from natural biogenic to biomass burning conditions, Faraday Discuss., 2013

Bastable H., Shuttleworth W. J., Dallarosa R., Fisch G., Nobre C. A., Observations of climate, albedo, and surface radiation over cleared and undisturbed Amazonian forest, International Journal of Climatology, 1993, vol. 13, p. 783

Betts A. K., Fuentes J. D., Garstang M., Ball J. H., Surface diurnal cycle and boundary layer structure over Rondônia during the rainy season, Journal of Geophysical Research: Atmospheres (1984–2012), 2002, vol. 107, p. LBA

Bolton D., The computation of equivalent potential temperature, Monthly weather review, 1980, vol. 108, p. 1046

Borma L. d. S., Da Rocha H., Cabral O., Von Randow C., Collicchio E., Kurzatkowski D., Brugger P., Freitas H., Tannus R., Oliveira L., et al., Atmosphere and hydrological controls of the evapotranspiration over a floodplain forest in the Bananal Island region, Amazonia, Journal of Geophysical Research: Biogeosciences, 2009, vol. 114

Broxton P. D., Zeng X., Scheftic W., Troch P. A., A MODIS-based global 1-km maximum green vegetation fraction dataset, Journal of Applied Meteorology and Climatology, 2014, vol. 53, p. 1996

Buarque D. C., Paiva R. C. D., Clarke R. T., Mendes C. A., A comparison of Amazon rainfall characteristics derived from TRMM, CMORPH and the Brazilian national

rain gauge network, Journal of Geophysical Research: Atmospheres (1984–2012), 2011, vol. 116, p. D19105

Burleyson C. D., Feng Z., Hagos S. M., Fast J., Machado L. A., Martin S. T., Spatial Variability of the Background Diurnal Cycle of Deep Convection around the GoAmazon2014/5 Field Campaign Sites, Journal of Applied Meteorology and Climatology, 2016

Cantelli A., Monti P., Leuzzi G., A subgrid surface scheme for the analysis of the urban heat island of rome, Hrvatski meteorološki časopis, 2008, vol. 43, p. 354

Chemel C., Sokhi R. S., Response of London's urban heat island to a marine air intrusion in an easterly wind regime, Boundary-layer meteorology, 2012, vol. 144, p. 65

Chen F., Miao S., Tewari M., Bao J.-W., Kusaka H., A numerical study of interactions between surface forcing and sea breeze circulations and their effects on stagnation in the greater Houston area, Journal of Geophysical Research: Atmospheres, 2011, vol. 116

Crosman E. T., Horel J. D., Sea and lake breezes: a review of numerical studies, Boundary-layer meteorology, 2010, vol. 137, p. 1

Cuartas L. A., Tomasella J., Nobre A. D., Nobre C. A., Hodnett M. G., Waterloo M. J., de Oliveira S. M., von Randow R. d. C., Trancoso R., Ferreira M., Distributed hydrological modeling of a micro-scale rainforest watershed in Amazonia: Model evaluation and advances in calibration using the new HAND terrain model, Journal of hydrology, 2012, vol. 462, p. 15

Culf A. D., Esteves J. L., Marques Filho A. O., da Rocha H. R., , 1996 in Gash J. H. C., Nobre C. A., Roberts J. M., Victoria R. L., eds, , Amazonian deforestation and climate. John Wiley & Son Ltd New York pp 175–192

Cutrim E., Martin D. W., Rabin R., Enhancement of cumulus clouds over deforested lands in Amazonia, Bulletin of the American Meteorological Society, 1995, vol. 76, p. 1801

Da Silva R. R., Gandu A. W., Sá L. D., Dias M. A. S., Cloud streets and land–water interactions in the Amazon, Biogeochemistry, 2011, vol. 105, p. 201

Dadson S. J., Ashpole I., Harris P., Davies H. N., Clark D. B., Blyth E., Taylor C. M., Wetland inundation dynamics in a model of land surface climate: Evaluation in the Niger inland delta region, Journal of Geophysical Research: Atmospheres, 2010, vol. 115

Davidson E. A., de Araújo A. C., Artaxo P., Balch J. K., Brown I. F., Bustamante M. M., Coe M. T., DeFries R. S., Keller M., Longo M., et al., The Amazon basin in transition, Nature, 2012, vol. 481, p. 321

de Souza D. O., Alvalá R. C., Observational evidence of the urban heat island of Manaus City, Brazil, Meteorological Applications, 2014, vol. 21, p. 186

De Souza D. O., Alvalá R. C., do Nascimento M. G., Urbanization effects on the microclimate of Manaus: A modeling study, Atmospheric Research, 2016, vol. 167, p. 237

Dos Santos M. J., Silva Dias M. A., Freitas E. D., Influence of local circulations on wind, moisture, and precipitation close to Manaus City, Amazon Region, Brazil, Journal of Geophysical Research: Atmospheres, 2014, vol. 119

Dos Santos M. J., Silva Dias M. A., Freitas E. D., Kim H., Seasonal Flooding Causes Intensification of the River Breeze in the Central Amazon. Manuscript in preparation., 2017

Doughty C. E., Goulden M. L., Seasonal patterns of tropical forest leaf area index and CO2 exchange, Journal of Geophysical Research: Biogeosciences, 2008, vol. 113

Durieux L., Machado L. A. T., Henri L., The impact of deforestation on cloud cover over the Amazon arc of deforestation, Remote Sensing of Environment, 2003, vol. 86, p. 132

Espinoza J. C., Ronchail J., Frappart F., Lavado W., Santini W., Guyot J. L., The major floods in the Amazonas River and tributaries (western Amazon basin) during the 1970–2012 period: a focus on the 2012 flood, Journal of Hydrometeorology, 2013, vol. 14, p. 1000

Fitzjarrald D. R., Sakai R. K., Moraes O. L. L., Oliveira R. C., Acevedo O. C., Beldini M. J. C. T., Spatial and temporal rainfall variability near the Amazon-Tapajós confluence, Journal of Geophysical Research: Biogeosciences (2005–2012), 2008, vol. 113

Freitas E. D., Rozoff C. M., Cotton W. R., Dias P. L. S., Interactions of an urban heat island and sea-breeze circulations during winter over the metropolitan area of São Paulo, Brazil, Boundary-Layer Meteorology, 2007, vol. 122, p. 43

Gan M. A., Kousky V. E., Ropelewski C. F., The south america monsoon circulation and its relationship to rainfall over west-central Brazil, Journal of climate, 2004, vol. 17, p. 47

Gartland L. M., Heat islands: understanding and mitigating heat in urban areas. Routledge, 2012

Gash J., Nobre C., Climatic effects of Amazonian deforestation: Some results from ABRACOS, Bulletin of the American Meteorological Society, 1997, vol. 78, p. 823

Grell G. A., Freitas S. R., A scale and aerosol aware stochastic convective parameterization for weather and air quality modeling, Atmos. Chem. Phys. Discuss, 2013, vol. 13, p. 23845

Gutman G., Ignatov A., The derivation of the green vegetation fraction from NOAA/AVHRR data for use in numerical weather prediction models, International Journal of remote sensing, 1998, vol. 19, p. 1533

Hess L. L., Melack J. M., Novo E. M., Barbosa C. C., Gastil M., Dual-season mapping of wetland inundation and vegetation for the central Amazon basin, Remote Sensing of Environment, 2003, vol. 87, p. 404

Hill G. E., Factors controlling the size and spacing of cumulus clouds as revealed by numerical experiments, Journal of the Atmospheric Sciences, 1974, vol. 31, p. 646

Huffman G. J., Bolvin D. T., Nelkin E. J., Wolff D. B., Adler R. F., Gu G., Hong Y., Bowman K. P., Stocker E. F., The TRMM Multisatellite Precipitation Analysis (TMPA): Quasi-global, multiyear, combined-sensor precipitation estimates at fine scales, Journal of Hydrometeorology, 2007, vol. 8, p. 38

Iacono M. J., Delamere J. S., Mlawer E. J., Shephard M. W., Clough S. A., Collins W. D., Radiative forcing by long-lived greenhouse gases: Calculations with the AER radiative transfer models, Journal of Geophysical Research: Atmospheres, 2008, vol. 113

IBGE I. B. d. G. e. E., , 2010 Instituto Brasileiro de Geografia e Estatística - IBGE

Jolliffe I. T., Stephenson D. B., Forecast verification: a practitioner's guide in atmospheric science. John Wiley & Sons, 2003

Joyce R. J., Janowiak J. E., Arkin P. A., Xie P., CMORPH: A method that produces global precipitation estimates from passive microwave and infrared data at high spatial and temporal resolution, Journal of Hydrometeorology, 2004, vol. 5, p. 487

Khanna J., Medvigy D., Strong control of surface roughness variations on the simulated dry season regional atmospheric response to contemporary deforestation in Rondônia, Brazil, Journal of Geophysical Research: Atmospheres, 2014, vol. 119

Khanna J., Medvigy D., Fueglistaler S., Walko R., Regional dry-season climate changes due to three decades of Amazonian deforestation, Nature Climate Change, 2017, vol. 7, p. 200

Kim H., Yeh P. J.-F., Oki T., Kanae S., Role of rivers in the seasonal variations of terrestrial water storage over global basins, Geophysical Research Letters, 2009, vol. 36

Klein Goldewijk K., Ramankutty N., Land cover change over the last three centuries due to human activities: the availability of new global data sets, GeoJournal, 2004, vol. 61, p. 335

Lapola D. M., Oyama M. D., Nobre C. A., Sampaio G., A new world natural vegetation map for global change studies, Anais da Academia Brasileira de Ciências, 2008, vol. 80, p. 397

Lee X., Goulden M. L., Hollinger D. Y., Barr A., Black T. A., Bohrer G., Bracho R., Drake B., Goldstein A., Gu L., et al., Observed increase in local cooling effect of deforestation at higher latitudes, Nature, 2011, vol. 479, p. 384

Lilly D. K., On the numerical simulation of buoyant convection, Tellus, 1962, vol. 14, p. 148

Lu L., Denning A. S., da Silva-Dias M. A. F., da Silva-Dias P. L., Longo M., Freitas S. R., Saatchi S., Mesoscale circulations and atmospheric CO_2 variations in the Tapajós

Region, Pará, Brazil, Journal of Geophysical Research: Atmospheres (1984–2012), 2005, vol. 110

Machado L., Laurent H., Dessay N., Miranda I., Seasonal and diurnal variability of convection over the Amazonia: a comparison of different vegetation types and large scale forcing, Theoretical and Applied Climatology, 2004, vol. 78, p. 61

Mahmood R., Leeper R., Quintanar A. I., Sensitivity of planetary boundary layer atmosphere to historical and future changes of land use/land cover, vegetation fraction, and soil moisture in Western Kentucky, USA, Global and Planetary Change, 2011, vol. 78, p. 36

Maitelli G. T., Wright I. R., , 1996 in Gash J. H. C., Nobre C. A., Roberts J. M., Victoria R. L., eds, , Amazonian deforestation and climate. John Wiley & Son Ltd New York pp 193–206

Malhado A. C., Costa M. H., de Lima F. Z., Portilho K. C., Figueiredo D. N., Seasonal leaf dynamics in an Amazonian tropical forest, Forest ecology and management, 2009, vol. 258, p. 1161

Marengo J. A., Characteristics and spatio-temporal variability of the Amazon River Basin Water Budget, Climate Dynamics, 2005, vol. 24, p. 11

Marengo J. A., On the hydrological cycle of the Amazon Basin: A historical review and current state-of-the-art, Revista Brasileira de Meteorologia, 2006, vol. 21, p. 1

Marengo J. A., Long-term trends and cycles in the hydrometeorology of the Amazon basin since the late 1920s, Hydrological Processes, 2009, vol. 23, p. 3236

Marengo J. A., Alves L. M., Soares W. R., Rodriguez D. A., Camargo H., Riveros M. P., Pabló A. D., Two contrasting severe seasonal extremes in tropical South America in 2012: flood in Amazonia and drought in northeast Brazil, Journal of climate, 2013, vol. 26, p. 9137

Marengo J. A., Nobre C. A., Culf A. D., Climatic impacts of *friagens* in forested and deforested areas of the Amazon basin, Journal of applied meteorology, 1997, vol. 36, p. 1553

Marengo J. A., Tomasella J., Soares W. R., Alves L. M., Nobre C. A., Extreme climatic events in the Amazon basin, Theoretical and Applied Climatology, 2012, vol. 107, p. 73

Margulis S., Causes of deforestation of the Brazilian Amazon. Washington, DC: World Bank, 2004

Martin C. L., Fitzjarrald D., Garstang M., Oliveira A. P., Greco S., Browell E., Structure and growth of the mixing layer over the Amazonian rain forest, Journal of Geophysical Research: Atmospheres (1984–2012), 1988, vol. 93, p. 1361

Masson V., A physically-based scheme for the urban energy budget in atmospheric models, Boundary-layer meteorology, 2000, vol. 94, p. 357

Medvigy D., Walko R., Avissar R., Modeling interannual variability of the Amazon hydroclimate, Geophysical Research Letters, 2008, vol. 35

Medvigy D., Walko R. L., Avissar R., Effects of deforestation on spatiotemporal distributions of precipitation in South America, Journal of Climate, 2011, vol. 24, p. 2147

Molion L. C. B., Dallarosa R. L. G., Pluviometria da Amazônia: são os dados confiáveis, Climanálise-Boletim de Monitoramento e Análise Climática, 1990, vol. 5, p. 40

NASA L. D., MODIS Land Cover Type Yearly L3 Global 500 m SIN Grid (MCD12Q1), NASA EOSDIS Land Processes DAAC, USGS Earth Resources Observation and Science (EROS) Center, Sioux Falls, South Dakota (https://lpdaac. usgs. gov), 2014

NOAA/NESDIS GOES Level 3 6km Near Real Time SST 1 Hour, 2014

Nobre A., Cuartas L., Hodnett M., Rennó C., Rodrigues G., Silveira A., Waterloo M., Saleska S., Height above the nearest drainage–a hydrologically relevant new terrain model, Journal of Hydrology, 2011, vol. 404, p. 13

Oke T. R., Boundary layer climates. Routledge, 2002

Oliveira A. P., Fitzjarrald D. R., The Amazon river breeze and the local boundary layer: I. Observations, Boundary-Layer Meteorology, 1993, vol. 63, p. 141

Oliveira A. P., Fitzjarrald D. R., The Amazon river breeze and the local boundary layer: II. Linear analysis and modelling, Boundary-Layer Meteorology, 1994, vol. 67, p. 75

Ometto J. P., Aguiar A. P. D., Martinelli L. A., Amazon deforestation in Brazil: effects, drivers and challenges, Carbon Management, 2011, vol. 2, p. 575

Paiva R. C. D., Buarque D. C., Clarke R. T., Collischonn W., Allasia D. G., Reduced precipitation over large water bodies in the Brazilian Amazon shown from TRMM data, Geophysical Research Letters, 2011, vol. 38

Papa F., Prigent C., Aires F., Jimenez C., Rossow W., Matthews E., Interannual variability of surface water extent at the global scale, 1993–2004, Journal of Geophysical Research: Atmospheres, 2010, vol. 115

Pielke Sr R. A., Mesoscale meteorological modeling 2nd edn. Academic press, 2002

Pitman A. J., Narisma G. T., Pielke R., Holbrook N., Impact of land cover change on the climate of southwest Western Australia, Journal of Geophysical Research: Atmospheres, 2004, vol. 109

Prigent C., Papa F., Aires F., Rossow W., Matthews E., Global inundation dynamics inferred from multiple satellite observations, 1993–2000, Journal of Geophysical Research: Atmospheres, 2007, vol. 112

Raia A., Cavalcanti I. F. A., The life cycle of the South American monsoon system, Journal of climate, 2008, vol. 21, p. 6227

Ramankutty N., Gibbs H. K., Achard F., Defries R., Foley J. A., Houghton R., Challenges to estimating carbon emissions from tropical deforestation, Global change biology, 2007, vol. 13, p. 51

Ramos da Silva R., Gandú A. W., Cohen J. C., Kuhn P., Mota M. A., Weather forecasting for Eastern Amazon with OLAM model, Revista Brasileira de Meteorologia, 2014, vol. 29, p. 11

Ramos da Silva R., Haas R., Ocean Global Warming Impacts on the South America Climate, Frontiers in Earth Science, 2016, vol. 4, p. 30

Ramos da Silva R., Vitorino M. I., Kuhn P., Ananias D. d. S., Climate estimates for Eastern Amazon with OLAM model, Revista Brasileira de Meteorologia, 2014, vol. 29, p. 2

Bibliography

Rao V. B., Cavalcanti I. F. A., Hada K., Annual variation of rainfall over Brazil and water vapor characteristics over South America, Journal of Geophysical Research, 1996, vol. 101, p. 26539

Ribeiro M., Adis J., Local rainfall variability, a potential bias for bioecological studies in the Central Amazon, Acta Amazonica, 1984, vol. 14, p. 159

Rizwan A. M., Dennis L. Y., Chunho L., A review on the generation, determination and mitigation of Urban Heat Island, Journal of Environmental Sciences, 2008, vol. 20, p. 120

Saad S. I., Da Rocha H. R., Silva Dias M. A., Rosolem R., Can the deforestation breeze change the rainfall in Amazonia? A case study for the BR-163 highway region, Earth Interactions, 2010, vol. 14, p. 1

Saha S., Moorthi S., Wu X., Wang J., Nadiga S., Tripp P., Behringer D., Hou Y.-T., Chuang H.-y., Iredell M., et al., The NCEP climate forecast system version 2, Journal of Climate, 2014, vol. 27, p. 2185

Satyamurty P., Costa C. P. W., Manzi A. O., Candido L. A., A quick look at the 2012 record flood in the Amazon Basin, Geophysical Research Letters, 2013, vol. 40, p. 1396

Schedlbauer J. L., Oberbauer S. F., Starr G., Jimenez K. L., Controls on sensible heat and latent energy fluxes from a short-hydroperiod Florida Everglades marsh, Journal of Hydrology, 2011, vol. 411, p. 331

Sharma A., Fernando H. J., Hamlet A. F., Hellmann J. J., Barlage M., Chen F., Urban meteorological modeling using WRF: a sensitivity study, International Journal of Climatology, 2017, vol. 37, p. 1885

Shukla J., Nobre C., Sellers P., et al., Amazon deforestation and climate change., Science(Washington), 1990, vol. 247, p. 1322

Silva C. M. S., Gielow R., Freitas S. R., Diurnal and semidiurnal rainfall cycles during the rain season in SW Amazonia, observed via rain gauges and estimated using S-band radar, Atmospheric Science Letters, 2009, vol. 10, p. 87

Silva Dias M. A. F., Dias P. L. S., Longo M., Fitzjarrald D. R., Denning A. S., River breeze circulation in eastern Amazonia: observations and modelling results, Theoretical and Applied Climatology, 2004, vol. 78, p. 111

Simard M., Pinto N., Fisher J. B., Baccini A., Mapping forest canopy height globally with spaceborne lidar, Journal of Geophysical Research: Biogeosciences, 2011, vol. 116

Sippel S. J., Hamilton S. K., Melack J. M., Choudhury B. J., Determination of inundation area in the Amazon River floodplain using the SMMR 37 GHz polarization difference, Remote Sensing of Environment, 1994, vol. 48, p. 70

Smagorinsky J., General circulation experiments with the primitive equations: I. the basic experiment*, Monthly weather review, 1963, vol. 91, p. 99

Sorribas M. V., Paiva R. C., Melack J. M., Bravo J. M., Jones C., Carvalho L., Beighley E., Forsberg B., Costa M. H., Projections of climate change effects on discharge and inundation in the Amazon basin, Climatic Change, 2016, pp 1–16

Souza D. O., Alvalá R. C. S., Observational evidence of the urban heat island of Manaus City, Brazil, Meteorological Applications, 2012

Tanaka L. d. S., Satyamurty P., Machado L., Diurnal variation of precipitation in central Amazon Basin, International Journal of Climatology, 2014, vol. 34, p. 3574

Vitousek P. M., Mooney H. A., Lubchenco J., Melillo J. M., Human domination of Earth's ecosystems, Science, 1997, vol. 277, p. 494

Walko R. L., Avissar R., The ocean-land-atmosphere model (OLAM). Part I: Shallow-water tests, Monthly Weather Review, 2008a, vol. 136, p. 4033

Walko R. L., Avissar R., The Ocean-Land-Atmosphere Model (OLAM). Part II: Formulation and tests of the nonhydrostatic dynamic core, Monthly Weather Review, 2008b, vol. 136, p. 4045

Walko R. L., Avissar R., A direct method for constructing refined regions in unstructured conforming triangular–hexagonal computational grids: Application to OLAM, Monthly Weather Review, 2011, vol. 139, p. 3923

Walko R. L., Band L. E., Baron J., Kittel T. G., Lammers R., Lee T. J., Ojima D., Pielke Sr R. A., Taylor C., Tague C., et al., Coupled atmosphere-biophysics-hydrology models for environmental modeling, Journal of applied meteorology, 2000, vol. 39, p. 931

Walko R. L., Cotton W. R., Meyers M., Harrington J., New RAMS cloud microphysics parameterization part I: the single-moment scheme, Atmospheric Research, 1995, vol. 38, p. 29

Wang L., Good S. P., Caylor K. K., Global synthesis of vegetation control on evapotranspiration partitioning, Geophysical Research Letters, 2014, vol. 41, p. 6753

Wu C.-L., Shukla S., Shrestha N. K., Evapotranspiration from drained wetlands with different hydrologic regimes: Drivers, modeling, and storage functions, Journal of Hydrology, 2016, vol. 538, p. 416

Yamazaki D., Almeida G. A., Bates P. D., Improving computational efficiency in global river models by implementing the local inertial flow equation and a vector-based river network map, Water Resources Research, 2013, vol. 49, p. 7221

Yamazaki D., Kanae S., Kim H., Oki T., A physically based description of floodplain inundation dynamics in a global river routing model, Water Resources Research, 2011, vol. 47

Yamazaki D., Lee H., Alsdorf D. E., Dutra E., Kim H., Kanae S., Oki T., Analysis of the water level dynamics simulated by a global river model: A case study in the Amazon River, Water Resources Research, 2012, vol. 48

Yamazaki D., Oki T., Kanae S., Deriving a global river network map and its sub-grid topographic characteristics from a fine-resolution flow direction map, Hydrology and Earth System Sciences, 2009, vol. 13, p. 2241

Zeng Z., Piao S., Lin X., Yin G., Peng S., Ciais P., Myneni R. B., Global evapotranspiration over the past three decades: estimation based on the water balance equation combined with empirical models, Environmental Research Letters, 2012, vol. 7, p. 14026

Zhang H., Sato N., Izumi T., Hanaki K., Aramaki T., Modified RAMS-urban canopy model for heat island simulation in Chongqing, China, Journal of Applied Meteorology and Climatology, 2008, vol. 47, p. 509

Zhong S., Jr J. M. L., Takle E. S., Interaction of the sea breeze with a river breeze in an area of complex coastal heating, Boundary-Layer Meteorology, 1991, vol. 56, p. 101

Zhou J., Lau K.-M., Does a monsoon climate exist over South America?, Journal of climate, 1998, vol. 11, p. 1020

Appendix

Appendix A

Model Parameters

Table A.1 - Vegetation parameters used in the OLAM simulations.

Parameters	Evergreen broad-leaf forest	Floodplain
Albedo	0.17	0.17
Vegetation Height [m]	32.0	21.0
Root Depth [m]	5.0	5.0
Minimal stomatal resistance [sm^1]	500.0	500.0

In the microphysical scheme, the concentration of the hydrometers was prognosed and the diameter was diagnosed. The other parameters of this physical scheme are shown in the below table.

Table A.2 - Parameters of the microphysical scheme.

Parameters	Value
Source or sink	0 (off)
Transport rain/graupel/hail internal energy	1 (on)
CCN concen [$\#/kg_{air}$]	$3\mathrm{x}10^8$
GCCN concen [$\#/kg_{air}$]	10
Median radius of the CCN dist [m]	$4\mathrm{x}10^{-8}$
Median radius of the GCCN dist[m]	$3\mathrm{x}10^{-6}$

Fluxes of Energy and Radiation
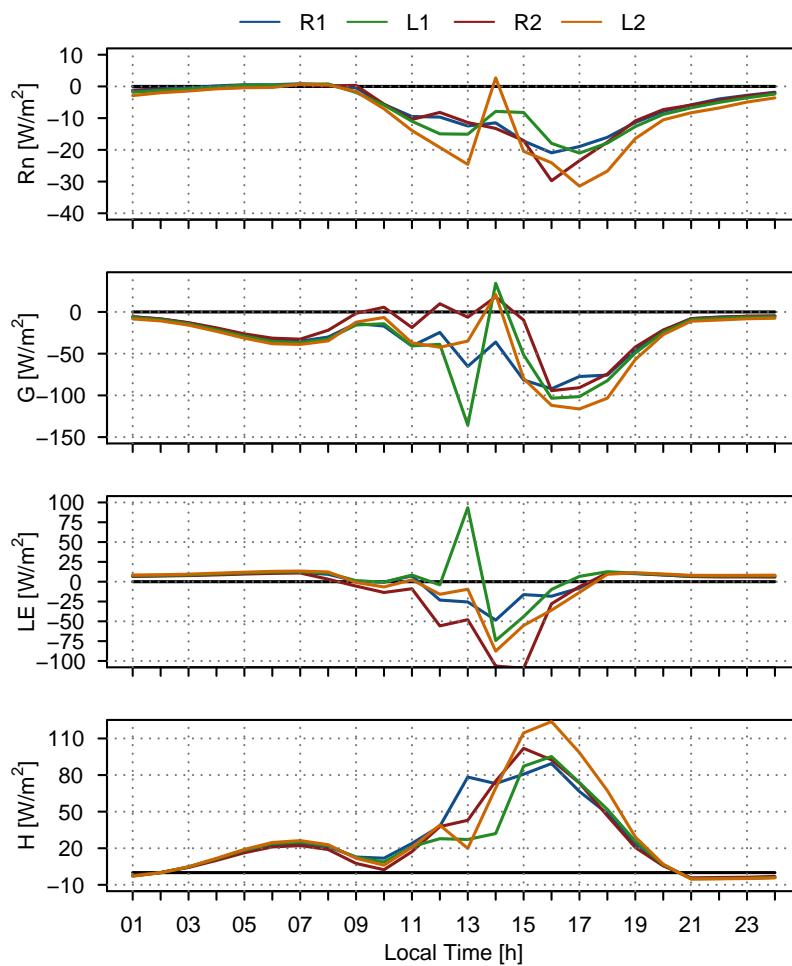
Figure B.1: Diurnal cycles of the surface energy fluxes difference between CTL and NonRiver experiments for four regions of the Manaus city (L1, L2 ,R1, R2 – see Figure 3.2)
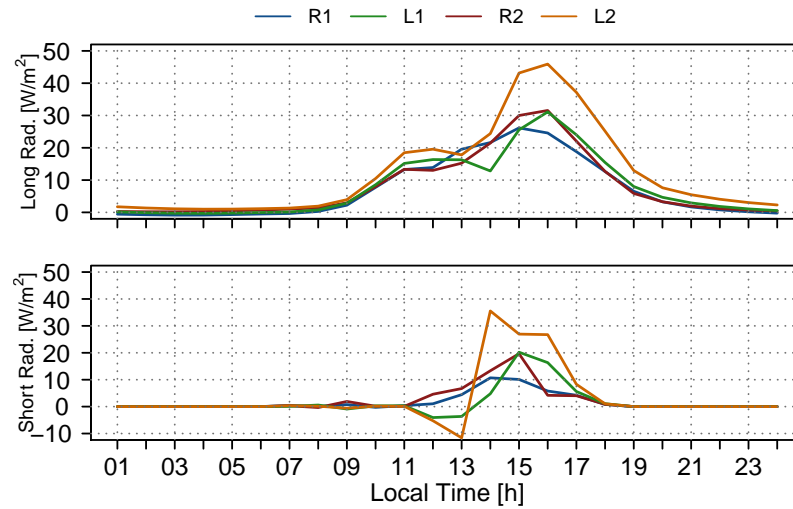
Figure B.2: Diurnal cycles of the radiation difference between CTL and NonRiver experiments for four regions of the Manaus city (L1, L2 ,R1, R2 – see Figure 3.2)
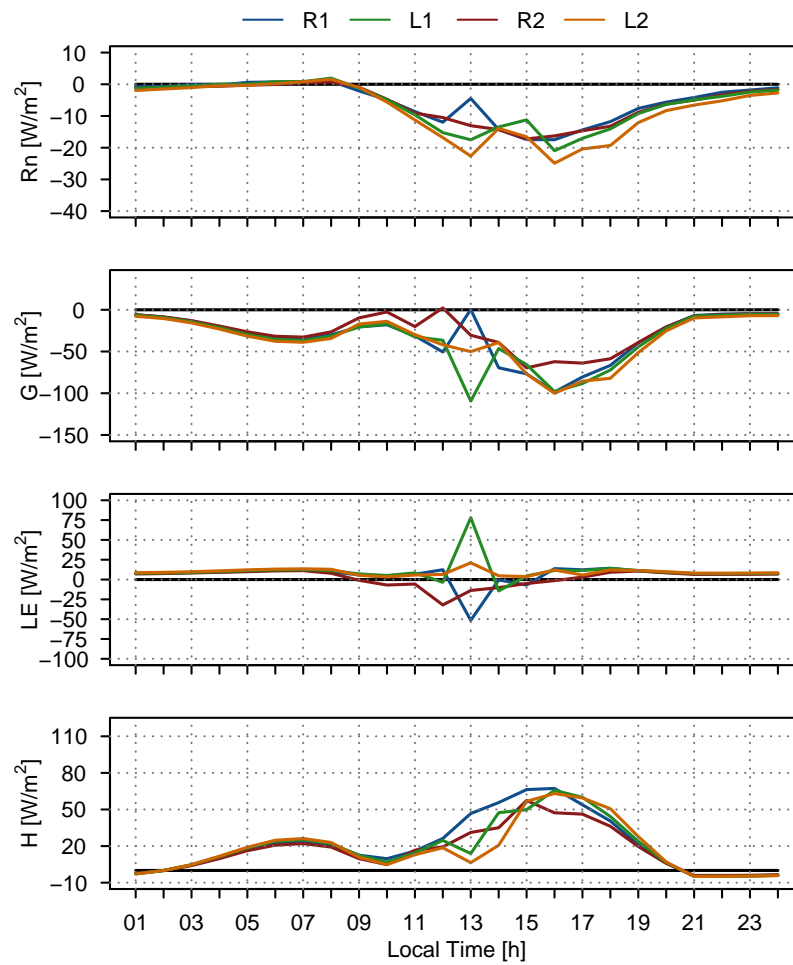
Figure B.3: Diurnal cycles of the surface energy fluxes difference between CTL and NonFlood experiments for four regions of the Manaus city (L1, L2 ,R1, R2 – see Figure 3.2)
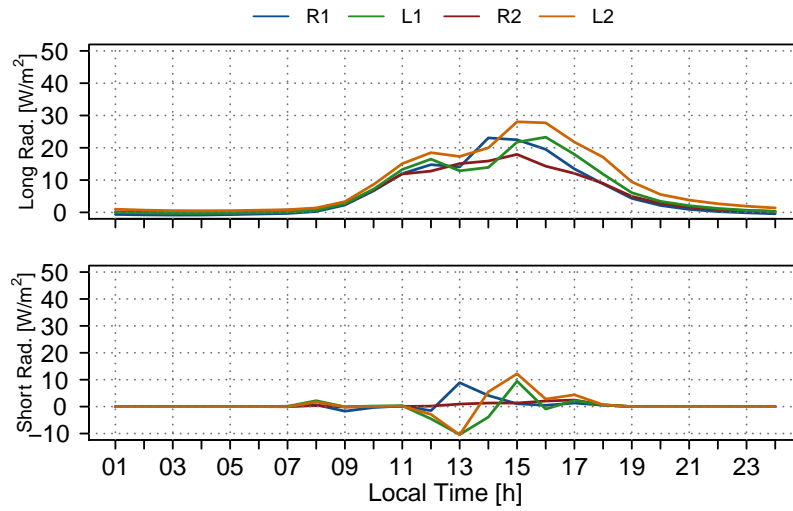
Figure B.4: Diurnal cycles of the radiation difference between CTL and NonFlood experiments for four regions of the Manaus city (L1, L2 ,R1, R2 – see Figure 3.2)